METRICS AND PERFORMANCE ANALYSIS OF NEXT GENERATION HANDHELD MINE DETECTORS

by

Marie Talbott
A Thesis
Submitted to the
Graduate Faculty
of
George Mason University
in Partial Fulfillment of
The Requirements for the Degree
of
Master of Science
Electrical Engineering

Committee:

_____	Dr. Gerald Cook, Earle C. Williams Professor, Thesis Director
_____	Dr. Lloyd Griffiths, Dean Emeritus, Committee Member
_____	Dr. Dimitris Ioannou, Committee Member
_____	Dr. Monson Hayes, Department Chair
_____	Dr. Kenneth S. Ball, Dean, Volgenau School of Engineering
Date:_____	Spring Semester 2017 George Mason University Fairfax, VA

Metrics and Performance Analysis of Next Generation Handheld Mine Detectors

A Thesis submitted in partial fulfillment of the requirements for the degree of Master of Science at George Mason University

by

Marie Talbott
Bachelor of Science
Physics and Electrical Engineering, 2012

Director: Gerald Cook of Electrical Engineering
Department of Electrical and Computer Engineering

Spring Semester 2017
George Mason University
Fairfax, VA

DISTRIBUTION STATEMENT

Distribution Statement A: Approved for public release; distribution is unlimited.

ACKNOWLEDGEMENTS

This work is funded by the Countermine Division of the Night Vision and Electronic Sensors Directorate (NVESD) of the U.S. Army through the author's place of employment at the Institute for Defense Analysis (IDA).

TABLE OF CONTENTS

LIST OF TABLES

LIST OF FIGURES

ABSTRACT

METRICS AND PERFORMANCE ANALYSIS OF NEXT GENERATION HANDHELD MINE DETECTORS

Marie Talbott, M.S.

George Mason University, 2017

Thesis Director: Dr. Gerald Cook

Soldiers in theater face the threat of mines and improvised explosive devices (IEDs) which grow more sophisticated and more dangerous each year. In current conflicts, insurgents regularly use IEDs along well-traveled roads or even in urban environments to disrupt and delay soldiers during missions, as soldiers must first clear a safe path forward before proceeding. Mine and IED detection systems in theater can be integrated onto a vehicle, robotic platform, or a handheld system and use a variety of sensors to detect potential threats.

In this thesis, we will analyze data collected by three handheld mine detectors that utilize Ground Penetrating Radar (GPR) to detect mines and IEDs. These detectors are prototypes intended to improve upon the handheld detector currently fielded by the US Army. We will assess each GPR system's capabilities for detecting targets as well as the system's limitations, particularly targets with little or no metal content.

Data used in this thesis is from a collection that occurred in April and May 2016 at a US Army test site over relevant targets and threats. Data was collected with all three prototype systems and the currently fielded handheld detector over a short time period so

that any environmental or weather issues that may impact system performance would be experienced by all systems.

These systems are prototypes and thus a signal over background metric will be applied to the data collected with each system to calculate detections of targets (GPR response at a target location) and false alarms (GPR response not due to a target). Several methods for selecting the background for the signal over background will be investigated as there are varying levels of position information available for each detector. Once the signal over background metric is calculated for all data collected with each system, alarms will be created using a simple peak picking algorithm and using a blobbing technique. These alarms will then be scored using methodology identical to the analysis the author performs at her place of employment (The Institute for Defense Analyses) in support of the Countermine Division of Night Visions and Electronic Sensors Directorate (NVESD) based in Fort Belvoir, to assess a variety of mine and IED detection systems. Results will be shown for each system broken down into target type and target depth. Because there was rainfall during the data collection, results will also be compared for dry and wet conditions.

CHAPTER 1: INTRODUCTION

1.1 Background

There are an estimated 110 million landmines emplaced in the world that kill 15,000 to 20,000 people a year [1]. These landmines exist in areas previously or currently engaged in conflict. In Iraq and Afghanistan, mines and Improvised Explosive Devices (IEDs) were the cause of roughly half of all United States soldier casualties between 2007 and 2013 [2].

Whereas landmines are manufactured by various countries around the world, IEDs are often homemade and comprised of cheap or easily attainable materials. Landmines are typically described as high or low metal, but IEDs can consist of low-metal or completely non-metallic materials which will not be detected by a metal detector. Both landmines and IEDs are categorized as Anti-Personal (AP) or Anti-Tank (AT). AP landmines and IEDs are smaller than AT landmines and IEDs because AT targets are intended to damage a vehicle. Ground Penetrating Radar (GPR) is effective at finding buried threats with little or no metal content depending on the burial depth and soil conditions.

The strength of ground penetrating radar return depends on the contrast in dielectric properties of the target and surrounding soil. Soil moisture plays a critical role in target detection and discrimination from clutter as it can enhance the contrast between

the target and surrounding soil, but too much moisture can limit the radar waves' penetration of the ground. [3] The equation for GPR attenuation is:

$$\alpha = \omega \sqrt{\frac{\mu\varepsilon}{2}\left[\sqrt{1+\left(\frac{\sigma}{\omega\varepsilon}\right)^2}-1\right]}$$

In the above equation, μ is the permeability, ε is the permittivity, ω is the frequency in radians, and σ is the conductivity which gives the attenuation coefficient for the medium [4].

As seen in Table 1.1 wet soil has a larger permittivity value or ε, which means that it also has a larger attenuation coefficient and that the radar waves cannot penetrate as far into the ground. However, dry sand and explosives, such as TNT or TNT simulants, have very similar relative permittivity values which means there is little contrast between the target and the surrounding soil. Saturated sand has a significantly higher relative permittivity, which heightens the contrast between a target and its surrounding soil, but too much moisture results in a large attenuation coefficient.

Table 1.1: Relative Permittivity Values for Relevant Materials [5] [6]

Material	Relative Permittivity
Air	1
Fresh Water	80
Dry Sand	3-5
Saturated Sand	20-30
Clay	5-40
TNT	3-3.5
Dow Corning (TNT Simulant)	3-3.5

Relative permittivity values of the above mediums also impact the reflection and transmission coefficients of radar propagation [7]. Radar waves from GPR systems travel through three different regions: air, soil, and target (or explosive/simulant within the target) as seen in the figure below.

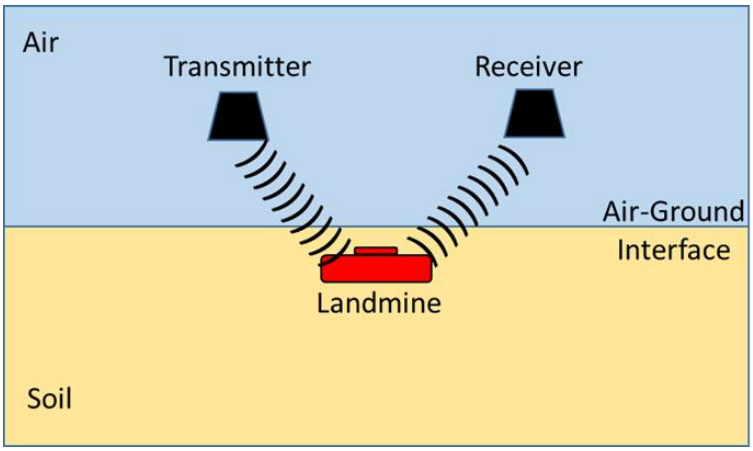

Figure 1.1: GPR Propagation in Soil

Contrast between the target and surrounding soil is a function of the portion of incident signal that is reflected or scattered from the objects of interest. If the encounter is between the soil and target (or landmine), the reflection coefficient is the ratio of the amplitude of the reflected wave to the amplitude of the incident wave. A perfect reflector has a reflection coefficient of 1. There is no true perfect reflector, but metal objects are very close. Non-metal objects, such as low-metal landmines or IEDs, have a reflection

coefficient much less than 1. The reflection coefficient between two mediums is given by the following equation [8].

$$R = \frac{\sqrt{\varepsilon_2} - \sqrt{\varepsilon_1}}{\sqrt{\sqrt{\varepsilon_2} + \sqrt{\varepsilon_1}}}$$

In the above equation ε_1 is the permittivity of the soil, ε_2 is the permittivity of the target, and the soil is assumed to be non-magnetic, which is a reasonable assumption for the data analyzed in this thesis [9].

The radar cross section (RCS) of a target is a strong function of the reflection coefficient. The RCS of a target depends on the reflection coefficient and target geometry and orientation and is described generally in the following equation [10].

$$\sigma = \lim_{R \to \infty} 4\pi R^2 \frac{|E_s|^2}{|E_i|^2}$$

The radar cross section, denoted as σ, is the limit of the incident signal E_i and the scattered signal E_s as the range goes to infinity. Metal targets, such as metal cased mines or IED components with large amounts of metal, have a high RCS since they are close to a perfect reflector, while non-metal targets like most IED components or plastic cased mines have a low RCS. RCS is also proportional to target size and thus larger targets are more detectable than smaller targets.

Another consideration in GPR performance and target detectability is the bandwidth of the GPR. A wide band GPR is required to detect targets at a variety of depths and sizes, while having enough range resolution to discriminate responses from targets and clutter. Clutter sources abound in GPR propagation from soil characteristics, subsurface rocks, response from the ground, and self-reflection from the antenna. GPR

performance is limited by the Signal to Clutter Ratio (SCR), not the Signal to Noise Ratio (SNR) of a system.

Most GPRs designed to detect shallow targets operate at frequencies between 200 MHz and 5000MHz. Range resolution, or depth resolution since the radar is ground penetrating, is calculated by the following equation.

$$\Delta R = \frac{c}{2B\sqrt{\varepsilon_r}}$$

The depth resolution is a function of c (the speed of light), the bandwidth (B), and εr which is the relative permittivity. While most GPRs are depth resolution limited, bandwidth helps since lower frequencies allow radar energy to penetrate deeper into the soil and the higher frequencies provide the resolution needed to discriminate targets from clutter, especially at shallow depths.

1.2 Ground Penetrating Radar Data

GPR data is typically viewed and presented by A scans, B scans, and C scans. A scans of a GPR signal correspond to the GPR response of a single antenna element into the ground. Below is an example of an A scan at the location of a buried target where the GPR response is in arbitrary units (A.U.) on the y axis and the x axis corresponds to the time that the GPR signal penetrates into the ground and has been collected into time bins.

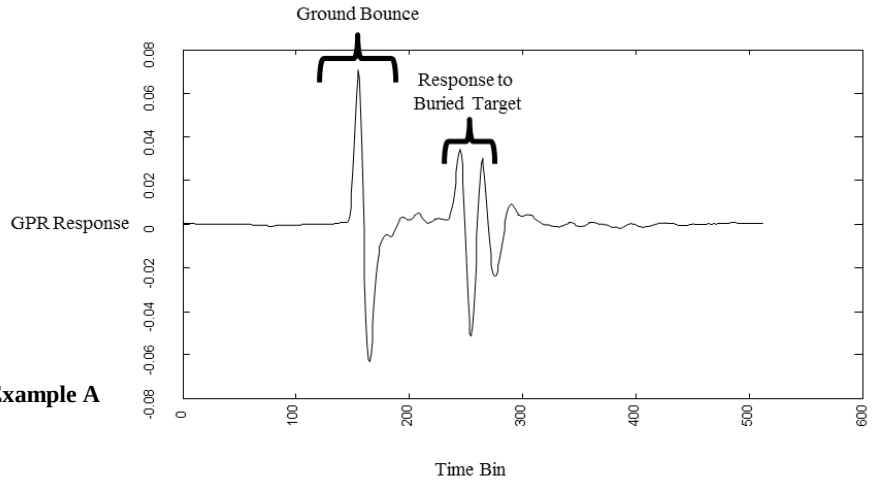

Figure 1.2: Example A scan

In the A scan, the radar wave travels through the air then through the air-ground interface which is the largest magnitude response and called the ground bounce. The radar wave then responds to the target at time bin 250. Time bins of the GPR signal can be thought of as depth into the ground.

The B scan is a two dimensional plot that shows the GPR response of adjacent A scans as the GPR collects data. To create a B scan, the A scan is rotated 90 degrees. Then adjacent A scans are plotted and the GPR response is mapped to a gray scale to create an image. B scan plots have units of time bins (time of GPR penetration into the ground) as the y axis and the number of scans over which the GPR data is collected as the x axis. This process is illustrated in the Figure below.

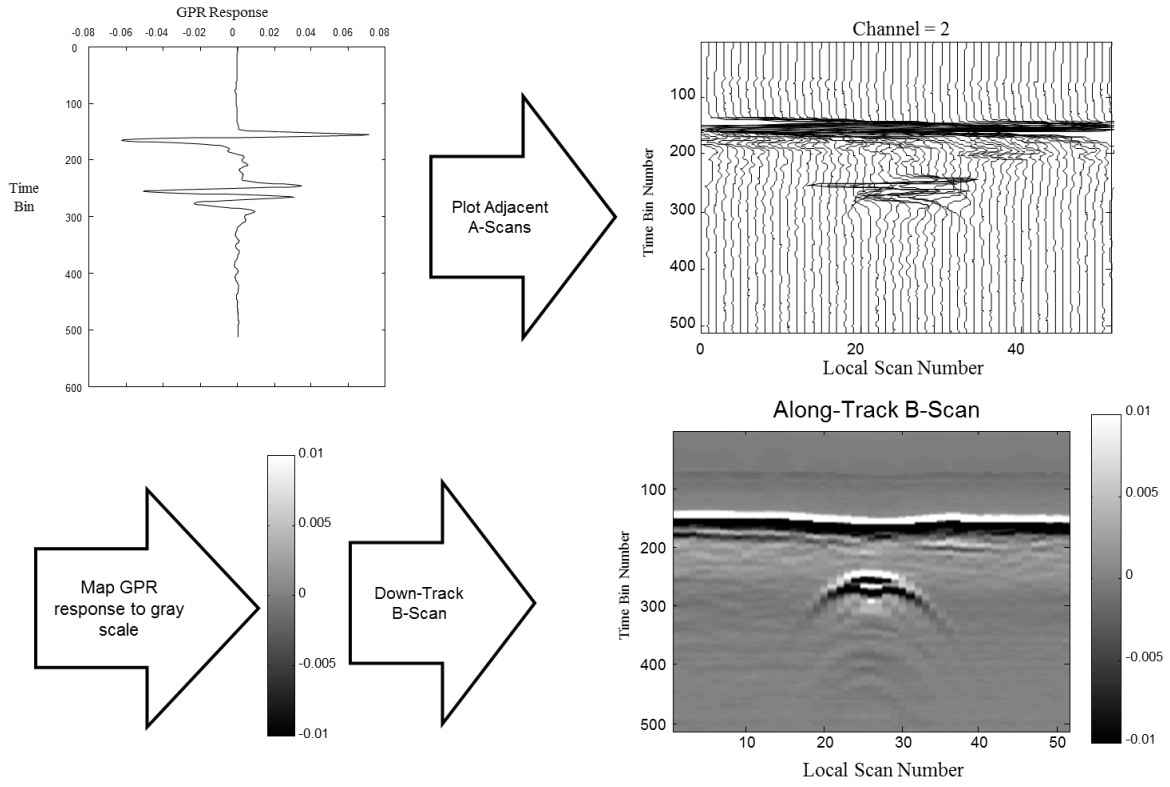

Figure 1.3: B scan Creation from GPR A scans

Targets manifest as hyperbolic curves in a B scan, which can be observed around the time bin location 250 in the plot. Also in the plot, the Ground Bounce or GPR response to the ground is observed as a very strong response around time bin 150. The gray scale color map limits were chosen by examining the range of GPR response values in the A scan and choosing values that would provide the best contrast for viewing the data. Here the range -0.01 to 0.01 was chosen since the ground bounce and target response saturates the color map at these limits.

A C scan is a two dimensional plot of the summed energy in each A scan. This plot provides a bird's eye view look at the GPR response over an area. When analyzing GPR data collected from a vehicle system, C scans have the dimensions of the number of channels by the number of scans since a vehicle GPR will have an antenna array with enough channels to cover the width of the road and collect data as the vehicle drives down the road. A C scan from a vehicle system with 51 channels, which covers about 3 meters, driving for 600 scans or about 30 meters is shown in Figure 1.4

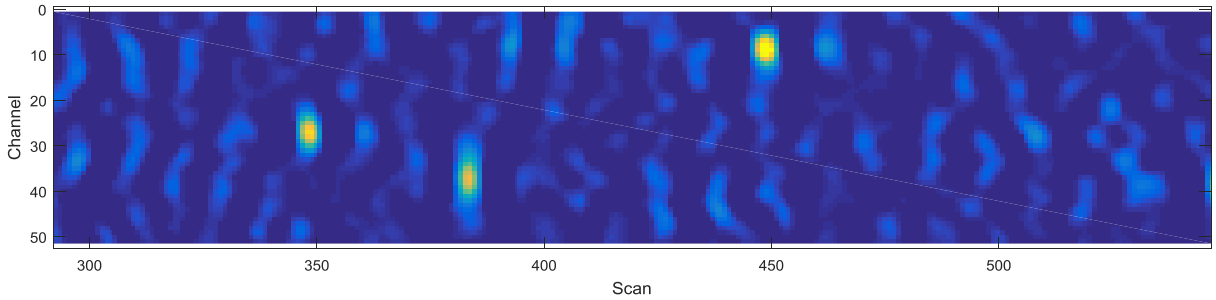

Figure 1.4: C scan from Vehicle Based GPR

Handheld detectors generally have one or two GPR antenna channels and are swung by an operator back and forth to cover the width of a data collection lane as they progress down the lane. An example of how a handheld detector is operated is shown in Figure 1.5

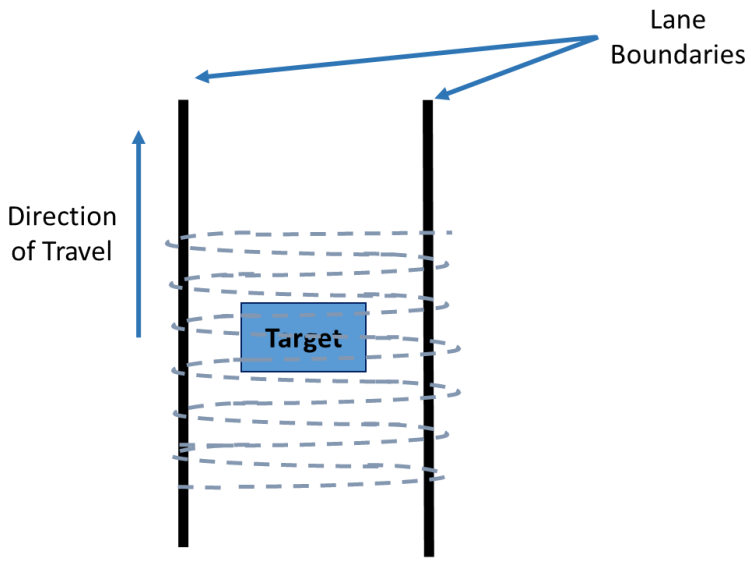

Figure 1.5: Handheld GPR Detector Operation

In Figure 1.5, the dotted line represents the path of the GPR handheld detector as the operator swings the detector back and forth to cover a 1.5 meter wide lane. This back and forth motion is overlapped as the operator moves down the lane to ensure full coverage of the lane. Due to the nature of how handheld detectors are used, the operator will swing back and forth over the target several times. In a fielded system the detector would give audio feedback to the operator to alert him to investigate this location further. The data analyzed in this thesis is from a data collection where the operator swung the detector up to, over, and past the target as shown in Figure 1.5 and then did a condensed set of scans over the target for additional data directly at the target location.

Current handheld detector systems do not have any GPS or position information and thus B scans and C scans are plotted as one continuous data stream of GPR response as a function of scan as the operator swings the detector back and forth across the lane and progressing down-track. Figure 1.6 shows an example of a B scan (left) and a C scan (right) of the GPR response from a handheld detector as an operator swings up to, over, and past a target.

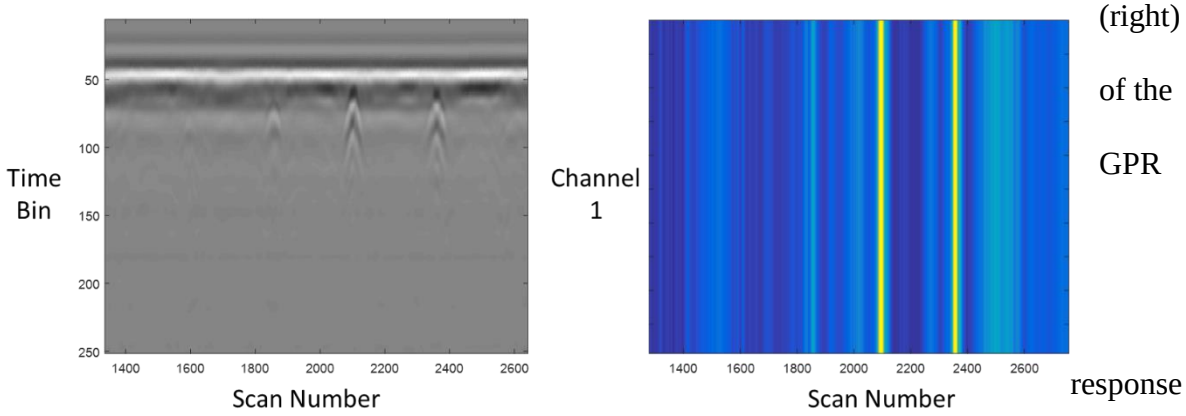

Figure 1.6: B scan and C scan From Handheld GPR

1.3 Motivation

Soldiers in theater face the threat of mines and improvised explosive devices (IEDs) which can be victim operated (VOIED) or radio controlled (RCIED). Anti-personnel, anti-tank mines, and victim operated IEDs have been used since World War II and are very effective. RCIEDs are a more modern occurrence and can be detonated by any device that sends a signal, such as a cell phone or remote control. The RCIED itself will be buried in the ground along or beside a road, just like VOIEDs, however the victim need not come into contact with the device for it to be detonated. In these cases someone will place the RCIED and wait for a victim to reach an appointed location near the RCIED at which point he/she would detonate the device.

The technology to detect these mines and IEDs has advanced since World War II, when handheld metal detectors were used. Metal detectors (MD) are capable of finding high metal targets but have difficulty detecting targets with low metal content, especially in the presence of metal clutter. The inability to distinguish between low metal targets and metallic clutter can result in a high false alarm rate, where the detector mistakenly identifies the metal clutter as a target. Though metal detectors are still used in some cases, a more advanced detection technique is required because current mines and IEDs that are used in theater may have little or no metal content. Thus handheld detectors evolved to couple a GPR with a MD to detect low metallic targets. A GPR only detector has a higher false alarm rate (FAR) since it will respond to natural clutter in the ground such as rocks, changes in soil density, or subsurface vegetation. By coupling the GPR and MD, the FAR will be lower than a GPR only detector, but some metal content is still required for the coupled system to respond so targets with very little or no metal can still

be missed. The next iteration of handheld detectors also had a GPR and MD, but ran in decoupled mode where each sensor operated independently to detect targets. The uncoupled system allows for detection of non-metal targets, but at the price of increasing the FAR due to GPR only alarms to natural and manmade clutter.

1.4 Problem Definition

The currently fielded handheld detector is a dual-sensor system that contains a metal detector and GPR for detecting mines and IEDs. Algorithms that use GPR response, metal detector response, or a fusion of both run in real-time and give the operator an audio tone if a suspected threat is present. The operator must sweep back and forth over an area to investigate when an audio alert is heard and attempt to mentally map out the response from a potential threat. There is no display for the operator to examine the response from either sensor and there is no position information available to create a local map to help the operator determine if multiple alerts are correlated to the same location or same threat.

The Dismounted Soldier Branch of the Countermine Division of the NVESD has begun the first phase of a long term program to fund development of the Next Generation Handheld Detector that improves upon the currently fielded system. This Next Generation Handheld must also be a dual-sensor system that utilizes the response of both the GPR and the metal detector to find threats. The system must also employ a position sensor to provide local position information, which will give not only more information to the operator, but also open the opportunity for more sophisticated algorithm development.

Data was collected with all three initial prototypes of these systems at a temperate test site in Virginia over a three week period in April and May of 2016. This work will focus on assessing the detection capability of each sensor in an effort to baseline the system performance as two more iterations of each prototype will be delivered to NVESD over the next few years. These initial prototype systems do not have any algorithms implemented in real time, contain only a GPR sensor, and have intermittent local position data. This work will deal primarily with cleaning up the GPR data collected and implementing two metrics to calculate signal over background which will be used to assess each system's capability to detect various targets.

1.5 Previous Work

Significant progress in the field of mine and IED detection has been made since landmines were first introduced in World War II. Ground Penetrating Radar systems have had improvements in both hardware and software and are now used by militaries around the world in conflict zones as well as by civilians and Government organizations for humanitarian demining.

The Ksum metric applied to handheld GPR data in this thesis was applied to vehicle mounted GPR systems in [11]. This metric was applied to four different vehicle based GPR systems in the referenced work as a measure of signal over background. In this work, the Ksum will be utilized in a similar manner, but will be applied to data with no algorithms or any kind of processing applied. In the referenced work all systems had GPS information so that the data was tagged with accurate location information and it is

easy to determine when the sensor was collecting data over targets. The handheld detectors used for the data collection for this thesis were not outfitted with any type of GPS. Two of the four sensors had a stereo camera position sensor that yielded relative position information and the remaining sensors had a trigger that the operator would press when over the target. Thus in this thesis, the Ksum will be calculated using three different options for the background, each with varying levels of location information.

The scoring methodology used to assess the Ksum metric results and determine the performance of each handheld detector is described in Chapter 4. The outlined methodology defines how alarms, which are a list of potential threat locations, are classified as a detection of the target or as a false alarm by comparing the alarm location with the ground truth location. The same scoring methodology will be used to calculate the probability of detection and false alarm rate for all sensors so that performance can be compared.

1.6 Thesis Scope

The scope of this thesis is to utilize previously developed signal over background metrics on data collected with three prototype handheld GPR systems during a three week data collection. The results of applying these metrics will be used to create alarm files in two different ways. The first way utilizes position information along with each metric output to create a C scan of the GPR response of the system and applying a blobbing technique to create alarms. The second method, which does not utilize position information, simply applies a peak picking algorithm on the metric output to create

alarms. Both types of alarms will be matched to the known target locations to calculate probability of detection (Pd) and false alarm rate (FAR) for each system

It is not the intent of this thesis to develop algorithms for the handheld systems to be run in real time, but only to apply known metrics to data from these new prototype sensors to attain a measure of system performance.

1.7 Structure of Thesis

This research is intended to gain insight into the detection capability of the three Next Generation Handheld prototypes as a baseline of their respective potential. No algorithms run in real-time on any of the prototype systems, thus metrics that calculate signal response over targets to background will be applied to the data. These metrics will then be used to create C scan maps of GPR response at target locations and to create alarm files for scoring. Results will be presented for each system as a function of target type and depth.

Chapter 2 will describe the data collection that occurred in spring 2016. This section will include a general description of each system, the targets encountered during the collection, the procedure for collecting the data, and the quantity of data collected.

Chapter 3 will give details about the metric implemented onto the collected data, as well as describe the process used to filter out the operator feet from the data. The process for creating alarms or nominations for each metric will also be described.

Chapter 4 describes the analysis methodology for assessing system performance by comparing alarms on suspected threat locations to ground truth. The process to calculate probability of detection (Pd) and false alarm rate (FAR) is explained as well as

Receiver Operating Characteristic (ROC) curve generation to illustrate the performance tradeoff between Pd and FAR.

In Chapter 5, the performance results for each system will be presented as well as a comparison between the three systems. ROC curves will be shown to illustrate overall performance as well as performance against target type. The results will also be shown for each metric implemented both with and without the operator feet removed for comparison.

Chapter 6 will summarize work done on this thesis and describe the conclusions of this effort. Lessons learned and proposed future work will also be discussed in this section.

CHAPTER 2: DATA COLLECTION PLAN

2.1 Data Collection Objective

The work described in this thesis utilizes radar data collected by three prototype handheld mine and IED detection systems from three different contractors and the current US Army fielded system. This data was collected in April and May of 2016 at a temperate test range in Virginia.

The objective of the data collection event was to baseline the capability of the three prototype handheld detectors, which were acquired by NVESD Countermine, as compared to the US Army fielded handheld detector. This thesis is one of the deliverables from the data collection that will analyze the collected data, apply metrics, and assess performance against various target types.

The goal is to collect a balanced set of data such that, even with a limited set of operators, all detectors will encounter similar targets at similar depths under similar conditions so that direct comparisons can be made with A) later iterations of each vendor's capability upgrade with its original baseline offering at the onset of the Next-Gen handheld initiative, and B) with the currently fielded system that has been exhaustively baselined in prior Army testing.

Results can vary greatly from operator to operator. Therefore, data collected from a small number of operators cannot capture average expected performance. To get an estimate of the average expected performance, data must be collected in the field with a statistically significant number of soldier operators, which is beyond the scope of this data collection.

2.2 Performance Sampling Procedure

Each prototype system was operated by two Government operators (one expert, one former soldier) and one contractor operator from the system developer (experience levels vary). The numbers and types of data collection lanes, the number and types of detectors, and the number of operators all define the elements of the data collection matrix:

- **Equipment (4)**
    - System A
    - System B
    - System C
    - Currently Fielded System
- **Operators (3)**
    - Operator 1: Government Expert Operator
    - Operator 2: Government Former Solider
    - Operator 3: Vendor Operator
- **Data Collectors (3)**

A data collector was needed for every operator interrogating lanes. It was the responsibility of the data collectors to follow the operators to record the file names that correspond to each operator sweep over a particular target. The data collector will also record the date, time, operator, detector, and any meta-data and comments from the operator in a data collection sheet or data collection logging software provided by each vendor for the prototype systems.

The data collection matrix describes the order in which each operator used each detector. This high level matrix notionally illustrates that each operator utilized a detector for Period 1, which includes collecting data over all targets outlined in the Summary of Targets section. After the conclusion of Period 1, the operators switched detectors and proceeded to collect data over all targets in Period 2. This procedure will be repeated for Period 3.

Each period in the high level matrix corresponds to a one and a half day window to collect data over the thirty-eight target emplacements identified. There was extra time after the completion of each period, so data was collected over the secondary target list in Table 2.3

Thus, the data collection matrix outlines one week of data collection where all operators collect data with one vendor system. This matrix was executed for each vendor and so the data collection was executed over three weeks, with one week dedicated to data collection for each vendor system in conjunction with currently fielded system. Note that only the Government operators use the currently fielded system to prevent operator bias by the competing vendor operator.

Table 2.1: High Level Data Collection Matrix

Operator	Period 1	Period 2	Period 3

Government Expert	Fielded System	Next Gen HH Prototype	Collection with Additional Sensors
Government Former Soldier	Collection with Additional Sensors	Fielded System	Next Gen HH Prototype
Vendor Operator	Next Gen HH Prototype	Collection with Additional Sensors	Collection with Additional Sensors

2.3 System Descriptions

A single prototype system from three different vendors will be utilized for this data collection as well as a fielded production system. All systems are handheld systems and are meant to be swung by a human operator. The specifications for each system are summarized below.

- System A is a dual sensor system comprised of a pulsed GPR antenna and continuous wave metal detector. It is also outfitted with a stereo-vision camera that provides relative position information. During the data collection, information from all three sensors was saved for post-processing. This system required a laptop for data collection management, organization, and data storage.
- System B is a dual sensor system comprised of a stepped-frequency GPR and a continuous wave metal detector. It is also outfitted with a stereo-vision camera that provides relative position information. During this data collection, the metal detector was not functional and thus no metal detector data was collected. As the position sensor on this system worked intermittently, there is minimal relative position information for the GPR data. This system required a laptop for data collection management,

organization, and data storage for collections where the position sensor was operational. Otherwise, a handheld storage device was used for data collection management and data storage.

- System C is a dual sensor system comprised of a pulsed GPR antenna and continuous wave metal detector, however the metal detector was turned off for this data collection due to a data rights conflict. This system is outfitted with a trigger that the operator can press to indicate when the sensor is over the target and thus tag the GPR data over target locations. This system required a tablet for data collection management, organization, and data storage.
- The Fielded System is a dual sensor system comprised of a step frequency GPR and EMI coil. During the data collection information from both sensors was saved as well as all outputs from the algorithms running in real-time on the detector. A handheld storage device is used for data collection management and data storage.

2.4: Test Site Information

There are two areas at the temperate test site that contain handheld data collection lanes. For this data collection, both areas will be utilized so that operator interference is not an issue and in an effort to collect data in a range of soils. Although the overall soil composition may not be different between the areas since the base of all lanes is clay soil, local soil changes, such as layering or subsurface rocks, could be different from area to

area and moisture content could vary from area to area because some areas may dry out quicker than others after rainfall.

The two areas utilized for this data collection will be designated as X and Y.

- Area X contains four data collection lanes that are 25 meters long by 1.5 meters wide that are divided into twenty-five 1 meter long by 1.5 meters wide grids. Targets are standalone components that are center emplaced in each grid. There is grass and other vegetation on the lanes in Area X, which results in more subsurface clutter and the lanes drying more quickly after rainfall.
- Area Y contains twenty-six data collections lanes that are 25.5 meters long by 1.5 meters wide that are divided into seventeen grids that are 1.5 meters long by 1.5 meters wide. Targets are standalone components that are center emplaced in each grid. There is little vegetation on the lanes in Area Y and, as a result, the wet soil in this area took longer to dry after rainfall.

A total of thirty-eight targets of interest, described in section 2.5, were chosen throughout the lanes in areas X and Y for this data collection. Additional secondary targets were also identified in the lanes in areas X and Y that could be utilized if the data collection matrix is completed before the end of the allotted time.

2.5 Summary of Targets

For this data collection, targets of interest were chosen from various target categories. Most of the targets were chosen because they are tactically relevant threats

and difficult to detect. Data will be collected over a metal cased landmine since it has a strong GPR response and will used as a form of quality assurance during the subsequent analysis of the data.

The targets of interest for this data collection are: Low-Metal AP Mine, Metal AT Mine, Low-Metal AT Mine, Low-Metal Pressure Plate, and Non-Metal Main Charge (emplaced horizontally). Pressure Plates and Main Charges are components of an IED target scenario. Data will also be collected for wire in various orientations as a standalone target or part of an IED scenario. The low-metal AP mine is a small plastic cased anti-personnel landmine that contains a minimum amount of metal. The low-metal AT mine is also plastic cased with very little metal content but is a larger landmine since it is anti-tank. The low-metal pressure plate is made of wood with low metal contacts. The non-metal main charge is a larger target that is entirely plastic and emplaced laying on its side in the data for this collect.

There are examples of all chosen targets of interest in multiple lanes throughout all the data collection areas. The table below identifies the unique number of target emplacements at each depth utilized for this data collection.

Table 2.2: Target Information for Data Collection

	Depth						
Target	A	B	C	D	E	F	G
Low-Metal AP Mine	4	4	0	0	0	0	0
Metal AT Mine	1	1	0	0	0	0	0
Low-Metal AT Mine	2	2	2	2	0	0	0
Low-Metal Pressure Plate	3	2	2	1	0	0	0
Non-Metal Main Charge	0	0	1	0	2	2	3
Wire	2	2	0	0	0	0	0

The data collection matrix was completed with time to spare and additional targets were visited. These secondary targets for data collection are also examples of tactically relevant targets that are difficult to detect and are located in the data collection areas of the test site. The number of unique secondary targets at each depth are identified in Table 2.3.

Table 2.3: Secondary Target Information for Data Collection

	Depth							
Target	A	B	C	D	H	E	F	G
Metal AP Mine	5	4	1	0	0	0	0	0
Low-Metal AT Mine	3	2	3	2	1	1	0	0
Low-Metal Pressure Plate	6	1	4	1	0	0	0	0
Non-Metal Main Charge	0	0	2	0	4	3	3	2

The secondary targets of interest have similar attributes to the primary targets. The metal AP Mine is a small anti-personnel mine that has a metal ring around it. The low-metal AT mine is plastic cased. The low-metal pressure plate is made of wood with wire contacts and thus has very little metal content. The secondary non-metal main charge is entirely plastic, but is smaller than the non-metal main charge in the primary target set.

2.6 Data Collection Procedure

All operators will collect data over all instances of specified targets of interest with a designated detector. The data collection procedure for each detector is outlined below.

The operator will proceed to specified target location and perform a skyshot. A skyshot consists of lifting the detector up so that the GPR is facing the air and taking a measure of the background. A skyshot is usually used during data processing to subtract background noise and self-clutter from the radar data. Then the data collector records the date, time, operator name, lane, and target information. The data collector will record the pertinent information listed on a data sheet for the fielded system or via the data collection software running on either a tablet or laptop for each of the prototype detectors.

For each target, the operator will collect five separate data files which correspond to each of the five swings specified below.

1. Blank: The operator will collect data in an area of ground near target location that contains no targets and that will serve as a measure of the background. This could be done in the area between grids, which is free of targets, or in a nearby blank grid space. This swing method is the same as "Search", only performed over blank ground.
2. Search: The operator collects data while sweeping per the detectors normal interrogation method and listens for a target response. This swing originates at the beginning of the grid and culminates just past the target location in the grid cell.

3. Localize: The operator collects data by sweeping back and forth directly over the target 10 times, which is center placed in the grid cell.
4. Side-Sweep Search: Step 2 is repeated with the operator perpendicular to the grid cell and normal down-track direction of travel. This sweep provides additional information for targets with asymmetrical footprints.
5. Side-Sweep Localize: Step 3 is repeated with the operator perpendicular to the grid cell and direction of travel.

The next generation handheld detectors will be outfitted with a position sensor that will be utilized during this collection to collect position information along with GPR data (as possible).

Each swing type will be saved as a separate data file and will be utilized in the data analysis. The Blank swing serves as a measure of the background of the soil near the target and is an important swing for calculating signal over background. The Search and Side-Sweep Search swings occur over the entire grid cell and give an opportunity for false alarms to be nominated by any implemented metrics that calculate signal over background. Calculating the false alarm rate (described in Chapter 4) is an important piece of understanding the system performance. During the Localize and Side-Sweep Localize sweeps, the operator swings the sensor back and forth directly over the target, which gives the greatest likelihood for detection. These swings are important to examine the system response for difficult to detect targets.

Figures 2.1 and 2.2 illustrate the swing types utilized in this data collection.

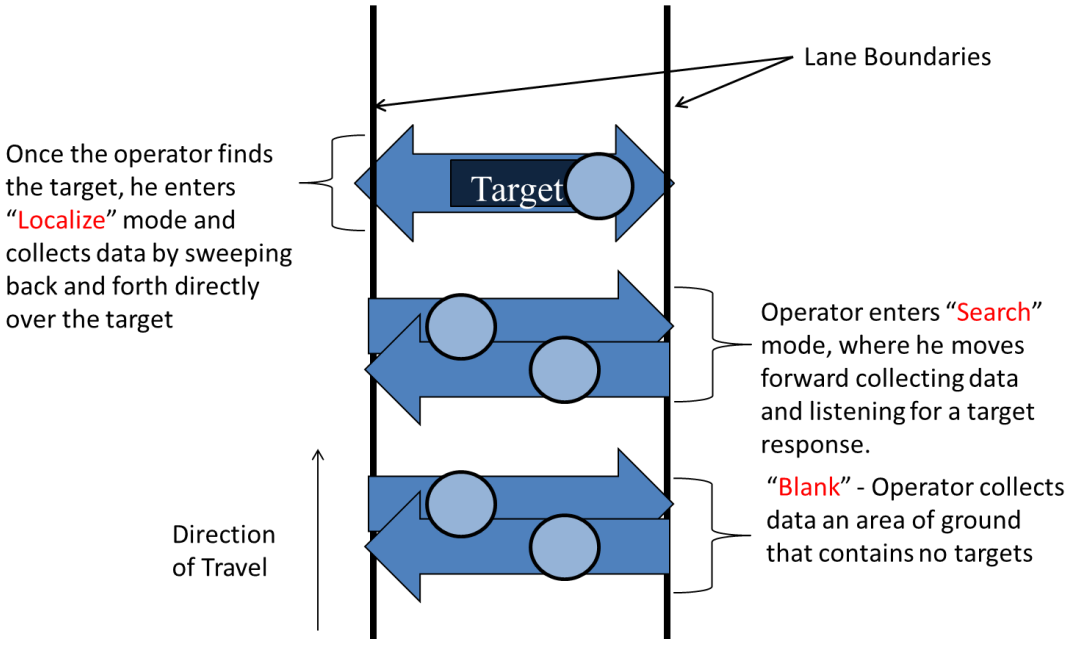

Figure 2.1: Illustration of Blank, Search, and Localize Swings for Data Collection

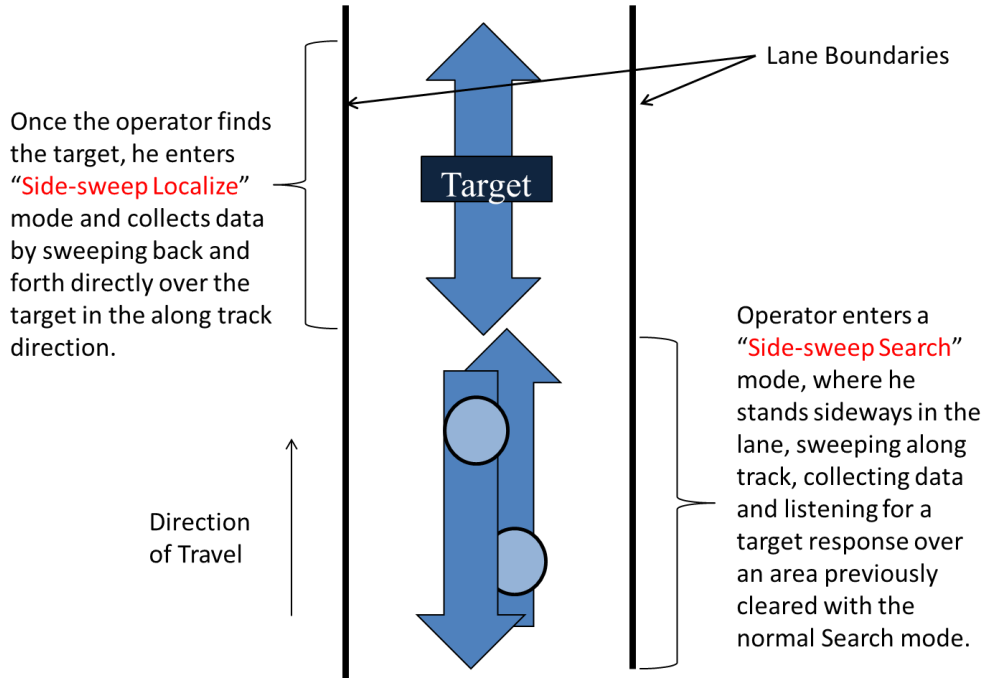

Figure 2.2: Illustration of Side-Sweep Search and Side-Sweep Localize Swings for Data Collection

The side-sweep search and localize swings are important for targets that are non-symmetrical, since the radar response can vary if the GPR is swung along or perpendicular to the length of the target.

2.7 Summary of Data Collected

The data that will be analyzed in this work was collected over a three week period at a temperate test site with three prototype sensors, each swung by three operators. One week was devoted to collecting data with each Next Generation Handheld system (A, B, and C) as well as with the currently fielded handheld system.

There was rainfall throughout the three weeks of data collection and thus, data was collected over the primary targets listed in Section 2.5 in both dry and wet conditions to attain a measure of how GPR performance for each system degrades in wet soil. If there was not enough time to collect data over the full set of primary targets in wet soil, targets with little or no metal content were prioritized since the response to these targets would degrade the most in wet soil conditions.

Table 2.4 summarizes how many targets were encountered by each system in wet and dry conditions as well as describing what position information is available for each system.

Table 2.4: Data Collection Summary

System	Primary Target Encounters	Secondary Target Encounters	Primary Target Encounters in Wet Soil	Position Information
A	150	53	90	Relative Position Information From Stereo Camera
B	66	86 (wet soil)	139	Small Set of Data With Relative Position Information From Stereo Camera, then Operator Trigger Information
C	150	30	106	Operator Trigger Information
Fielded System	297	164	248	Operator Trigger Information

During the first week of the data collection, System C and the fielded system were used to collect data over primary and secondary targets in both wet and dry soil. Both the fielded system and System C were outfitted with a trigger that the operator would press to indicate when the sensor is over the target. This trigger information is vital for scoring the results from any metric applied to System C's data since it provides context for the location of alarms. All three operators collected data over the set of 50 primary targets (150 encounters total) in dry conditions and a majority of the primary targets in wet conditions (106 encounters total).

Data was collected with System B and the fielded system during the second week of data collection. A small set of data was collected with System B before the stereo camera that provides relative position information began to have intermittent issues. The sensor was then adjusted so that a trigger could be used by the operator to indicate when the sensor is over the target. There was significant rainfall during the second week of the data collection and, as a result, most primary target encounters are in wet soil. Also, all secondary target encounters were in wet soil conditions.

The last week of the data collection was devoted to collecting data with System A and the fielded system. System A had a functioning stereo vision camera to provide relative position information for the entire collect. All three operators collected data over the set of 50 primary targets (150 encounters total) in dry conditions and a subset of the primary targets in wet conditions (90 encounters total).

CHAPTER 3: METRICS AND DATA PROCESSING

3.1 Ksum Description and Application

The metric for quantifying GPR response to targets that has been applied to the data collected for this work is called a Ksum. This metric is a measure of signal to clutter and thus the larger the magnitude of the GPR response to a target compared to the background, the larger the Ksum metric value will be. The Ksum metric is calculated by the equation below.

$$Ksum = \frac{1}{N}\sum_{i=1}^{N}\left[\frac{t_i - \mu_i}{\sigma_i}\right]^2$$

In the above equation, N_i is the total number of time bins in the A scan, t_i is the amplitude of the A scan at the i^{th} time bin, μ_i is the mean of a background A scan at the i^{th} time bin, and σ_i is the standard deviation of a background A scan at the i^{th} time bin.

The Ksum metric is calculated for each A scan. For each time bin the A scan value at that time bin is subtracted by the mean of the corresponding time bin in a collection of background A scans. The result is divided by the standard deviation of the collection of background A scans, squared, and then summed for all time bins in an A scan. This value is then divided by the number of time bins in the A scan to yield a single value for each A scan, which is the Ksum metric.

There are several options when determining which A scans to use as the background for calculating a Ksum. To calculate the most accurate Ksum the background should be chosen so that it is near the target location and thus contains the same

subsurface soil features that are present at the target location. The background should not contain any of the radar response to the target since some of the target response could be subtracted out which would result in a lower calculated Ksum metric for the target and may make the target undetectable.

As described the data collection procedures, operators collected a data file over blank ground before collecting data files for the various swings over a nearby target. This file could be used to calculate the mean and standard deviation of each time bin for the Ksum calculation as the file is known not to contain any responses to targets. However, there are disadvantages to using this file. One disadvantage is that it is not known how far away from the target location the blank file is collected and thus the ground subsurface structure could be different in the soil local to the target location than at the blank location.

The Ksum can be calculated for the down-track search, down-track localize, the across-track search, and the across-track localize sweeps using the blank data file as the background. The localize swings are the best opportunity for detecting the target since the operator is swinging the detector back and forth directly over the target. The search swings are more realistic for how the detector would be used in normal operation, as the operator is swinging over an entire area that contains a target with empty ground surrounding it. Thus, the Ksum results for the search swings are a better representation of the probability of detection and false alarm rate. An example of the Ksum results for a localize swing for all four detectors utilized in the data collection is shown in Figure 3.1.

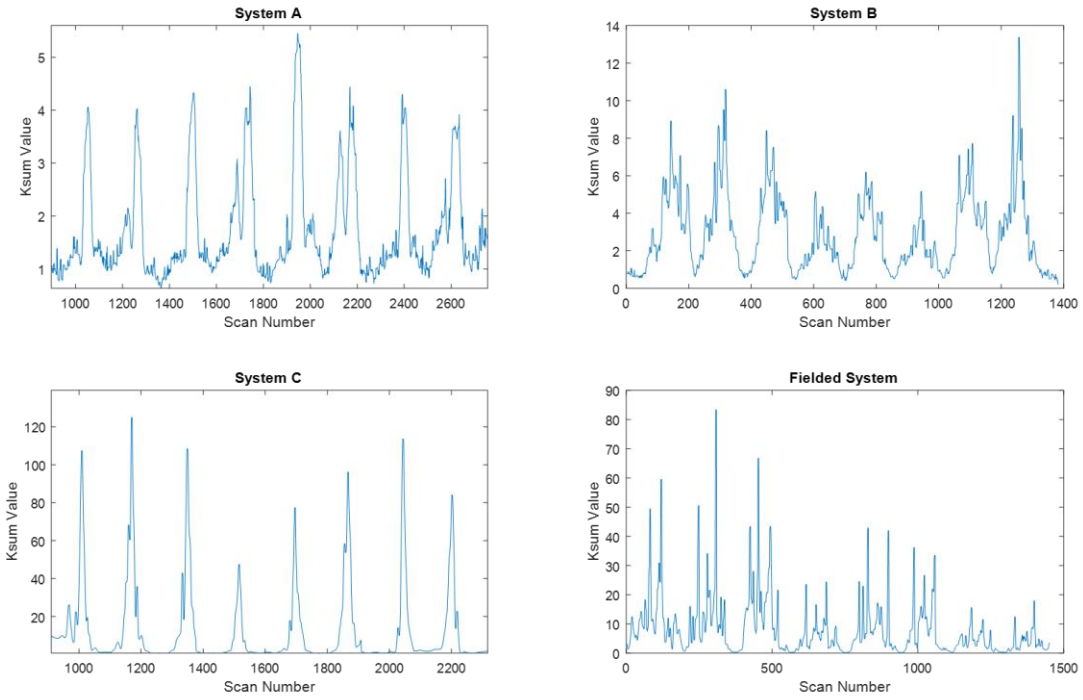

Figure 3.1: Ksum Results for All Systems Using Localize Swing

Figure 3.1 shows the Ksum result for the localize swing for each System for the metal AT landmine using the blank file as background. Recall that during the localize swing the operator knows the target location and sweeps back and forth over the target a set number of times. The Ksum results reflect this swing pattern: the operator swung each System back and forth over the target eight times. There is a spike in the Ksum plot for each system when the detector is over the target. This target is a large metal mine and thus the Ksum value corresponding to the target response is a large spike compared to the Ksum value to the ground around the target. The Ksum value is dimensionless and has no units. The magnitude of the Ksum value is different for each GPR and thus the threshold when creating alarms for scoring will be different for each system.

While the localize swings give the best opportunity to calculate the system response to the target, the search swings are useful since they provide the opportunity for the system to respond to the target while also having enough data surrounding the target to provide the opportunity for false alarms. The search data files contain GPR data from the operator swinging over an entire grid of a data collection lane where the target is emplaced in the center. Thus, the data within the grid and before the target is an accurate representation of the background and a reasonable choice for use in calculating the Ksum metric for a target.

To utilize the Search swing type data file and the ground surrounding the target as background for the Ksum calculation, one must know which A scans correspond to the background and which correspond to the GPR response due to the target. This information can be attained in three ways:

The first is to utilize relative position information attained from the stereo camera position sensor integrated onto the prototype system. Using the local position information for the Search data file and knowledge of the size of the grid cell and that the target is center emplaced in the grid cell, it is easy to identify which A scans correspond to background and which correspond to the target. A plot of the relative position information from System B as the operator sweeps back and forth over the target in Search mode is in Figure 3.2

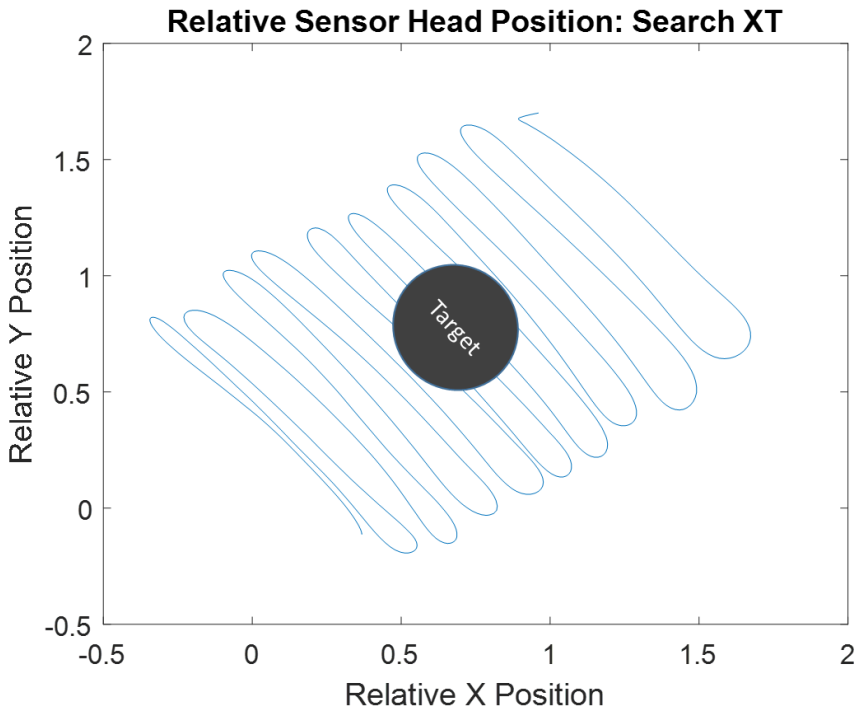

Figure 3.2: Relative Position Information for System B

The search sweep is of an entire grid of known size with the target centered in the grid. The target location and grid boundaries have been surveyed and thus the swing data can be pinned to Earth coordinates from the relative coordinates provided by the stereo camera position sensor. This pinning will require a rotation and a translation of the relative position data since the orientation of the sensor cannot be specified at startup and thus the position sensor picks an arbitrary heading when a new collection begins. The ability to set a heading when beginning a new collect will be implemented in a future firmware update to the position sensor.

A scans of the sweeps up to the target location can be used as the background for the Ksum calculation when relative position information is available. This method of Ksum calculation will be performed for a small subset of the data collected, because the position sensor was only implemented on two of the four systems and worked intermittently. This position sensor data can also be used to create Cscan maps of the Ksum response over a target location, which will be discussed in section 3.4

Only two of the four systems utilized during the data collection had a stereo camera position sensor. The other two systems had a trigger that the operator could press when he believed that he was swinging the detector over the target location. By using these marks in the data where the operator identified when the system is over the target for the A scans corresponding to the target location, the background could simply be a set number of A scans prior to the mark in the data. Figure 3.3 is a GPR B scan of an operator swinging up to the target, marking the target location in the data, and swinging past the target in Search mode.

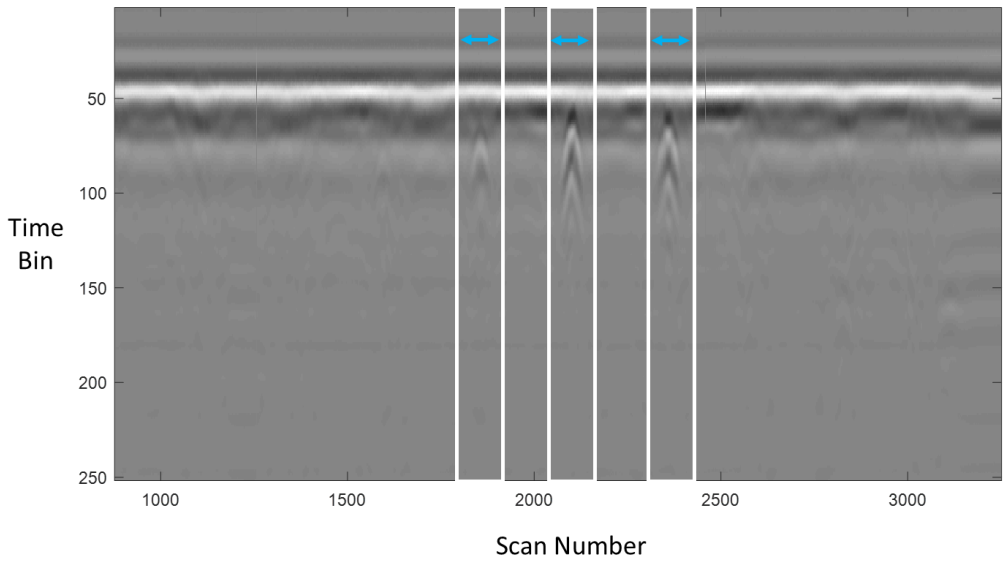

Figure 3.3: System C GPR B scan With Operator Trigger Information

The white lines in the figure above indicate when the operator begins and ends holding the trigger to indicate that the sensor is over the target location. The blue arrows indicate that the trigger is pressed for those scans. The packets prior to a trigger press could be utilized as the background for the Ksum calculation for the A scans during that respective trigger press.

This trigger information is available for search and localize swings with System C and the currently fielded system as well as System B when the position sensor had issues with overheating and could no longer be collected.

The third option for choosing the background for Ksum calculation for search sweeps assumes that no position information is known and thus there is no knowledge of

when the detector is over a target. In this case, the Search file will be used but a guard band window will be employed. As mentioned previously, the background A scans should not include any response to the target since it will be used to calculate the mean and standard deviation which is subtracted from the A scan over the target. To prevent this from happening when no location information is known, the background will be identified as a specific range of A scans prior to a guard band. The guard band can vary in size but is a specific range of A scans prior to the current one. Thus, if the system has begun to respond to a target the A scans immediately before the current one are not utilized in the Ksum calculation.

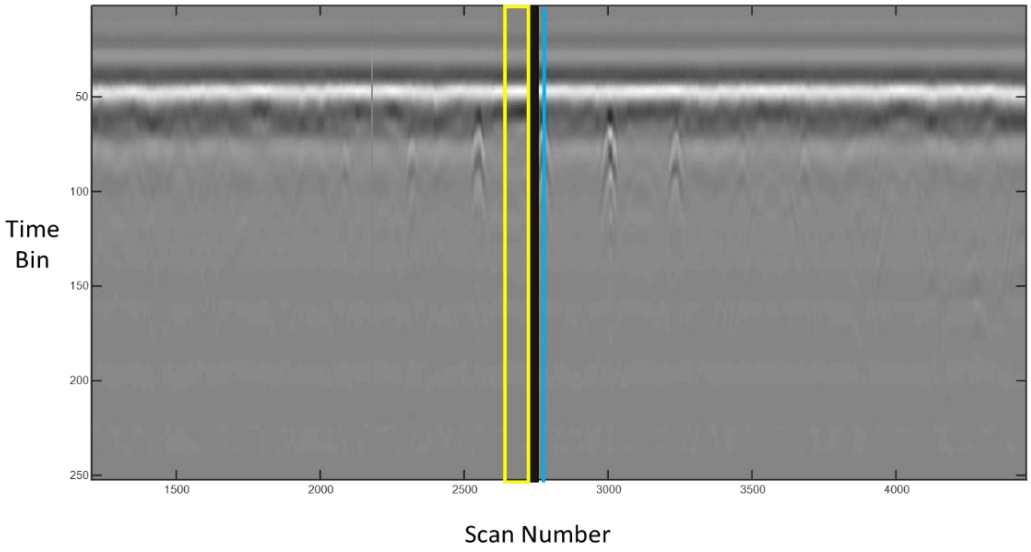

Figure 3.4: Guard band Background Implementation for System C

In Figure 3.4 the light blue line represents the A scan for which the Ksum is being calculated. The black area prior to the current A scan is the guard band, which contains A scans that will not be used for the background in the Ksum calculation. The yellow box bounds the A scans which will be used for the background when calculating the Ksum. For this work, the guard band will consist of 75 scans and the background A scans are the 100 A scans prior to the beginning of the guard band.

When creating alarms from the Ksum metric for scoring (discussed in Section 3.4), the Ksum result using the various background options will be used so that performance can be compared.

3.2 Required Preprocessing for System B

System A and System C collect GPR data in the time domain while System B collects GPR data in the frequency domain. Thus, the raw GPR data for System B are complex values. In order to visualize the GPR data in the usual A scan and B scan plots, the complex radar data must be transformed into the time domain. This transformation will standardize the format of the GPR data so that the data is real valued and has dimensions of the number of channels, number of time bins, and the number of scans and thus the Ksum metric described in section 3.1 can be applied uniformly to data from all systems for a fair comparison.

An example of the GPR response in the frequency domain for a shallow buried metal target for System B is in Figure 3.5.

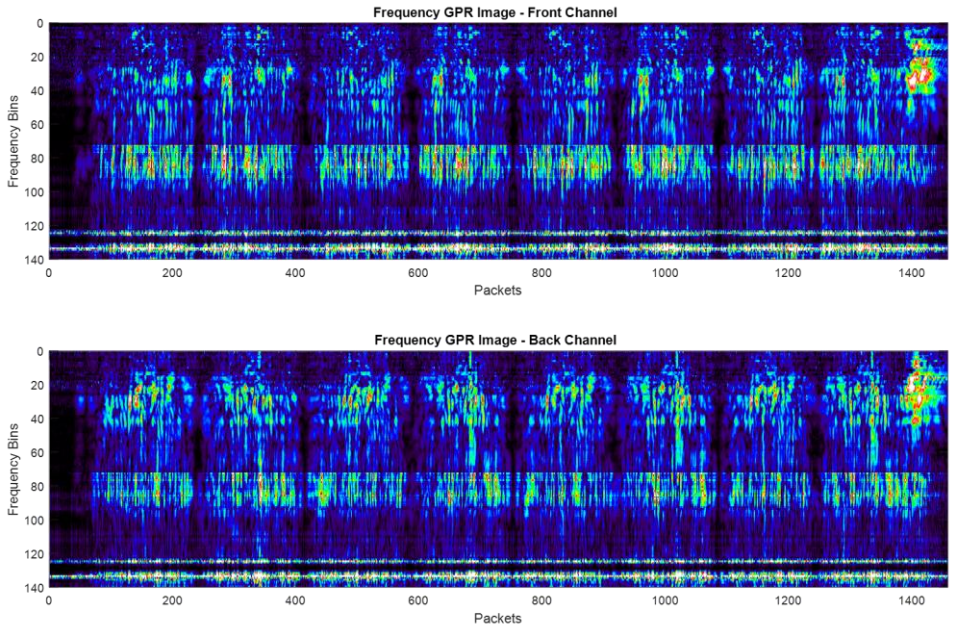

Figure 3.5: GPR Response in the Frequency Domain

System B has two receive antennas, commonly referred to as the Front and Back channel. The GPR response in the frequency domain for the Front channel is in the top plot and the response for the Back channel is in the bottom plot. The dimensions of each plot is the number of frequency bins, which is 140 for System B, by the number of data packets (or scans). The response to the target can be seen as the operator swings back and forth over the target.

To convert radar data from the frequency domain to the time domain, one simply needs to apply the inverse fast Fourier transform (IFFT) to the data. If this is performed blindly, the radar data will be in the time domain but will be complex valued. Since the radar data for Systems A and C are real valued and in the time domain, it is desired to have System B's radar data also be real valued in the time domain.

There are 140 frequencies for System B and the dimensions of the A scan is the magnitude of the GPR response by the number of frequencies. The number of time bins of the GPR in the time domain should be a factor of 2. To ensure that the GPR response after the IFFT is applied is real valued, the signal is modified in the frequency domain prior to the IFFT being applied. The length of the IFFT is chosen to be 512. This allows the signal to be doubled in size in the frequency domain prior to the IFFT and is a factor of 2. The GPR response in the frequency domain is zero padded, some prior to the signal and some after the signal so that is the length of IFFT/2 or 256. Then the signal is flipped and the complex conjugate of the signal is taken and added to the end of the zero padded signal. The final signal length is 512, the length of the IFFT. The GPR response in in the frequency domain is shown in the left plot and the modified GPR response where the signal has been flipped and complex conjugated is in the right plot of Figure 3.7.

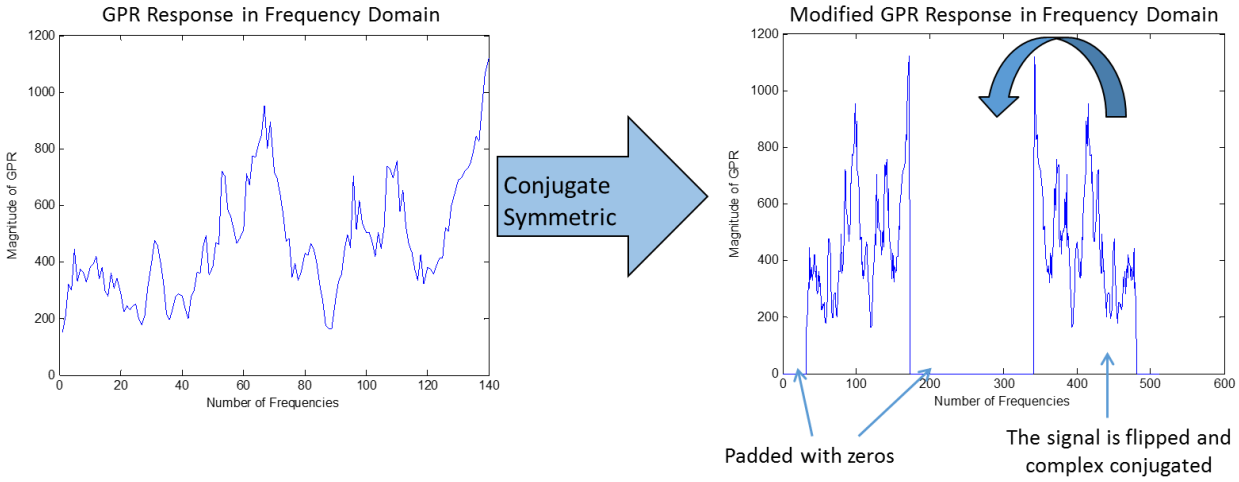

Figure 3.6: GPR Frequency Data Preparation for IFFT

Once the GPR data has been put into the format seen in the right plot of Figure 3.7, the IFFT is taken and the GPR data is now real valued and in the time domain. We can then plot the GPR B scan of the shallow buried metal target and examine the response to the target.

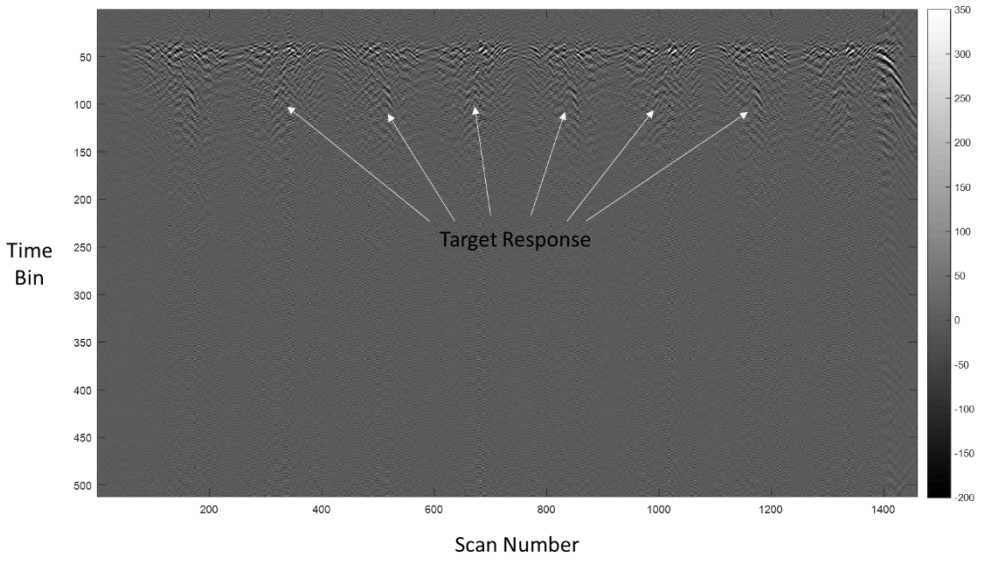

Figure 3.7: GPR Data after IFFT

3.3 Ksum C scan Creation

It is desired to utilize the position information from the sensor to create C scans where the Ksum metric plot is not a function of continuous scans, but plotted as a function of across-track and down-track. To create these C scan plots that have spatial information of the target response, the position information is used to characterize the swing over the target and the Ksum response is wrapped accordingly as the sensor moves back and forth across-track and progresses down-track. Plotting the C scan in this manner will allow spatial or geometric information from the target response to be used and could potentially reduce the number of false alarms.

The first step in creating Cscans with spatial information is to correct the orientation of the relative position information by applying a rotation. In Figure 3.8 below, the direction of travel is from the left side of the plot to the right side of the plot, but the beginning of the swing shows up in the lower right corner. The operators were instructed to collect search data files beginning in the lower left corner of the grid that contains the target and ending in the upper right corner of the grid, thus the relative position for the sensor in Figure 3.8 needs to be rotated by nearly 180 degrees or π.

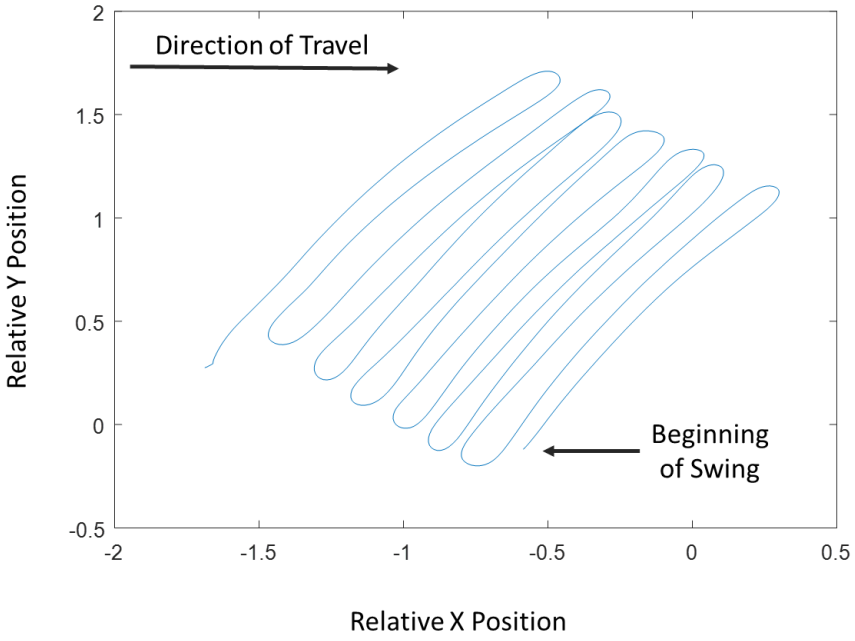

Figure 3.8: Relative Sensor Position Requiring Rotation

To rotate the position sensor data into the proper orientation, a rotation matrix was applied to the data as shown in the equation below:

$$\begin{bmatrix} x_r \\ y_r \end{bmatrix} = \begin{bmatrix} \cos(t) & -\sin(t) \\ \sin(t) & \cos(t) \end{bmatrix} * \begin{bmatrix} x \\ y \end{bmatrix}$$

In the equation, x and y are the original relative position coordinates, t is the angle in radians by which the coordinates need to be rotated, and x_r and y_r are the rotated relative position coordinates.

To calculate t, the rotation angle, the grid boundaries for the respective swing will be compared with the first swing information. Each operator was instructed to begin the search sweep in the lower left corner of the grid with respect to his orientation, thus different grid corners are used as the starting point for the down-track sweeps compared

to the across-track sweeps. A vector is created by subtracting the UTM coordinates (in Northing and Easting) for the lower left grid corner from the UTM coordinates for the lower right grid corner. This yields a vector in the direction of the operator's first swing. Then a peak picking algorithm finds the first change in direction of the operator swing in relative coordinates, which corresponds to the edge of the first sweep of the swing. A vector is then created by subtracting the relative position for the first scan of the swing from the relative position of the edge of the first swing. If the relative position data is properly rotated, then the vector from the lower left to lower right grid corner and the vector corresponding to the operator's first swing should be the same. Thus, the rotation angle t can be calculated by determining the angle between the two vectors using the following equation.

$$t = \cos^{-1}\left(\frac{\vec{u} \cdot \vec{v}}{\|\vec{u}\| \cdot \|\vec{v}\|}\right)$$

In the equation above, $\vec{u}$ and $\vec{v}$ are the vectors for the operators first swing and the lane coordinates, respectively. The angle between them is calculated by taking the inverse cosine of the dot product of the two vectors divided by the dot product of the length of the two vectors. The calculated angle t is in radians and can be used to calculate the rotation matrix to properly align the relative position of the operator's swing with the grid boundaries.

Since the stereo vision camera that provides relative position information selects a random starting point and heading, a translation and rotation must be applied to the relative position data to pin the relative position to UTM coordinates. First, the properly

rotated relative position information is pinned to the grid coordinates by adding the relative x position of the rotated data to the Easting value of the lower left grid corner and adding the relative y position of the rotated data to the Northing value of the lower left grid corner. The translation that must be applied is to subtract the relative x and y values of the first scan from all data points, which will yield a Northing and Easting UTM coordinate value for each scan in the search swing.

Figure 3.9 and 3.10 show examples of pinning the relative position information to UTM coordinates for a down-track and across-track search sweep. The left plot in each figure shows the original relative position information in blue and the rotated relative position information in red. The figure on the right shows the rotated and translated position data pinned to UTM coordinates in comparison to the surveyed grid corners and the target center, which are denoted by black circles.

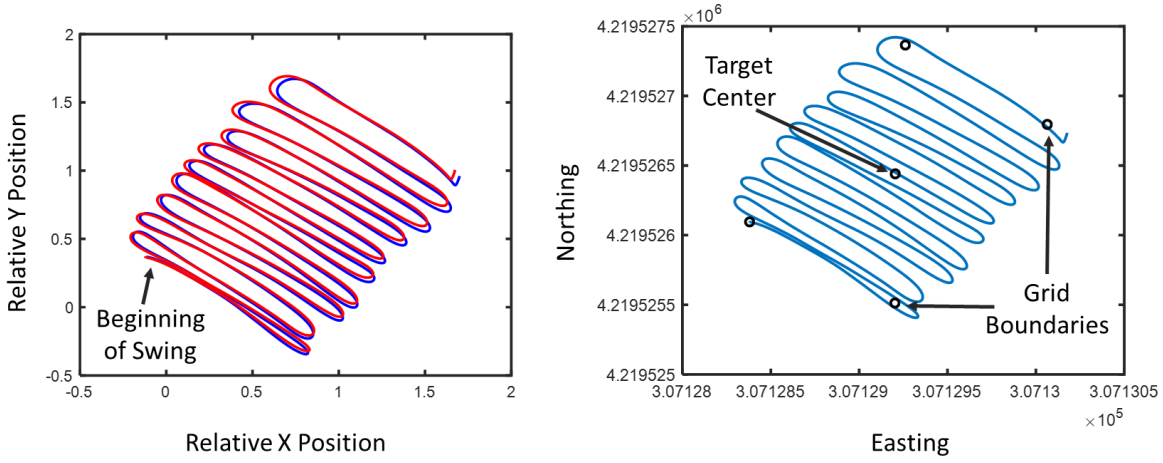

Figure 3.9: Position Data Pinned to UTM Coordinates for Across-track Search Sweep

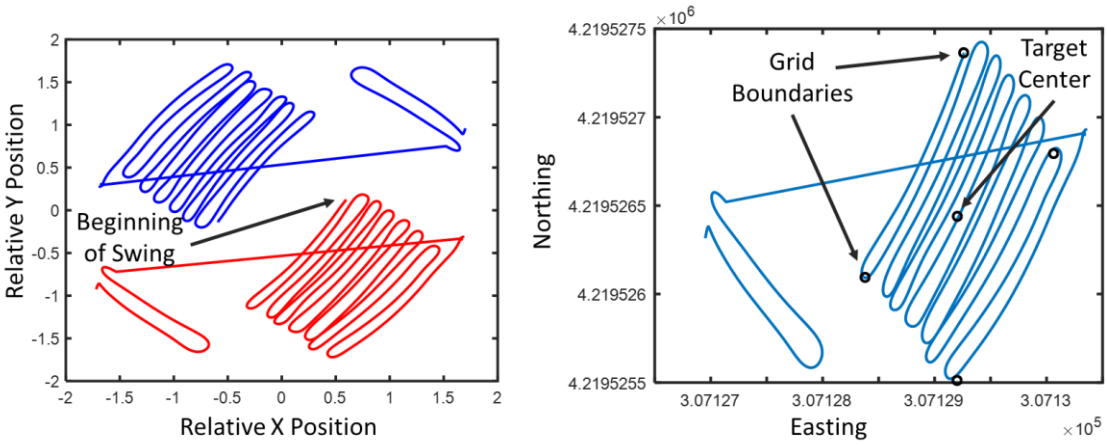

Figure 3.10: Position Data Pinned to UTM Coordinates for Down-track Search Sweep

The relative position information for the across-track search sweep shown in Figure 3.9 is an example of ideal relative position data. There are no jumps in position data and the relative position heading is accurate, so very little rotation is required. When the data is pinned to UTM coordinates, it is clear that the operator begins the search sweep on the lower left grid corner and ends on the upper right grid corner and that the target is centered in the grid and in the swing.

The down-track search sweep requires a large rotation, as seen in in the left plot in Figure 3.10 where the original position sensor data is plotted in blue and the rotated

position data is in red. The down-track search swing in not ideal but can still be utilized for this analysis since the jump in the position sensor data occurs at the end of the sweep. The relative position data at the beginning of the swing is accurate and can be used for pinning the data to UTM coordinates.

The position information is known for every data packet and thus the locations of edge of the sweep correspond to the scan number at which the Ksum should be wrapped to indicate that the sensor is at the edge of a swing and being moved down-track. Wrapping the Ksum value in this manner will create a matrix of data that corresponds to the sensor response as the operator sweeps across the lane, moves down-track and sweeps across the lane again. When this Ksum is plotted, it will have across-track and down-track dimensions similar to a C scan for a vehicle mounted GPR system. This process will be applied to the Ksum shown in Figure 3.11 to create the C scan shown in Figure 3.12.

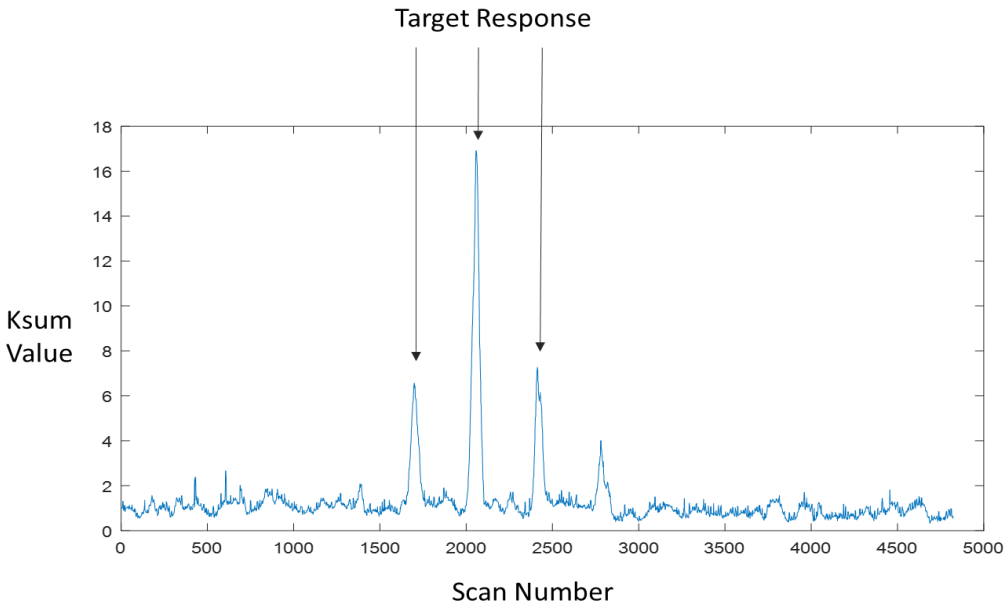

Figure 3.11: System A Ksum as a Function of Continuous Scans

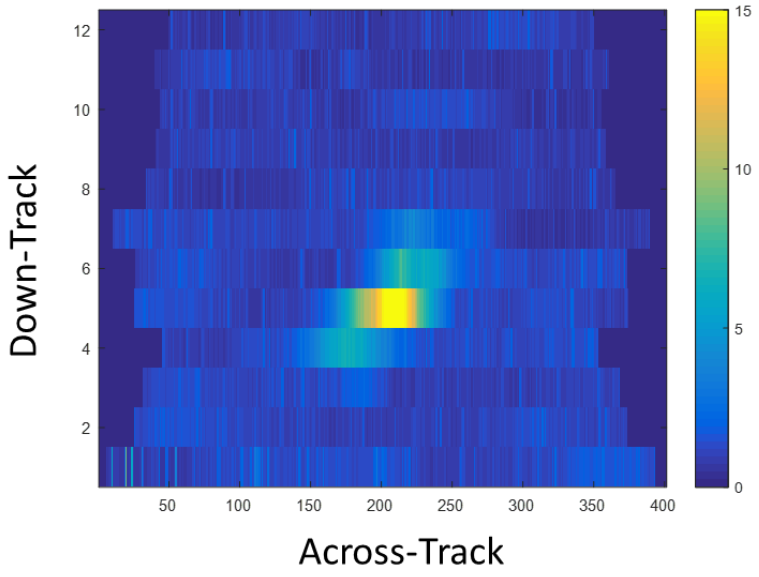

Figure 3.12: Ksum C scan

The Ksum as a function of continuous scans shown in Figure 3.11 is wrapped at the edge of the swing to create the Ksum C scan in Figure 3.12, which shows the Ksum values as a function of across-track and down-track as the operator swings the sensor over the grid. The response to the target is seen as the large yellow response in the center of the C scan since the target is center emplaced in the grid. This Ksum C scan will be used to create alarm files by using a blobbing technique to locate the center of the target response and identify the magnitude and location as an alarm. The magnitude of the response will be used as the confidence value for the alarm (discussed in Section 4.2).

3.4 Alarm File Generation

Two methods will be employed to create alarm files for scoring the Ksum metric. An alarm file consists of a unique alarm number, the location of the alarm (either in UTM coordinates if relative position information is available or the scan number of the alarm), and the magnitude of the Ksum metric at the alarm location which will be used as the confidence value of the alarm. The confidence value of an alarm is a measure of how confident the metric or algorithm is that the alarm is due to a target and not a false alarm. Details about the analysis methodology for scoring alarms to determine the probability of detection and false alarm rate can be found in Chapter 4.

The first method is to create alarms from the Ksum C scan using a blobbing technique. This technique finds the center of the blob of the target response and identifies the magnitude of the Ksum and the location as the alarm confidence value and location. This process will be done for all data files with good position sensor information.

For all other files that do not have good position sensor data, a peak picking algorithm will be used to identify the peaks and their locations of the Ksum metric. The locations of these peaks will be compared to trigger information (if available) for the sensor to determine if the alarm is a detection of a target or a false alarm. System B and the fielded system have trigger information for both the search and localize swings that will be used to determine if alarm locations are at the location of the target. System C has trigger information for the localize sweep only. For System C, the fact that targets are center emplaced in the grid will have to be utilized to determine if alarms during the search sweeps are due to targets or false alarms.

The peak picking algorithm used to create alarms from Ksum results in the absence of position information allows a threshold and peak width to be specified. These values will be chosen based on examining the Ksum results for each System, as the magnitude and width of Ksum peaks due to target response varies for each system. The table below identifies the threshold and minimum peak width (in scan number) that will be utilized when creating alarms for each system.

Table 3.1: Threshold and Minimum Peak Width for Alarm

System	Threshold	Minimum Peak Width
A	2	5
B	2	5
C	40	5
Fielded System	6	10

An example of the results of applying the peak picking algorithm to system C to create alarms can be seen in Figures 3.13 and 3.14.

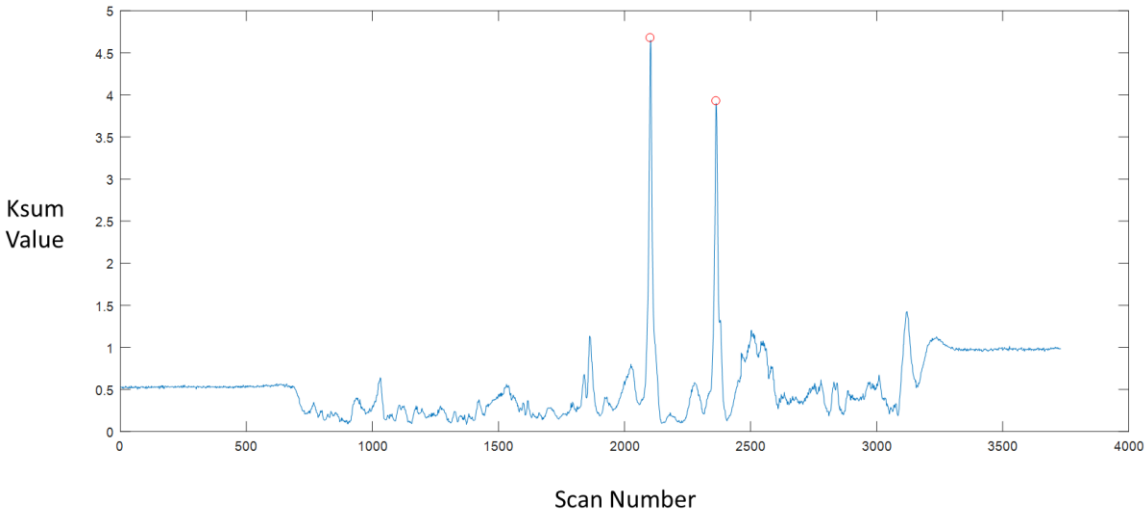

Figure 3.13: Ksum and Alarms for System C Search Sweep

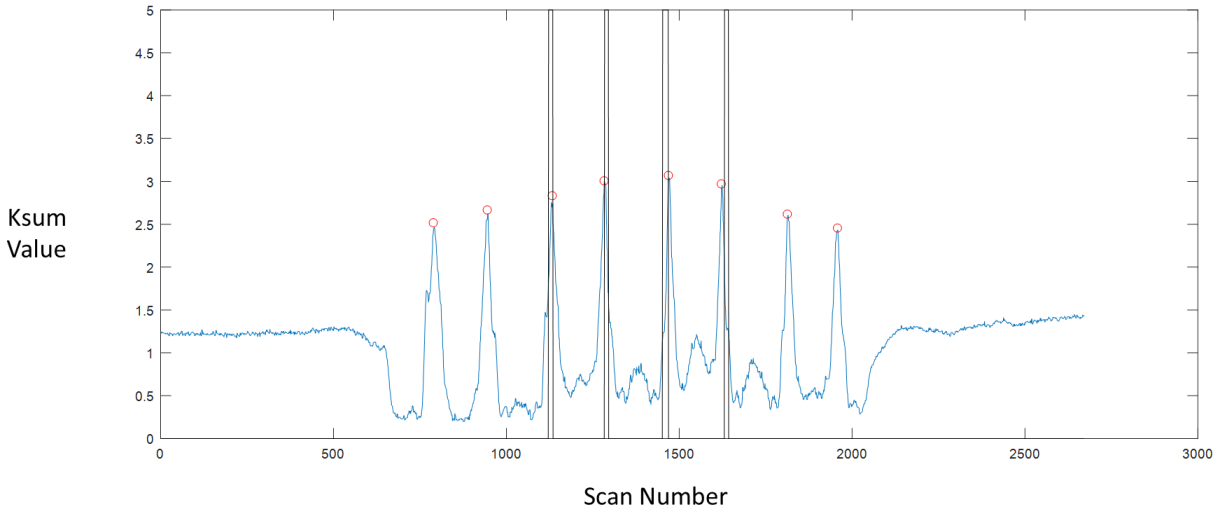

Figure 3.14: Ksum and Alarms for System C Localize Sweep with Trigger Information

In Figures 3.13 and 3.14, the Ksum metric output is plotted in blue and the location of alarms created by applying the peak picking algorithm are denoted by red circles. Figure 3.14 corresponds to a search sweep, where the operator sweeps up to and over the target, detecting the target twice. Figure 3.15 is a localize sweep where the operator swings back and forth over the target four times and the target is detected on all eight sweeps. The operator swept back and forth over the target once, then pressed the trigger while sweeping back and forth over the target twice, and then released the trigger and swept back and forth over the target again. The black lines in Figure 3.15 represent when the operator pressed the trigger to indicate that the sensor is over the target.

When creating the alarm file to be used for scoring, the Ksum will be calculated for each system for the localize and search sweeps in the down-track and across-track direction. Then, the peak peaking algorithm will identify the scan number and the value of the peak for all four swing types. The locations of the peaks in the localize sweeps will be compared with the trigger information and if a peak falls within the scans where the operator has identified that the sensor is over the target, the alarm will be assigned the UTM coordinates of the target. To identify false alarms, the search sweep will be utilized because it contains sweeps up to and past the location of the target. All targets are center emplaced in each grid and if we assume that the operator had a consistent swing speed, then we assume that any peaks in the Ksum metric that occur within the first and last quarter of the swing are due to false alarms. These false alarms will be assigned a UTM coordinate within the grid based on the scan number of the peak: all false alarms in the first quarter of the swing will be assigned coordinates after the beginning of the grid but

before the target location and all false alarms in the last quarter will be assigned coordinates after the target location but before the end of the grid. This method for creating alarms will be utilized for System C and the fielded system as well as data collected with System B when the position sensor stopped working since the data from these systems contains trigger information.

If good position sensor information is available and has been pinned to UTM coordinates, then all alarms in the search and localize files will be assigned their respective UTM coordinates when creating an alarm files for scoring. Unfortunately this was the case for a small subset of the data from System A and System B as the position sensors implemented on the prototype systems were early versions and worked reliably intermittently.

System A was not implemented with a trigger and when the position information from the stereo vision camera is bad or unreliable, the only background that can be used for calculating the Ksum is using the blank file or using the guardband background method described in Section 3.1. When creating the alarm file, the peak picking algorithm will identify the scan number of peaks in the search and localize files. Since there is no trigger information for System A, it is assumed that any peaks in the localize sweep file are due to the target and thus these peaks will result in alarms that have been assigned the UTM location of the target. Similar to Systems B, C, and the fielded system, any peaks that occur in the first or last quarter of the search sweep file will be assigned the UTM coordinates of a location in the grid either before or after the target location,

respectively. Again, this assumption is based on the target being center emplaced in the grid and the expectation that the operator swung the detector at a constant speed.

The alarms will be used to calculate performance of each system using the Ksum metric by the analysis methodology described in Chapter 4.

CHAPTER 4: ANALYSIS METHODOLOGY

4.1: Analysis Overview

The alarm files created from the metrics described in Chapter 3 will be utilized for calculating the performance measures used to assess each system. These measures are probability of detection (Pd) and false alarm rate (FAR). The process for calculating Pd and FAR will be explained as well as how to calculate the confidence levels for Pd and FAR, which are a measure of statistical accuracy. The Pd and FAR will then be plotted as a function of each other in a Receiver Operating Characteristic (ROC) curve to illustrate the tradeoff between the two measures for each system. This chapter will detail the analysis methodology used to score the alarms and calculate Pd and FAR as well as how ROC curves are created and should be interpreted.

4.2 Definitions of Probability of Detection and False Alarm Rate

The alarm files created by applying the metrics described in Chapter 3 to the GPR data from each system contain declarations of locations of potential targets. To calculate Pd and FAR, each of these alarm declarations are either matched to an emplaced target or not. Those declarations that are within a certain halo radius (R_{halo}) of the edge of the target is defined as a detection while the declarations that are not within the R_{halo} of the edge of a target is defined as a false alarm. A pictorial representation of these definitions is illustrated in Figure 4.1.

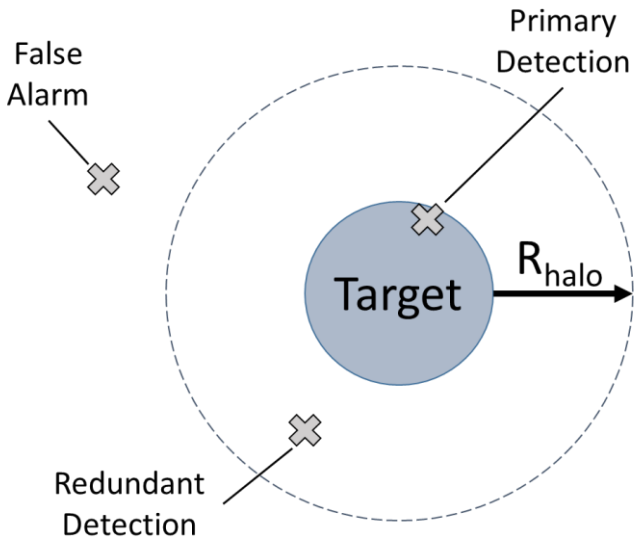

Figure 4.1: Definition of Declarations as Detections or False Alarms

In Figure 4.1, two alarm declarations fall within the halo radius from the edge of the target. In this case, the alarm closest to the target is identified as a primary detection and the alarm farther from the target is identified as a redundant detection. Redundant detections are not counted as false alarms but do not contribute to the Pd calculation since the target is already detected by the primary detection.

The type of scoring described in Figure 4.1 is scoring by distance, where the closest alarm to the target is counted as a primary detection of the target. If alarms are assigned a confidence value, scoring could be performed by confidence where the alarm within R_{halo} with the largest confidence value is identified as the primary detection. Scoring by confidence is illustrated in Figure 4.2.

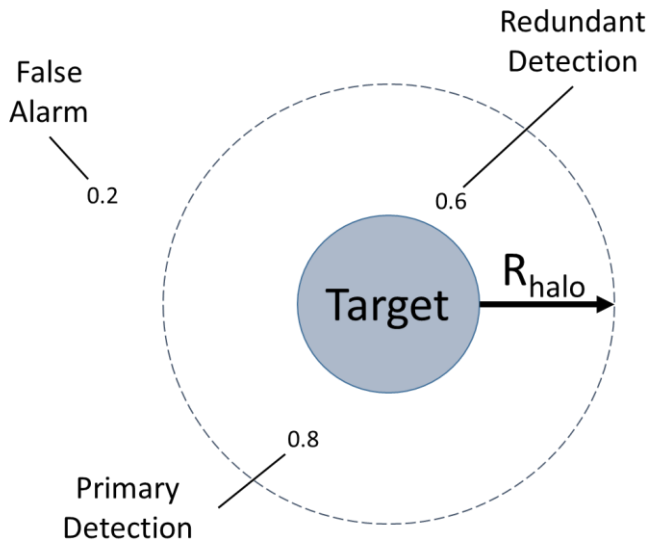

Figure 4.2: Scoring by Confidence

When scoring by confidence, the alarm with the highest confidence value is considered the primary detection while the closest alarm to the target is considered a redundant detection. The higher the confidence value, the more certain that the algorithm, metric, or operator is that the alarm is a declaration of a threat. Note that the false alarm has a lower confidence value than the two detections of the target. In an ideal GPR system, all alarms that are detections would have higher confidence values than false alarms, so that a system threshold could be set that would allow for maximum detections of targets with minimal false alarms.

Regardless of whether the alarms are scored by distance or confidence, the probability of detection and false alarm rate are calculated the same way. The probability of detection is the number of detected targets divided by the number of targets encountered, described in the equation below:

$$Pd = \frac{number\ of\ detected\ targets}{total\ number\ of\ encountered\ targets}$$

Probability of detection is a fraction and thus a Pd of 1 (or 100%) describes perfect detection. The false alarm rate is defined as the total number of false alarms divided by the covered area with the halo radius and target radius for each target subtracted. FAR is defined by the equation:

$$FAR = \frac{number\ of\ false\ alarms}{lane\ area - (target\ area + halo\ area)}$$

Probability of detection can be computed for all targets as well as by target type or target depth. It is important to compute the uncertainty on Pd and FAR calculations, especially if the results will be compared across different systems. These are defined as the ninety percent confidence level uncertainties on the Pd measurement and are calculated in MATLAB assuming a binomial distribution according to statistics laid out in [5]. The lower bound error is the value for Pd that would result in the measured Pd (or more) with a 5% probability and the upper bound error is the value for Pd that would yield the measured Pd (or less) with a 5% probability. These uncertainties are a function of the number of targets encountered, and thus the larger the number of encounters the greater statistical certainty in the resulting Pd and FAR calculations.

Table 4.1: 90% Confidence Levels for 0.50 Pd

Number of Targets	90% Confidence Level at Pd = 0.5	
	lo (%)	hi (%)
2	2.5	97.5
10	22.2	77.8
50	37.6	62.3
100	41.4	58.6

Table 4.1 shows how important it is to have a large sample size of targets, else the uncertainty in Pd can be large. For example, if performance against a particular target is calculated and there are only ten of these targets then the uncertainty in a Pd of 0.5 is ±27.8%. To attain results that have a small statistical uncertainty so that comparisons between systems can be made, it is vital to collect data over a large number of targets. This large sample size of targets for a data collection can become a resource issue because it will take a long test period to collect so much data. It is also a burden for test sites to manage a large sample size of targets given that each site has a limited amount of real estate and manpower is required to emplace, move, and maintain targets.

To calculate the uncertainty in FAR, the standard deviation in the number of false alarms is the square root of the number of false alarms. To attain the 90% confidence level uncertainty the standard deviation is multiplied by 1.65, which is a range that contains 90% of the statistical uncertainty.

4.3 Receiver Operator Characteristic (ROC) Curve Generation

Receiver Operator Characteristic (ROC) curves can only be generated for alarms that contain a confidence value. Alarm files that do not contain confidence values must be scored by distance and a single Pd and FAR can be computed. As mentioned

previously, the higher the confidence value of an alarm, the more confident an algorithm, metric or operator is that the alarm is due to a threat. The process by which alarm files with confidence values associated with each alarm are scored to calculate Pd and FAR, which are plotted as a function of each other in a ROC curve is described below.

Chapter 3 describes the two metrics applied to handheld GPR data and the creation of alarm files for each metric. Each alarm in an alarm file should have a unique number, location information, and a confidence value. The confidence value for the alarms generated in Chapter 3 is the scalar value of each metric that generated the alarm. A sample alarm file is shown in Table 4.2

Table 4.2: Sample Alarm File

Alarm Number	Confidence Value	Alarm Location
1	0.75	x_1,y_1
2	0.03	x_2,y_2
3	0.18	x_3,y_3
4	0.49	x_4,y_4
5	0.54	x_5,y_5
6	0.33	x_6,y_6
7	0.89	x_7,y_7
8	0.22	x_8,y_8
9	0.39	x_9,y_9
10	0.15	x_{10},y_{10}

The alarm location information is compared to the location of targets, and each alarm will either be labeled as a detection or false alarm. The comparison of alarms and ground truth is called scoring. Ground truth files contain information for all targets within a surveyed lane and contain a unique target number, name, burial depth, and location for each target. A sample ground truth file is shown in Table 4.3.

Table 4.3: Sample Ground Truth File

Target Number	Type	Burial Depth (in)	Alarm Location
1	AP Mine	2	x_1,y_1
2	AT Mine	4	x_2,y_2
3	Main Charge	1	x_3,y_3
4	Pressure Plate	3	x_4,y_4
5	AP Mine	1	x_5,y_5

Figure 4.3 illustrates the process of scoring the alarms from the sample alarm file in Table 4.2 against the targets listed in the sample ground truth file in Table 4.3. In Figure 4.3, the five targets from the ground truth file are plotted with their Rhalo in a test lane. The locations of the ten alarms are also plotted and any alarms that lie within the halo of a target is a detection, while alarms outside target halos are false alarms. In this example, all five targets are detected and there are five false alarms.

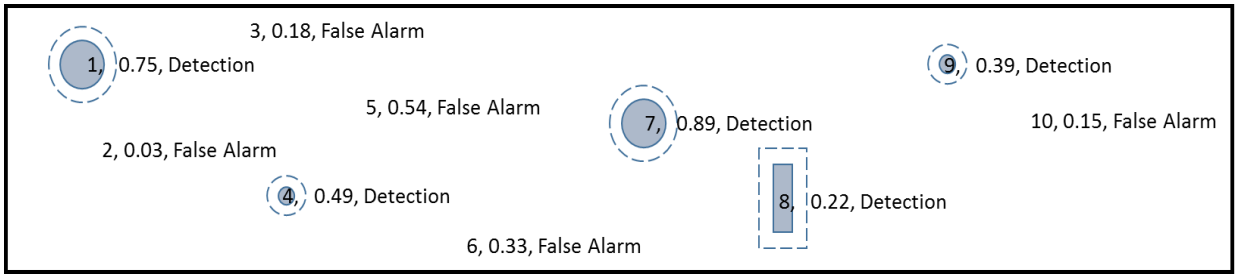

Figure 4.3: Scoring Results for Sample Alarm File

In Figure 4.3, alarms are numbered 1 through 10, have confidence values ranging from 0.03 to 0.89, and are labeled with the results of scoring (either a detection or false alarm). To illustrate the formation of a ROC curve, the alarms in the alarm file are sorted from highest to lowest. Once this is completed, a ROC curve can be generated by raising or lowering a threshold on the confidence values and determining the Pd and number of false alarms. Table 4.4 shows the result of ordering the alarm file from Table 4.2 by descending confidence value.

Table 4.4: Alarm File Ordered by Descending Confidence

Alarm Number	Confidence Value	Scoring Outcome
7	0.89	Detection
1	0.75	Detection
5	0.54	False Alarm
4	0.49	Detection
9	0.39	Detection
6	0.33	False Alarm
8	0.22	Detection
3	0.18	False Alarm
10	0.15	False Alarm
2	0.03	False Alarm

Once the alarm file is ordered by descending confidence value and each alarm has been assigned a scoring outcome, the ROC curve points can be identified. Table 4.5 lists the ROC curve information for each alarm in the alarm file, which will be used to plot the ROC curve.

Table 4.5: ROC Curve Information by Alarm

Alarm File			ROC Curve Points		
Alarm Number	Confidence Value	Scoring Outcome	Pd	# False Alarms	Point #
7	0.89	Detection	20%	0	2
1	0.75	Detection	40%	0	3
5	0.54	False Alarm	40%	1	4
4	0.49	Detection	60%	1	5
9	0.39	Detection	80%	1	6
6	0.33	False Alarm	80%	2	7
8	0.22	Detection	100%	2	8
3	0.18	False Alarm	100%	3	9
10	0.15	False Alarm	100%	4	10
2	0.03	False Alarm	100%	5	11

The Pd and number of false alarms are identified for each alarm in descending confidence value in Table 4.5. The first point on the ROC curve is the origin and would be the performance expected if a threshold was set so high that none of the alarms in the sample file are scored and there would be 0% Pd and 0 false alarms. Continuing down the table, the information for points 2 through 11 on the ROC curve is identified. The ROC curve is plotted in Figure 4.4.

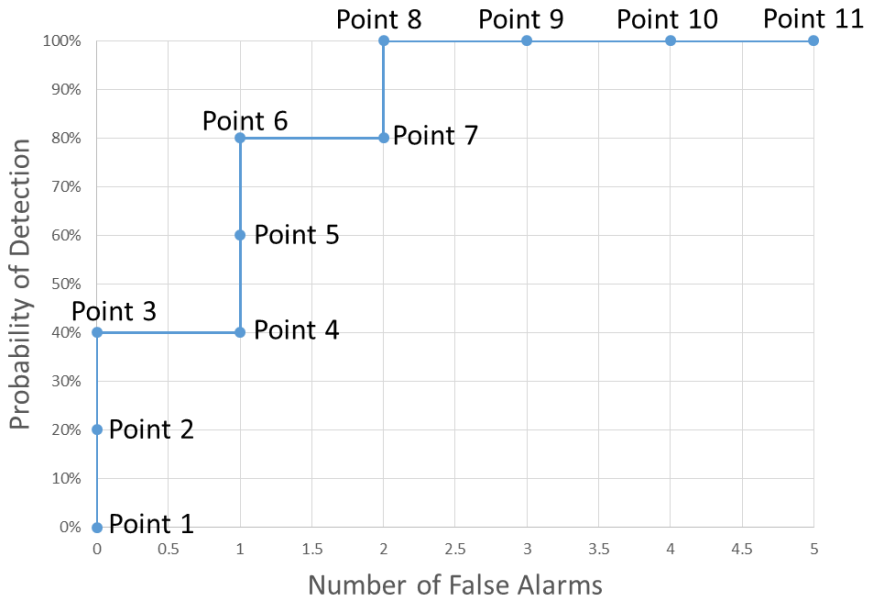

Figure 4.4: ROC Curve

The ROC curve in Figure 4.4 is the result of stepping through Table 4.5 and plotting the Pd and number of false alarms as the confidence value of the alarms decreases. Point 2 is the first calculated point in the ROC curve. At this point, one target out of five has been detected with no false alarms; thus at Point 2 the Pd is 20% and there are 0 false alarms. When stepping to Point 3 on the ROC curve, a second target is detected and thus the Pd at this point is 40% (two total detected targets out of five) with 0 false alarms. The next alarm is a false alarm and thus Point 4 on the ROC curve has a Pd of 40% and 1 false alarm. The next two alarms are detections and correspond to Points 5 and 6. By point 6 four out of the five targets have been detected with 1 false alarm, and so Point 6 has a Pd of 80% at 1 false alarm. The next alarm is a false alarm and so Point 7 has a Pd of 80% with 2 total false alarms. The next alarm is a detection of the final target and Point 8 has a Pd of 100% with 2 false alarms. The remaining three alarms are false alarms and accordingly points 9, 10, and 11 reflect an increasing number of false alarms with no further gains in Pd. By stepping down the table of alarms in descending confidence value, the ROC curve is mapped out from the lower left corner to the upper right corner.

CHAPTER 5: PERFORMANCE RESULTS

5.1 Results Overview

In Chapter 5 the performance results for each system will be discussed, where the Probability of Detection (Pd) and False Alarm Rate (FAR) will be presented in Receiver Operating Characteristic (ROC) curves. The analysis methodology to calculate Pd and FAR as well as how to interpret results on a ROC curve are explained in Chapter 4.

5.2 System A

System A had a stereo vision camera to provide relative position sensor information, though the prototype camera only worked intermittently during the data collection. Thus, most of the results shown for System A will be using the blank file as background, because there is no trigger information available for this system and the position sensor data was only available for a small subset of all data collected. For the small subset of data with position sensor information, Ksum C scans were created and a blobbing technique was used on the C scans to generate alarm files. A comparison of the C scan blobbing technique results will be compared with the peak picking algorithm results for this small data set.

The goal of the data collection was to attain a measure of performance of each prototype system compared to the currently fielded system. In Figure 5.1, the ROC curves are plotted for the results of scoring all operators and all targets for both systems. The dotted lines on the ROC curves are the error bars for the 90% confidence levels, which are a measure of the uncertainty and discussed in Chapter 4.

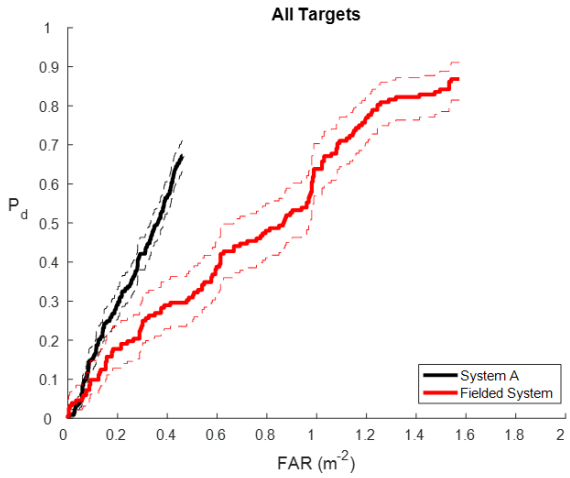

Figure 5.1: System A Performance Against All Targets Compared to the Fielded System

The ROC curves plotted in Figure 5.1 show the performance of System A and the currently fielded system against all targets utilized in the data collection. System A reaches a Pd of nearly 0.7 at a false alarm rate (FAR) of about 0.4 false alarms per square meter. While the currently fielded system has a higher overall Pd, this high Pd is not reached until a very high FAR.

A FAR greater than 0.2 false alarms per square meter is high and likely would limit the usefulness of the system as the operator will lose faith in the detector if most indicated threat locations are due to false alarms. The FAR for both systems could potentially be decreased with additional processing that uses additional information to classify alarms as targets or false alarms, as the Ksum metric simply finds the locations where there is a large signal compared to the background. In many GPR systems, an energy metric is used to identify potential threat locations and then a classification

algorithm runs on the identified threat locations and examines shape or spatial features of the GPR data to reduce the false alarm rate.

Figure 5.2 shows the performance of each system in the two different data collection areas used for this analysis: Area X and Area Y.

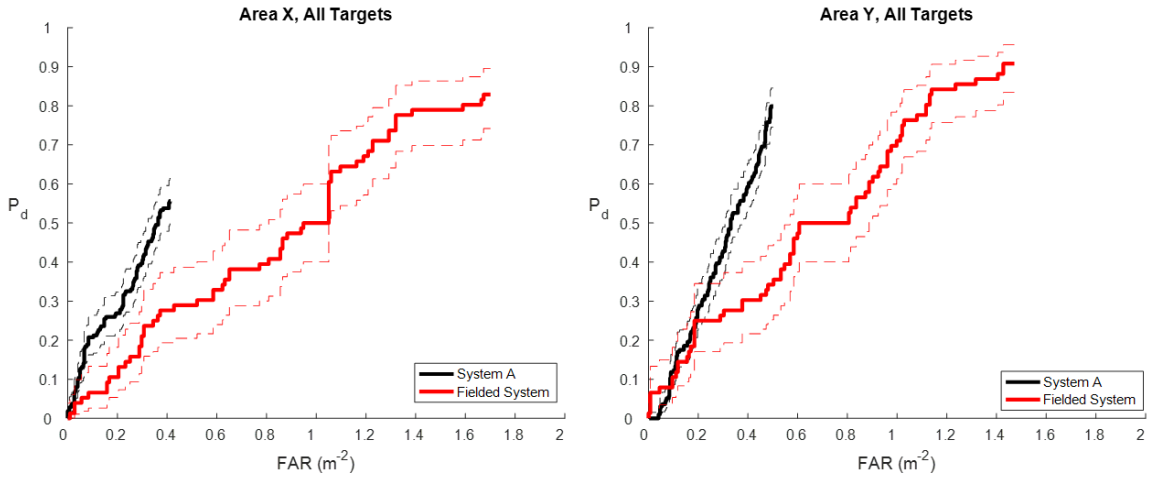

Figure 5.2: System A and Fielded System Performance by Data Collection Area

From Figure 5.2, it is clear that System A has a higher Pd in Area Y than in Area X, but there is no real location dependence on the performance of the currently fielded system. To better understand the performance differences between the two data collection areas, the confidence values of detections and false alarms can be examined. A plot of the distribution of confidence values for detections and false alarms can shed light on whether the performance difference is due to high confidence false alarms, low

confidence values for detections of certain targets, or a combination of both which would occur if the distributions for detections and false alarms overlapped.

Figure 5.3 shows the confidence value distributions for System A in Area X in the top plot and in Area Y on the bottom plot. The distributions are plotted as box plots with the 25 to 75 percentile measurements shown in yellow. For each distribution, the dots are individual detections or false alarms and the green line indicates the median confidence value. The y axis of this plot identifies the targets and their depth, and the x axis is the range of confidence values.

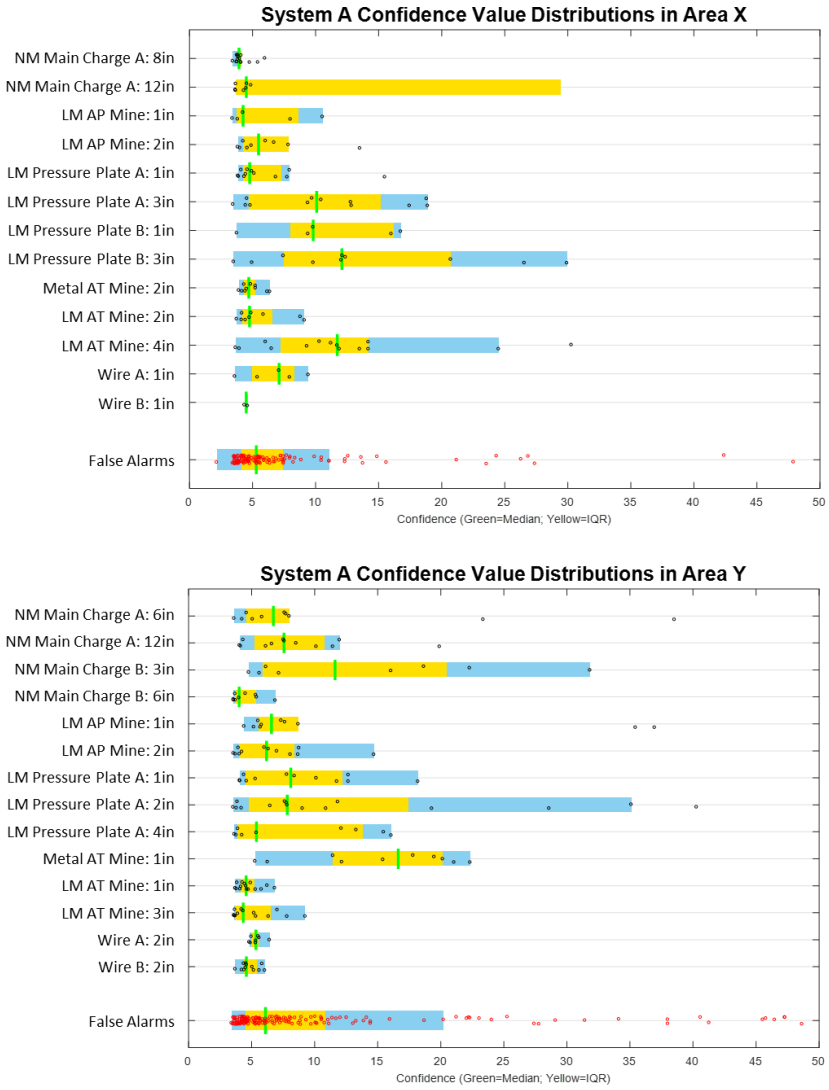

Figure 5.3: System A Confidence Value Distributions for Area X and Y

When comparing the confidence value distributions in the two data collection areas, Area Y has more detections and false alarms than Area X. This is also observed in the ROC curves for System A. In Figure 5.2, more Non-Metal Main Charges and Wire targets are detected in Area Y than in Area X and with higher confidence values than the detections in Area X. Confidence values are higher for detections of the Low-Metal AP

Mine at 2 inches and the Metal AT Mine in Area Y, but the detections of the Low-Metal AT Mines had higher confidence values in Area X. The median confidence value of the false alarm distributions is about the same in both data collection areas.

The ROC curves showed that performance of the fielded system is less dependent on the data collection area, but there are differences in performance when the confidence value distributions are examined for specific targets. The confidence value distributions for the fielded system by area are in Figure 5.4.

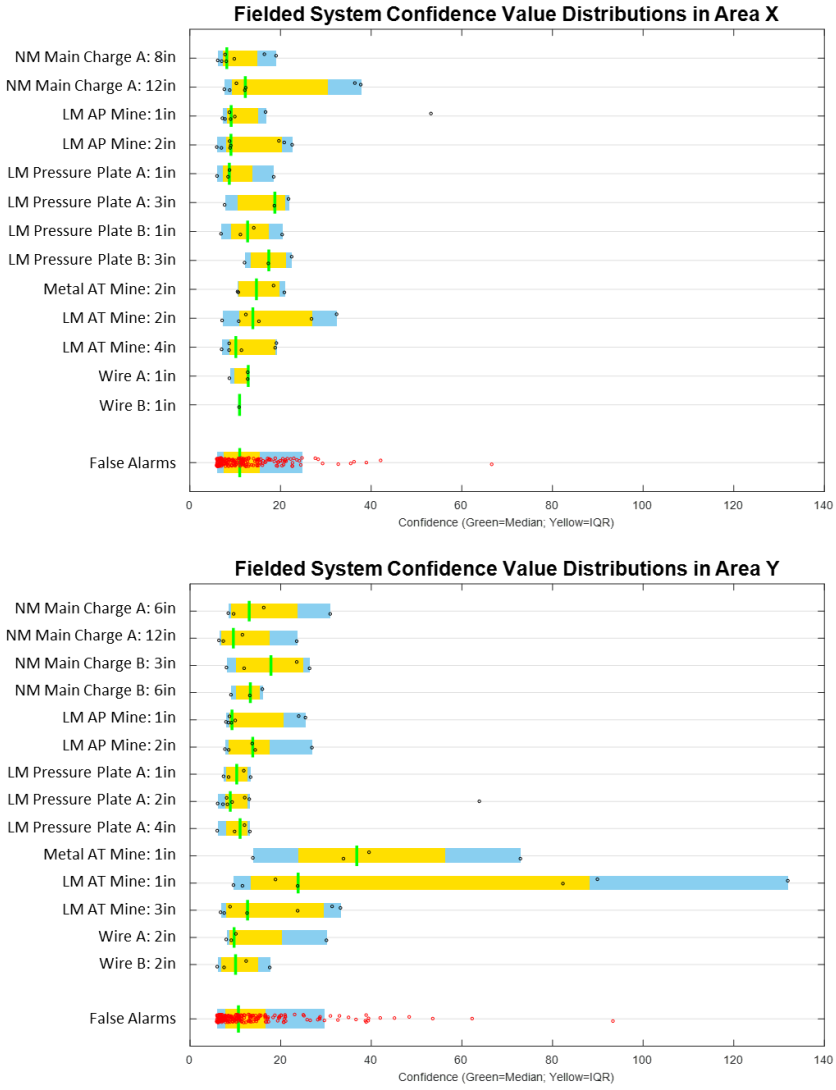

Figure 5.4: Fielded System Confidence Value Distributions for Area X and Y

The confidence values for detections of Metal AT Mines, Low-Metal AT Mines, and Non-Metal Main Charges at 12 inches are higher in Area Y than in Area X. A similar number of Low-Metal Pressure Plates were detected in both data collection areas, but the confidence values were higher for detections in Area X than in Area Y. More Wire targets were detected in Area Y than in Area X. There are more high confidence false

alarms in Area Y than in Area X, but the median confidence value of the false alarm distributions is the same for both data collection areas.

To further understand the performance of each system against the various target types, the ROC curves are plotted by target type for each system is in Figure 5.5.

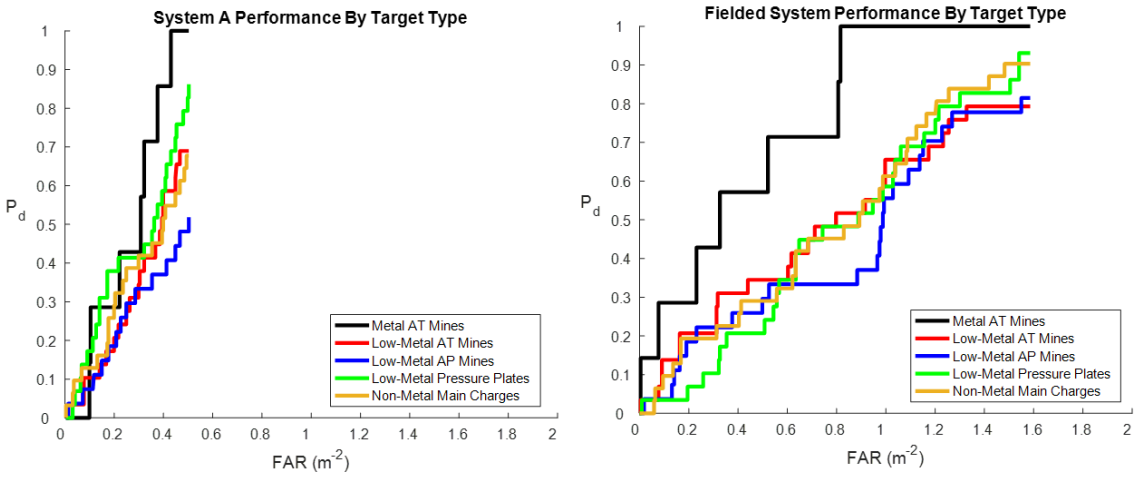

Figure 5.5: System A and Fielded System Performance by Target Type

In Figure 5.5, the performance for System A is plotted in the ROC curve plot on the left and the performance for the fielded system is plotted on the right. The performance is best for Metal AT Mines with both systems, which is intuitive since these targets are large and contain metal which improves the radar response. System A outperforms the currently fielded system for Low-Metal Pressure Plates, as they both detect a similar number of encounters, but System A does so at a smaller FAR. The Performance for Low-Metal AP Mines, Low-Metal AT Mine, and Non-Metal Main

Charges is about the same for each system respectively. The currently fielded system detects more of these targets overall, but at a FAR that is triple that of System A.

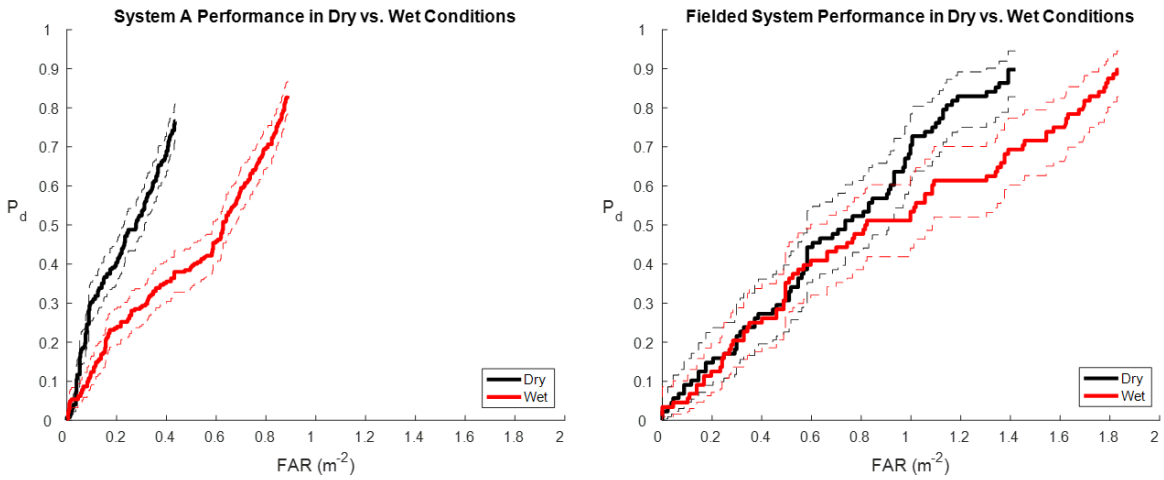

Figure 5.6: System A and Fielded System Performance in Dry and Wet Conditions

There was several inches of rainfall during the week of data collection with System A. Figure 5.6 above shows the performance of each system against the primary set of targets in wet and dry conditions. The Pd for System A is about 0.15 higher during wet conditions, but at nearly double the false alarm rate observed during dry conditions. Performance for the fielded system is about the same in wet and dry conditions, though the false alarm rate is higher in wet conditions.

Figure 5.7 contains the confidence value distributions for System A in dry and wet conditions.

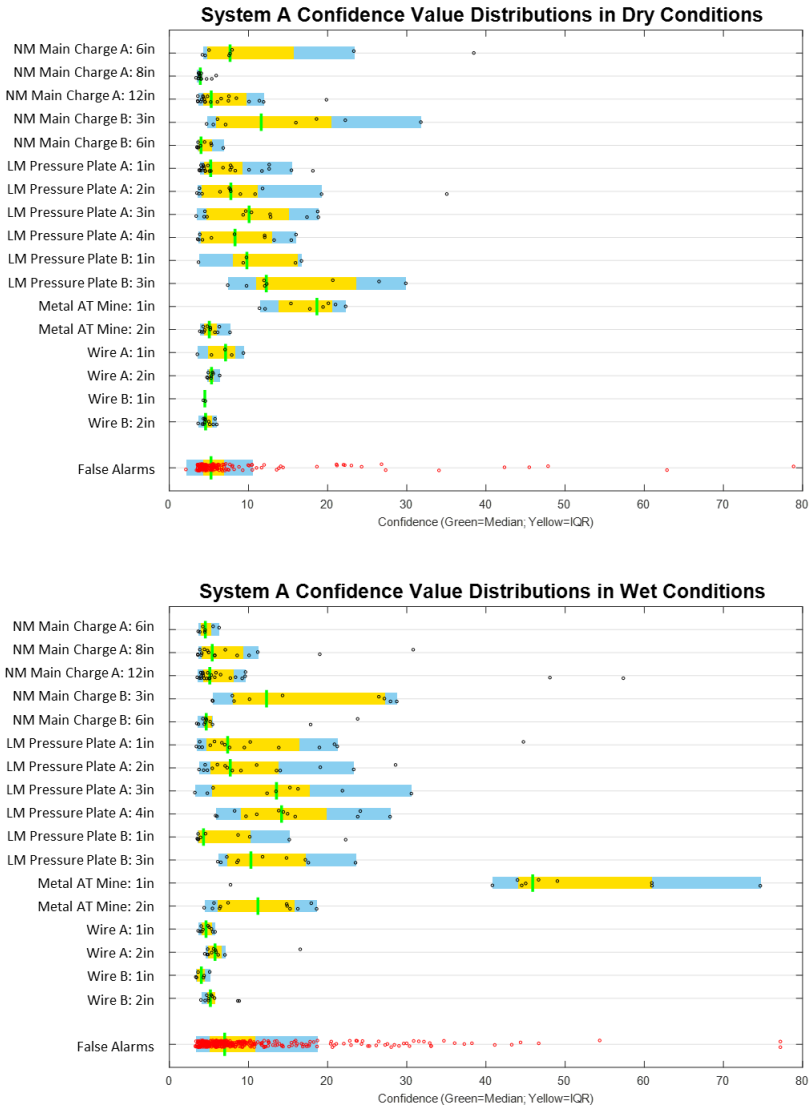

Figure 5.7: System A Confidence Value Distributions in Dry and Wet Conditions

The confidence values for detections of Non-Metal Main Charges at 6 and 12 inches and Wire targets at 1 inch are lower in wet conditions than in dry conditions. Detections of the Metal AT Mine and Low-Metal Pressure Plates had higher confidence values in wet conditions than dry conditions. The confidence value distribution for false

alarms is wider in wet conditions and there are more high confidence false alarms than in dry conditions.

Figure 5.8 contains the confidence value distributions for the fielded system in wet and dry conditions.

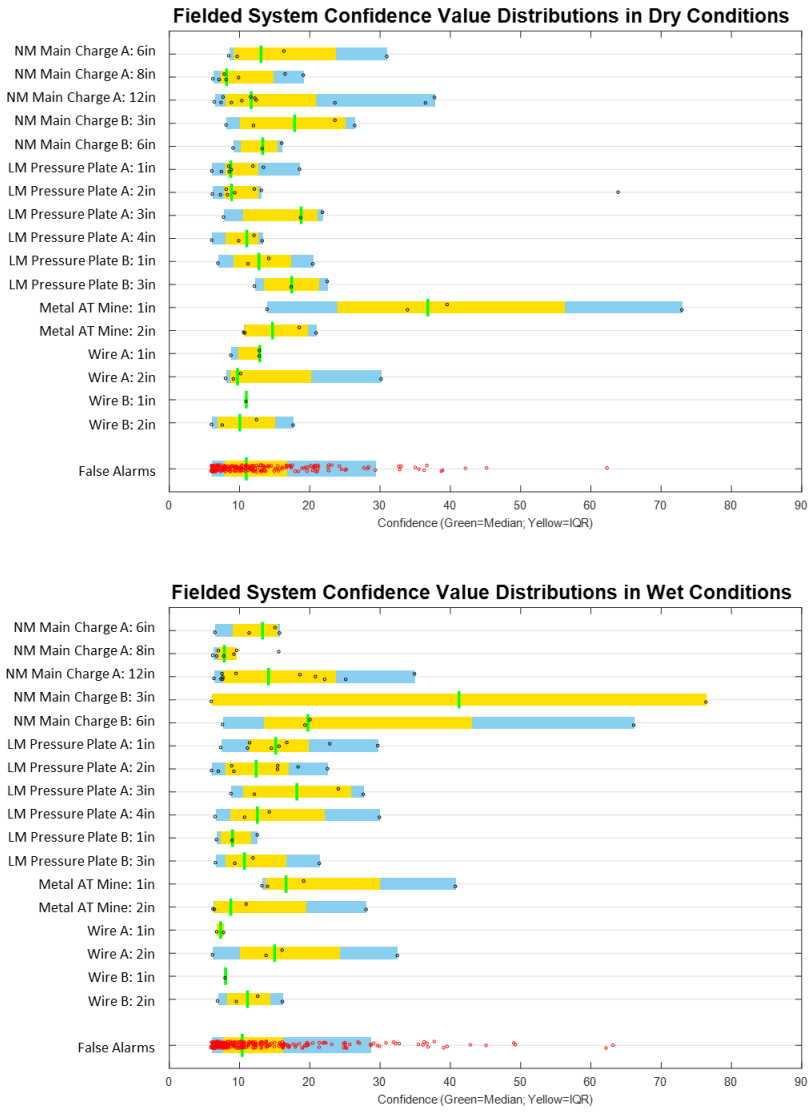

Figure 5.8: Fielded System Confidence Value Distributions in Dry and Wet Conditions

The detections of Metal AT Mines had higher confidence values in wet conditions than dry conditions. There were fewer detections of Non-Metal Main Charges in wet conditions than dry conditions with the currently fielded system, though a detection of Non-Metal Main Charge B at a 3 burial inch and at a 6 inch burial depth have very large confidence values. The false alarm confidence value distributions are similar in wet and dry conditions.

Three operators swung System A over the primary targets during the week of data collection: the operator provided by the vendor who developed the system, a Government expert operator, and a Government operator who is a retired soldier. Figure 5.9 compares the performance of the three operators who swung System A.

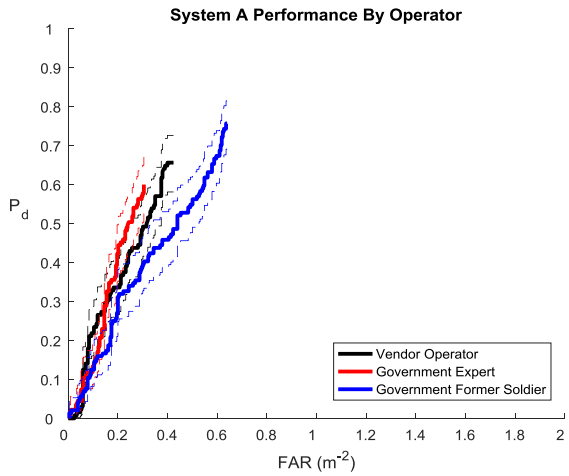

Figure 5.9: System A Performance by Operator

The Government expert operator had the best performance, with a comparable Pd to the other operators at the lowest FAR. The retired soldier had the highest Pd, but also

the highest FAR, while the vendor operator fell in between the Pd and FAR of the two Government operators.

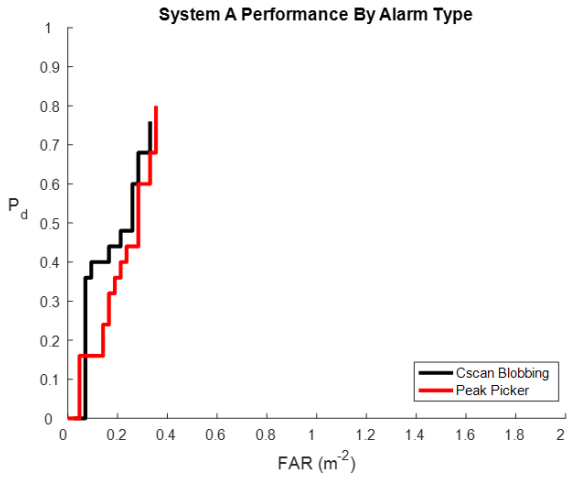

Figure 5.10: System A Performance by Alarm Type

In Figure 5.10, the performance between using the peak picking algorithm to create alarms from the Ksum metric is compared with using position information to create Ksum Cscans and to create alarms using a blobbing technique. This comparison is for a small subset of the data that had good position information that could be pinned to UTM coordinates. For this small dataset, the results are similar for the Cscan blobbing technique and the peak picking technique, though the Cscan blobbing technique is better in the low FAR region of 0 to 0.3 false alarms per square meter.

5.3 System B

System B had a stereo vision camera to provide relative position sensor information, but the prototype camera only worked intermittently during the data

collection. Thus, most of the data collected by System B uses trigger information and the blank data file to compute the Ksum.

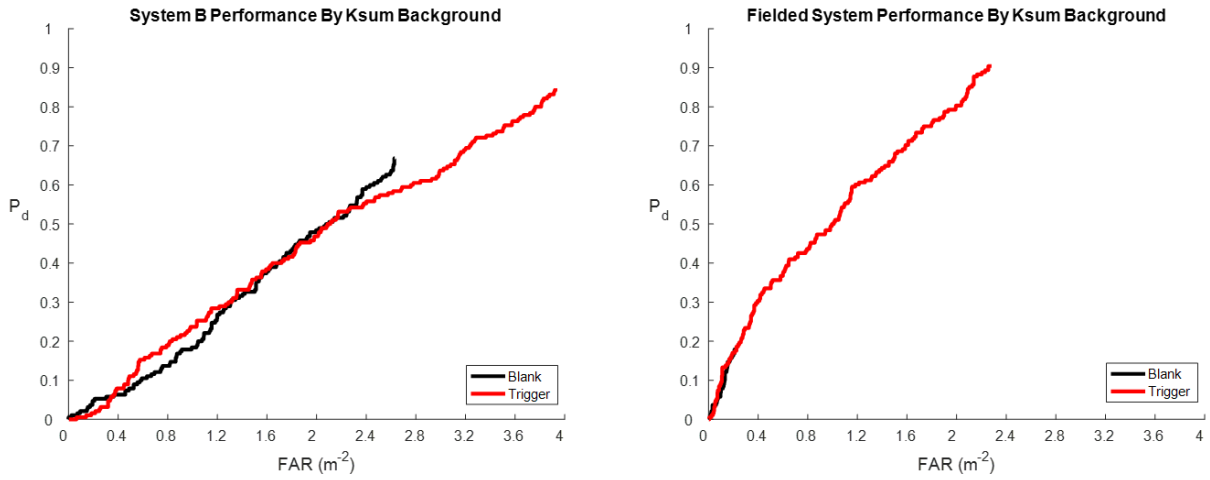

Figure 5.11: System B and Fielded System Performance by Ksum Background

The performance for System B is very similar for the two Ksum backgrounds, though the Pd and FAR are higher when the scans prior to the trigger are used as background. The Pd and FAR is significantly higher for the currently fielded system when the scans prior to the operator trigger press are used as the Ksum background. The Pd for both systems is higher using the trigger information, and so all results shown for System B and the fielded system will use this background.

The confidence value distributions for all detections and false alarms for System B for each background option are shown in Figure 5.12.

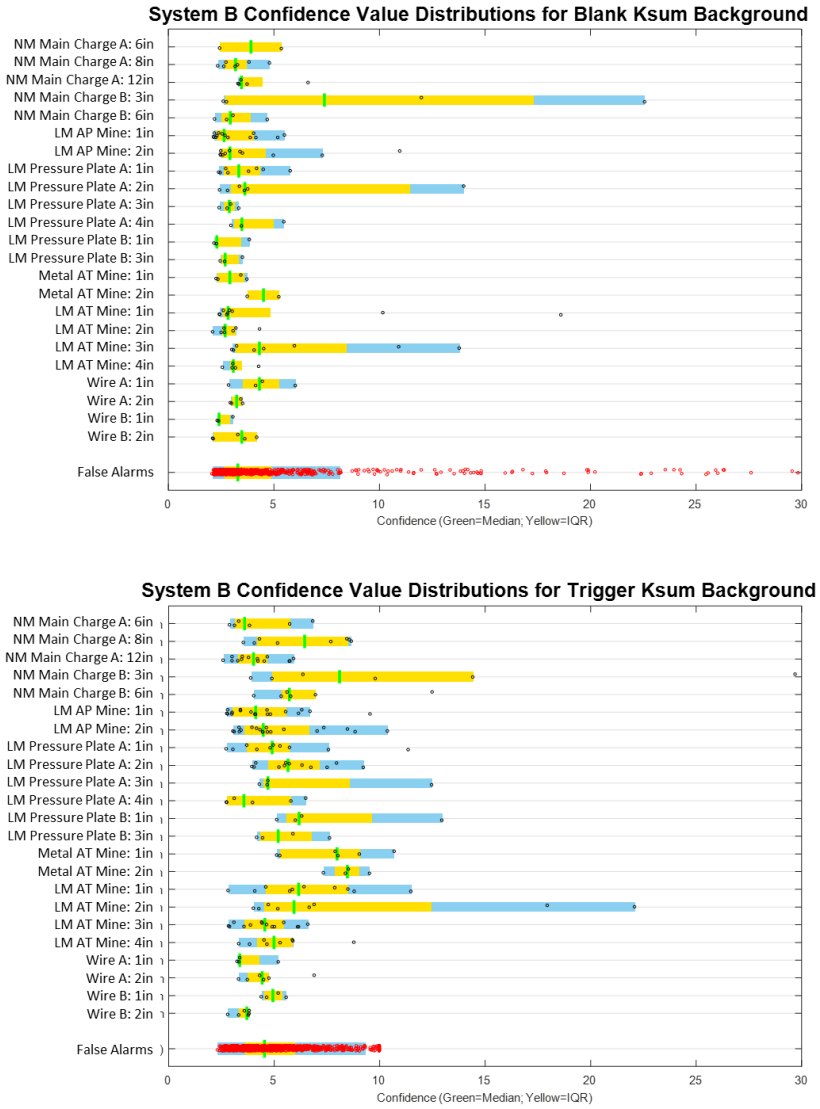

Figure 5.12: System B Confidence Value Distributions by Ksum Background

The detections of Non-Metal Main Charges, Metal AT Mines, and Low-Metal AT Mines at 1 and 2 inches have higher confidence values for the trigger Ksum background compared to the blank Ksum background. There are more false alarms for the trigger

Ksum background than the blank Ksum background and the median confidence value of the false alarm distribution.

The confidence value distributions for the fielded system for both Ksum backgrounds is in Figure 5.13.

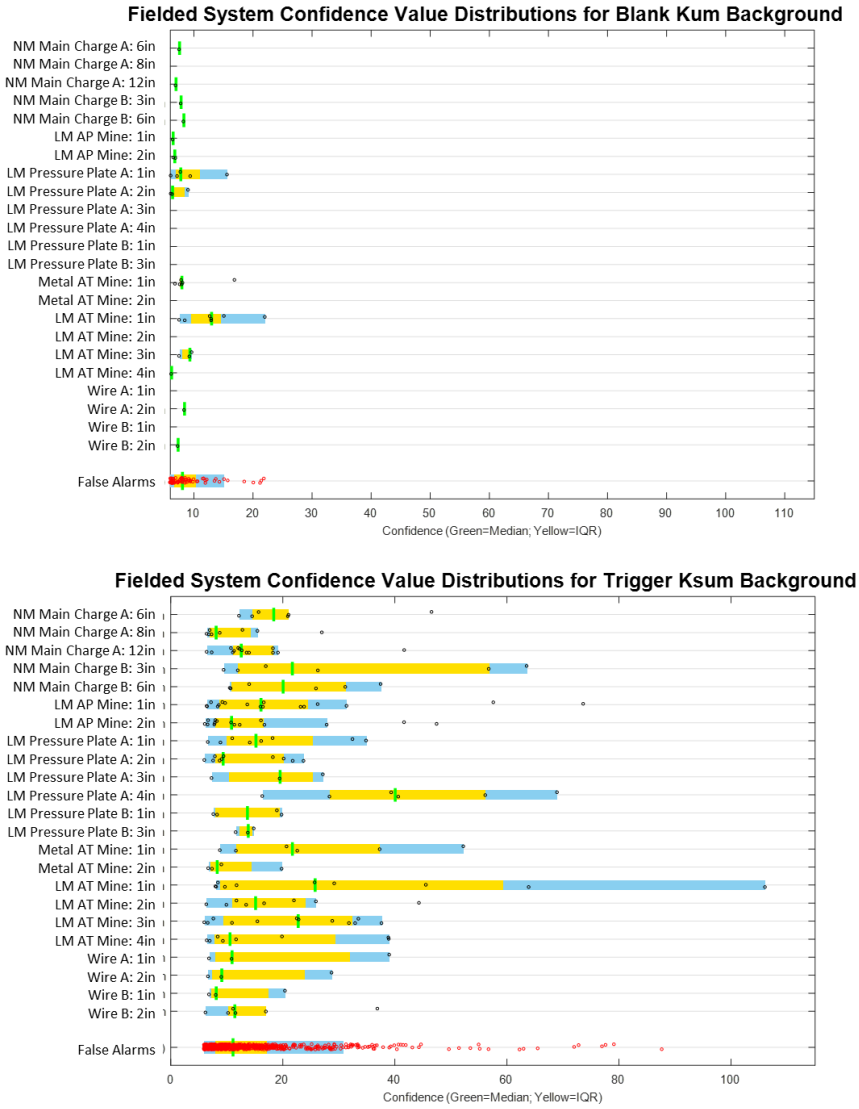

Figure 5.13: Fielded System Confidence Value Distributions by Ksum Background

In Figure 5.11, the Pd and FAR are significantly lower for the blank background for the Ksum compared to using trigger information. This is clear in Figure 5.13 as all targets are detected when the trigger information is used for the Ksum background and there are significantly more false alarms. The median confidence value of the false alarm distribution is higher for the trigger background than the blank Ksum background.

Figure 5.14 shows the performance of System B and the currently fielded system using the using the scans immediately prior to the operator pressing the trigger as background. The dotted lines on the ROC curves are the error bars for the 90% confidence levels.

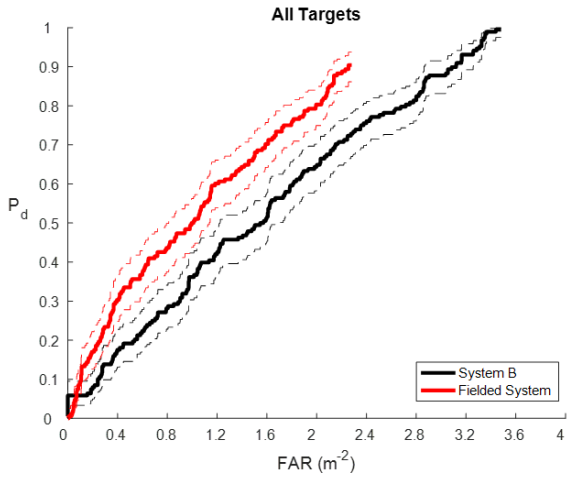

Figure 5.14: System B Performance Against All Targets Compared to the Fielded System

System B has a higher Pd and a higher FAR than the currently fielded system. A FAR of around 0.2 false alarms per square meter is the limit of system usability in normal

use and at this FAR the performance is poor for both systems and the fielded system Pd is higher than System B. However, the Ksum metric used to create the ROC curves is a metric of signal over background or of target energy. In many fielded systems, an energy metric is used as a prescreener to identify potential threat locations. Then a classification algorithm runs on these identified threat locations and examines shape or spatial features of the GPR data to reduce the false alarm rate. This approach could be useful for System B as it achieves a Pd of 1, but not until a very high FAR of 3.6 false alarms per square meter.

In Figure 5.15, the performance of System B and the fielded system are plotted for each data collection area separately.

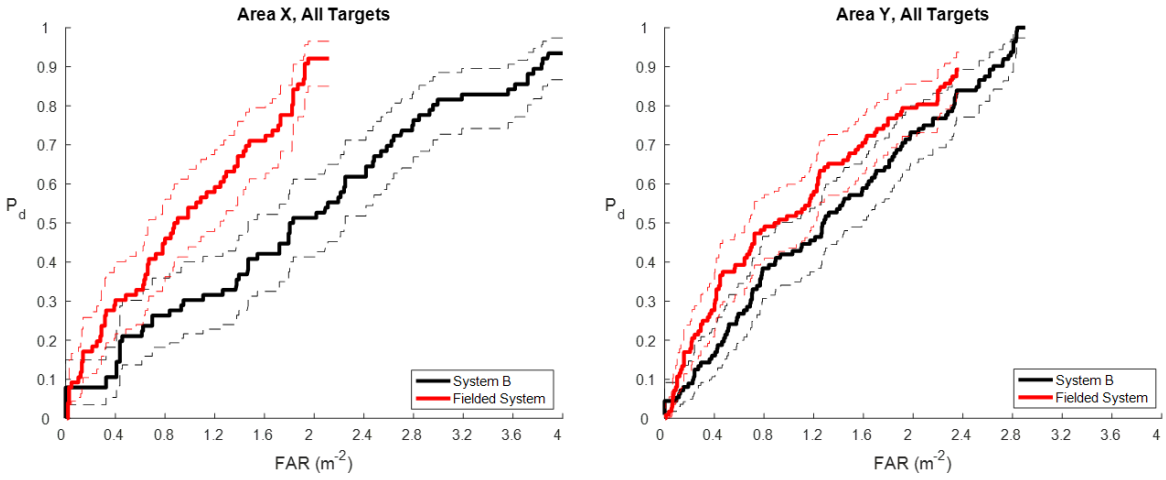

Figure 5.15: System B and Fielded System Performance by Data Collection Area

The fielded system outperforms System B in Area X: both systems have a 90% Pd, but the fielded system reaches that Pd at half of the FAR of System B. The ROC curves are much closer for Area Y. System B detects all targets, while the fielded system detects nearly 90% of all targets. System B has a higher FAR than the fielded system in both data collection areas.

To investigate the performance differences in the data collection areas, the confidence value distributions for all detections and false alarms in each area are plotted in Figure 5.16.

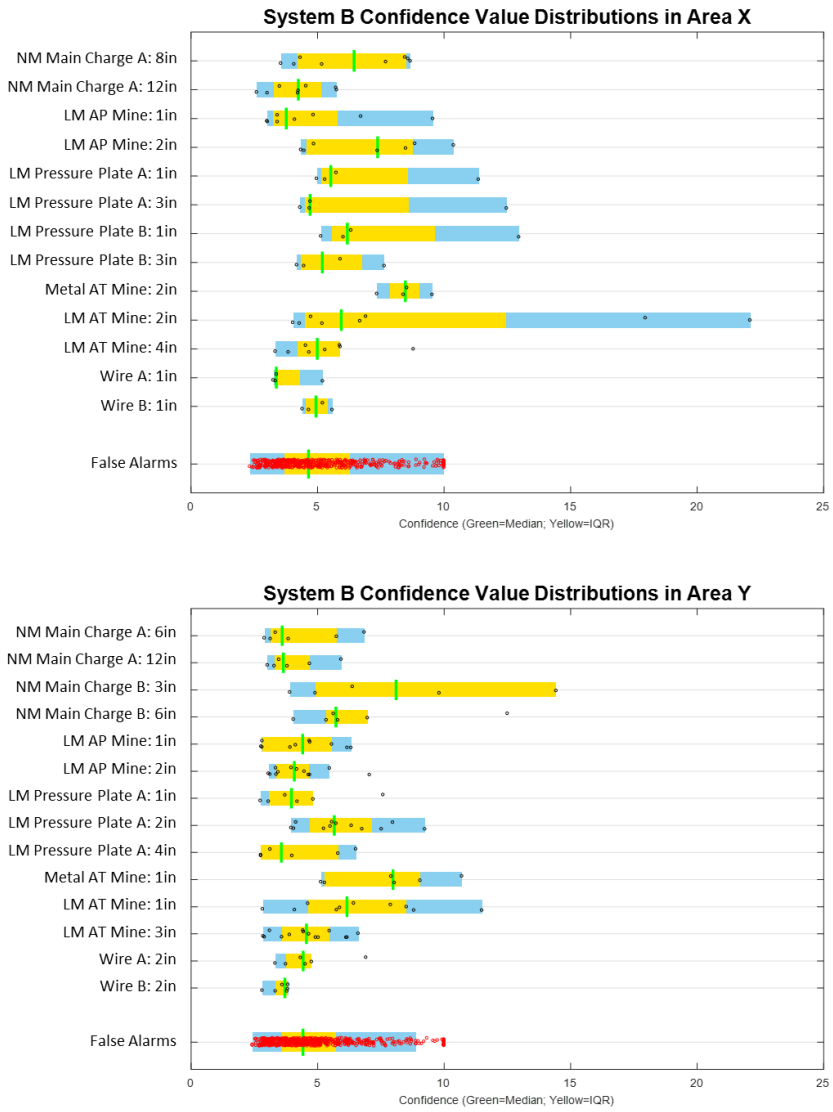

Figure 5.16: System B Confidence Value Distributions in Area X and Area Y

There are more false alarms in Area X than Area Y, though the median confidence value of the false alarm distribution is the same for both data collection areas. The confidence value distributions are wider for the Low-Metal AP Mines and Low-

Metal Pressure Plates in Area X compared to Area Y. The median of the confidence values distributions are approximately the same for Metal AT Mines and Low-Metal AT Mines in Area X and Area Y.

The confidence value distributions for the fielded system by area is in Figure 5.17.

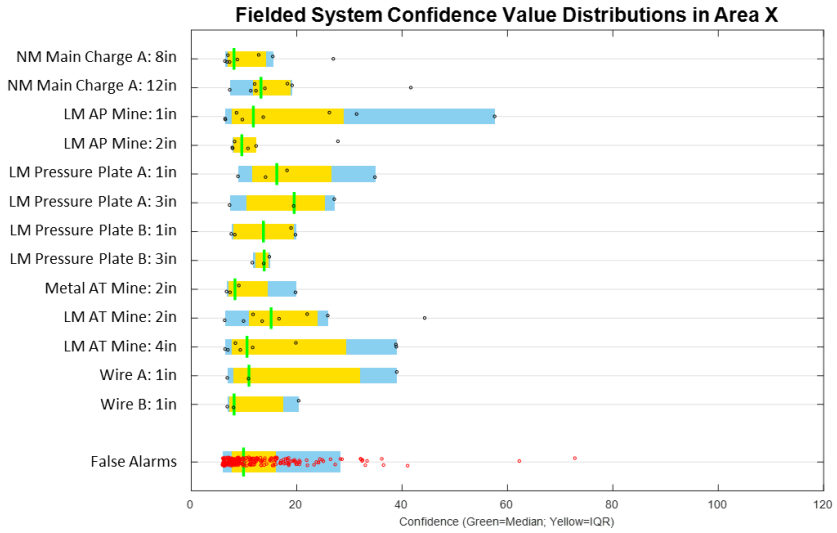

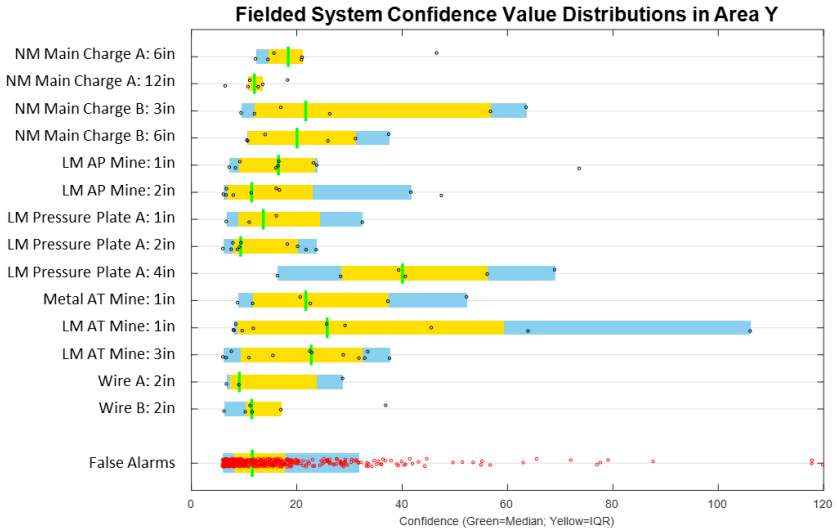

Figure 5.17: Fielded System Confidence Value Distributions in Area X and Area Y

The performance difference between data collection areas is larger for the fielded system than for System B. The confidence value distributions for detections of all targets, except Non-Metal Main Charges, are wider and have a higher median confidence value in Area Y than in Area X. There are more false alarms in Area Y than in Area X and the median confidence value in the false alarm distribution is slightly higher in Area Y than in Area X.

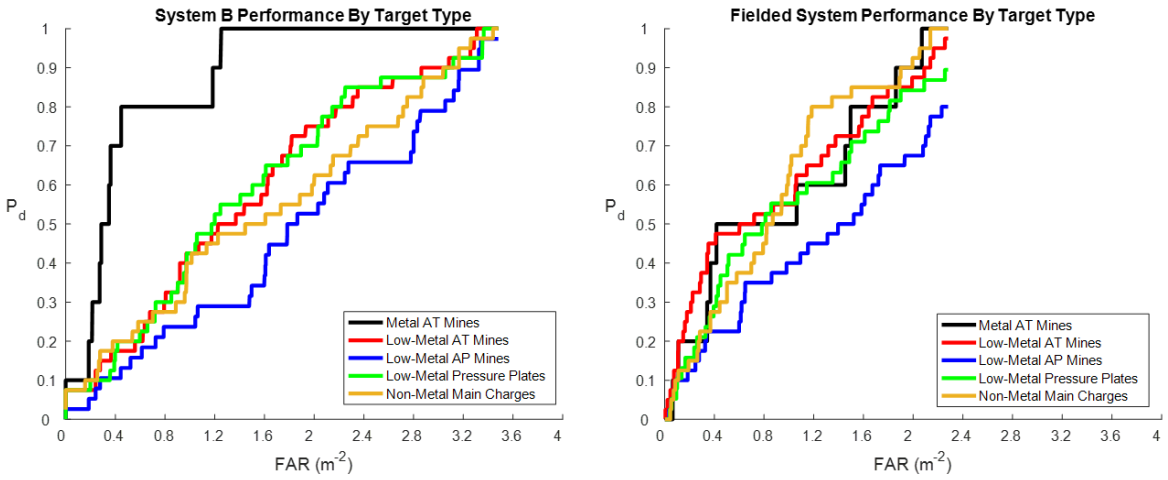

Figure 5.18: System B and Fielded System Performance by Target Type

The performance of System B and the fielded system is broken out by target type in Figure 5.18. System B and the fielded system have similar performance for low-metal AT mines and low-metal pressure plates, though System B has a higher FAR. System B

detects all metal AT mines at a FAR lower than the fielded system. System B also detects more low-metal AP mines than the fielded system, but at a high FAR.

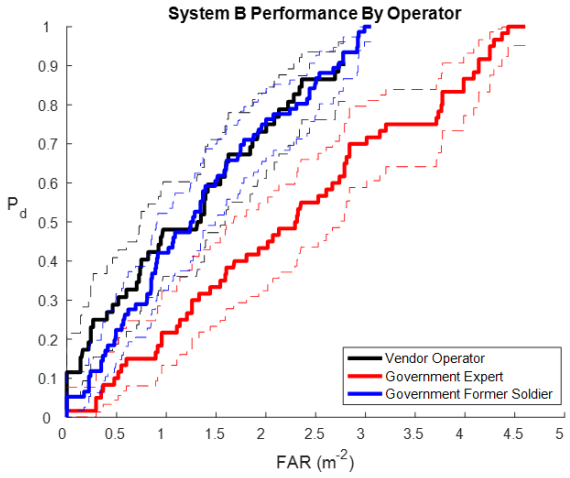

Figure 5.19: System B Performance by Operator

The vendor operator and government former soldier operator performance was similar for System B, while the government expert had the highest FAR. It should be noted that the vendor operator for System B is also an expert operator.

5.4 System C

System C did not have a stereo vision camera to provide relative position sensor information for the GPR data, thus the Ksum metric for System C will use the blank data files and trigger information and the results will be compared.

Figure 5.20 shows the performance of System C and the currently fielded system using the blank file and the trigger information as the background.

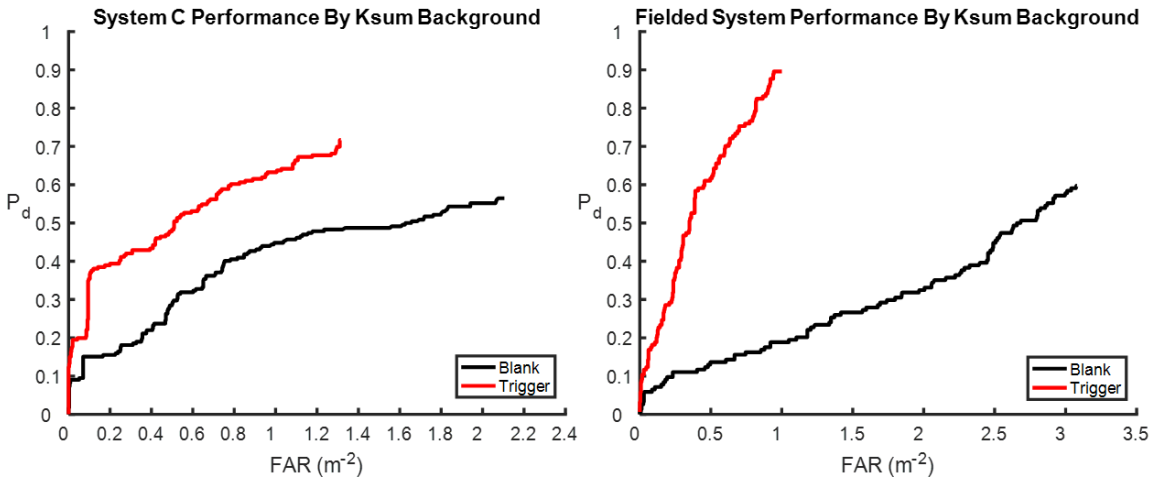

Figure 5.20: System C and Fielded System Performance as a Function of Ksum Background

The ROC curves above show that performance for both systems is significantly better when the trigger information is used as the background compared to using the blank file as the background. This result indicates that although the blank data files are collected near the target location, the blank patch of ground does not accurately capture subsurface features near the target location. Using the trigger information yields a more

realistic signal over background measure because the ground surrounding the target location is used for the background when calculating the Ksum. As the performance using the trigger information to determine the background is superior to using the blank data file for both detectors, all additional results for System C and the fielded system will correspond to Ksum results using the trigger for background information.

The difference between the Ksum results for each background is large. To understand this difference, the confidence value distributions for all targets and false alarms will be examined for each system for each background type. The confidence value distributions for System C for each background type are in Figure 5.21.

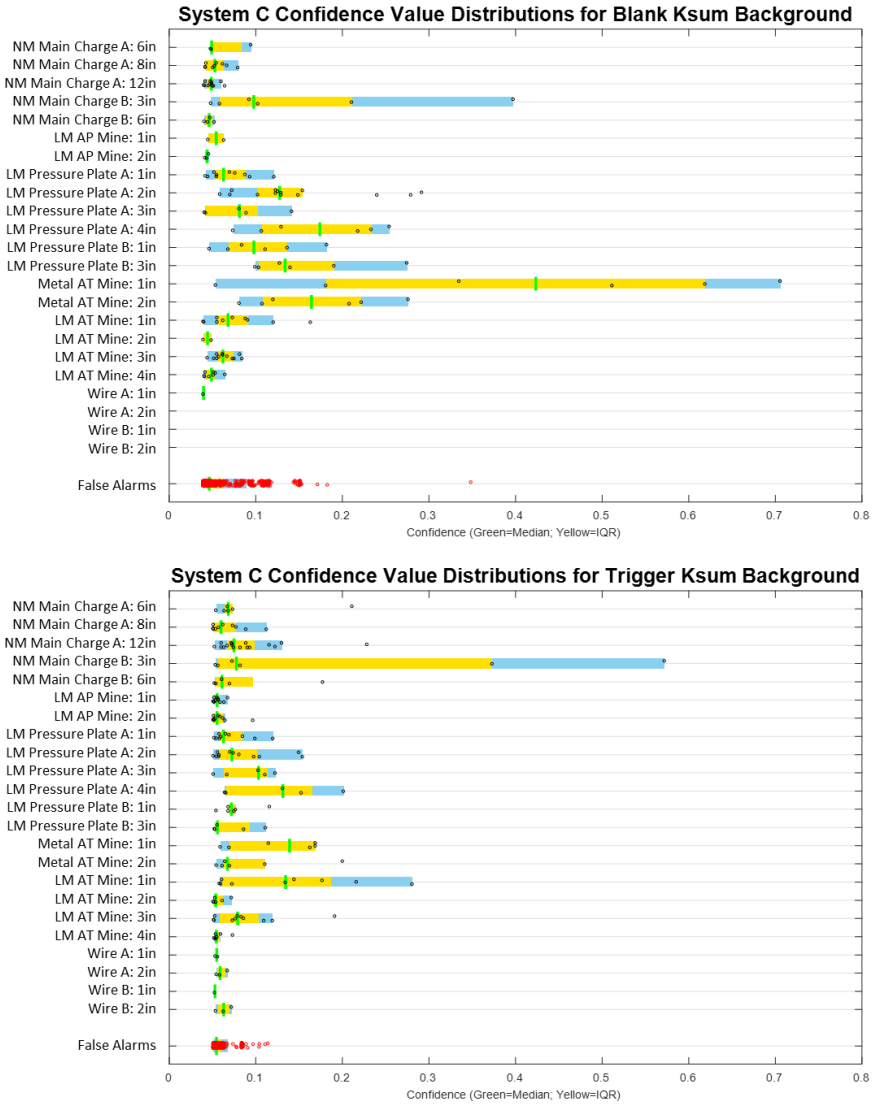

Figure 5.21: System C Confidence Value Distributions by Ksum Background

Though the median confidence value in the false alarm distribution is the same with both Ksum background types, there are fewer false alarms of both high and low confidence values when the trigger information is used for the Ksum background. When

the trigger information is used for the Ksum background, there are more detections of all Wire targets compared to the blank background where some Wire targets are not detected. There are more detections of Low-Metal AP Mines when the trigger information is used. Low-Metal AP Mines and Wire targets are difficult to detect since they are smaller than the rest of the targets in this target set. This indicates that the blank ground is a sufficient background for the Ksum calculation for larger targets, but the scans prior to the operator trigger press is a better background choice for the Ksum calculation of small targets, especially those buried at shallow depths.

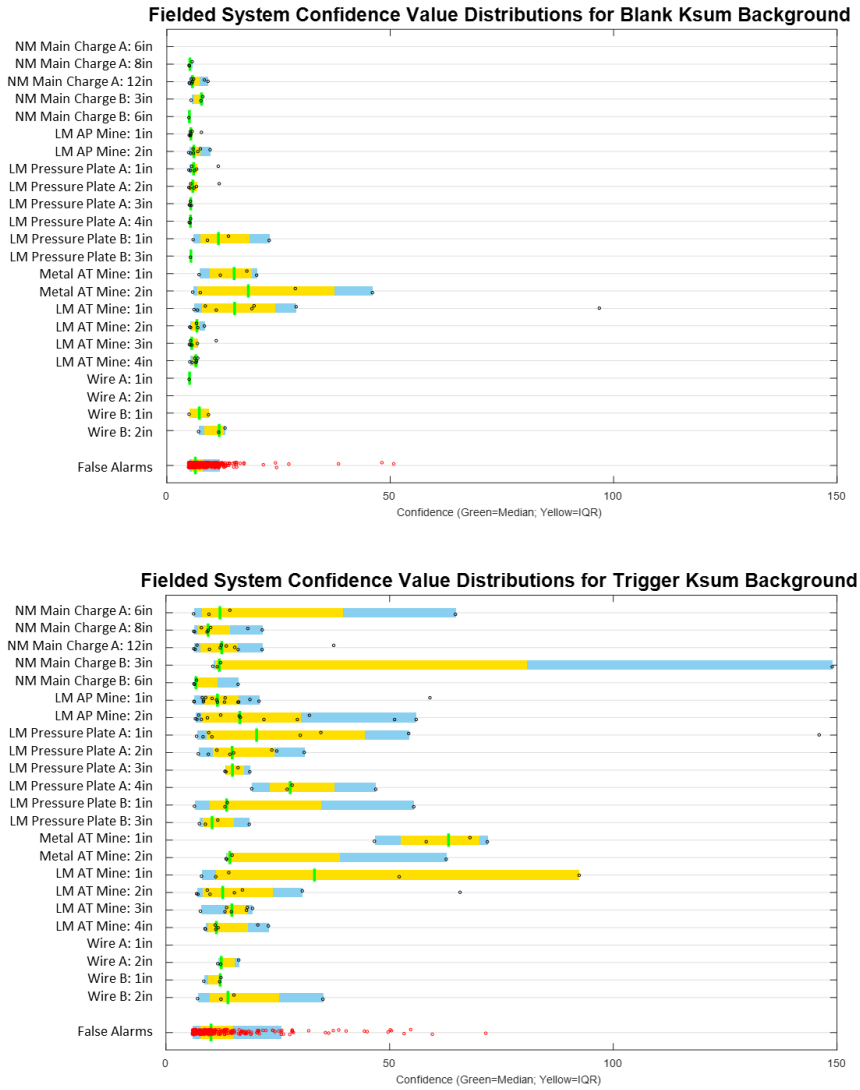

Figure 5.22: Fielded System Confidence Value Distributions by Ksum Background

The confidence value distributions for all targets are higher for the fielded system when the trigger information is used as the background for calculating the Ksum, except for Wire target A at 1 inch which is not detected. The higher confidence value distributions for detections result in better performance in the ROC curve because there is less overlap in the false alarm and detection confidence value distributions when the

trigger information is used than when the blank file is used as the background for calculating the Ksum.

The ROC curves comparing the performance of System C and the currently fielded system for all targets is in Figure 5.23.

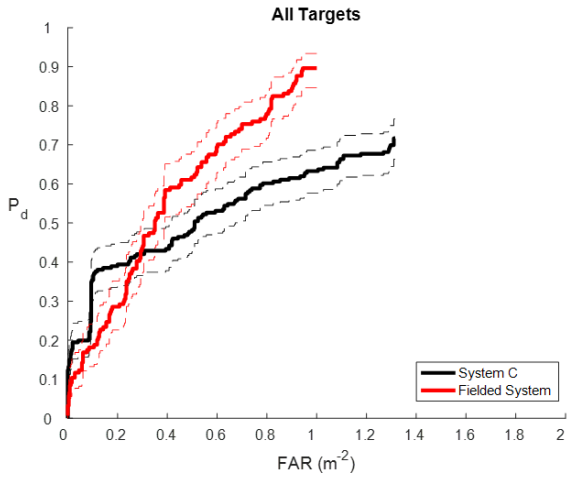

Figure 5.23: System C Performance Against All Targets Compared to the Fielded System

When the Ksum is calculated using the scans prior to the operator pressing the trigger, the fielded system has a higher Pd and lower FAR than the System C. However, System C outperforms the fielded system at low FAR.

The system performance broken out by data collection area is in Figure 5.24. From the ROC curves, it is clear that the performance difference between System C and the fielded system is primarily due to Area X. System C has a lower Pd and higher FAR in Area X compared to Area Y, where System C has a Pd and FAR more comparable to

the fielded system. System C also detects more than half of the targets in Area Y with no false alarms.

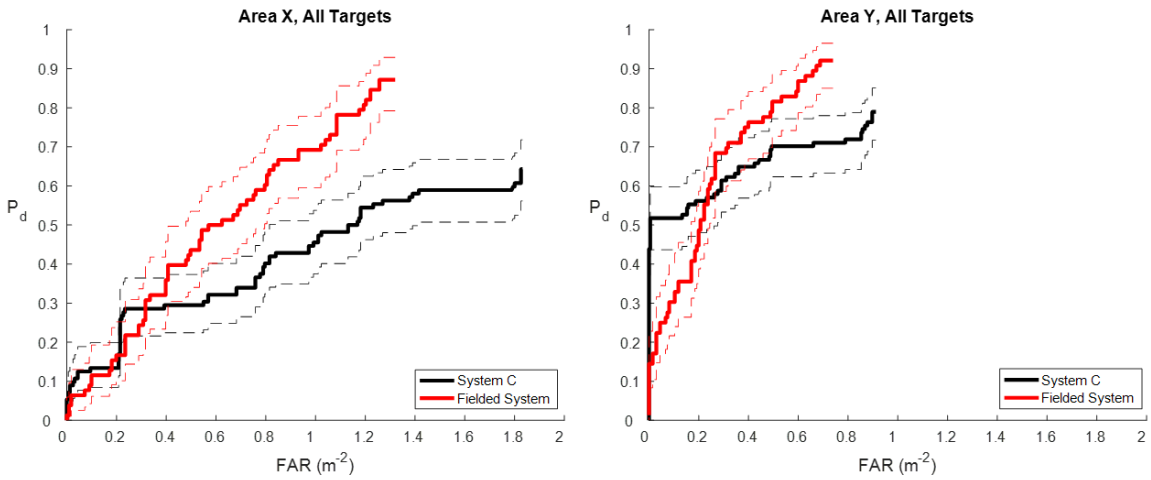

Figure 5.24: System C and Fielded System Performance by Data Collection Area

The confidence value distributions for System C in both data collections areas are plotted in Figure 5.25.

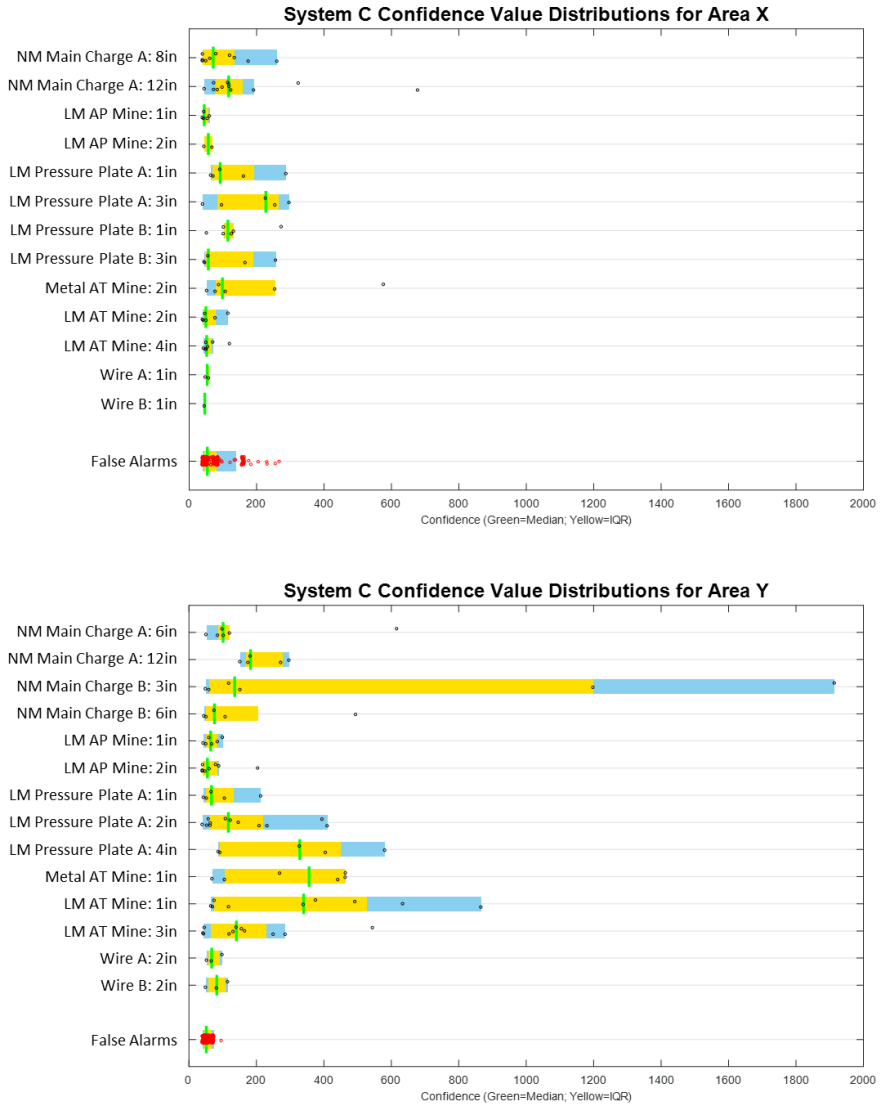

Figure 5.25: System C Confidence Value Distributions by Data Collection Area

The confidence value distributions for detections of all targets are higher in Area Y than data collection in Area X. There are fewer false alarms in Area Y than in Area X of both low and high confidence values. The increased separation between the confidence

values of the detections and false alarms in Area Y is the source of the better ROC curve for Area Y compared to Area X.

The confidence value distributions for the fielded system detections and false alarms in each data collection area are in Figure 5.26.

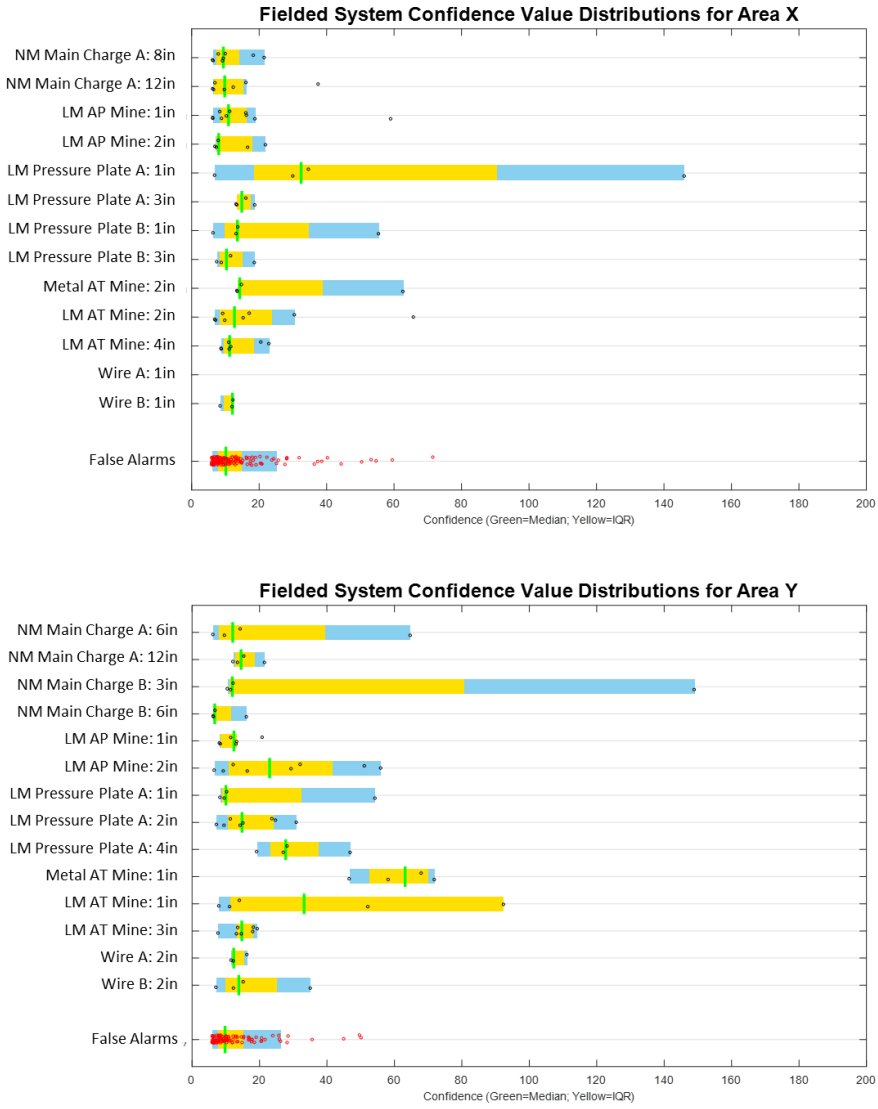

Figure 5.26: Fielded System Confidence Value Distributions by Data Collection Area

The fielded system has fewer high confidence false alarms in Area Y than in data collection Area X. The confidence value distributions for detections of Low-Metal AP Mines at 2 inches, Metal AT Mines, and all Wire targets have higher confidence values in Area Y than in Area X. Though the overall Pd for the fielded system is similar in Area X and Area Y, the reduced number of high confidence false alarms and the increased confidence values of detections of certain targets results in better performance at low FAR.

The performance for System C and the currently fielded system are plotted as a function of target type in Figure 5.27.

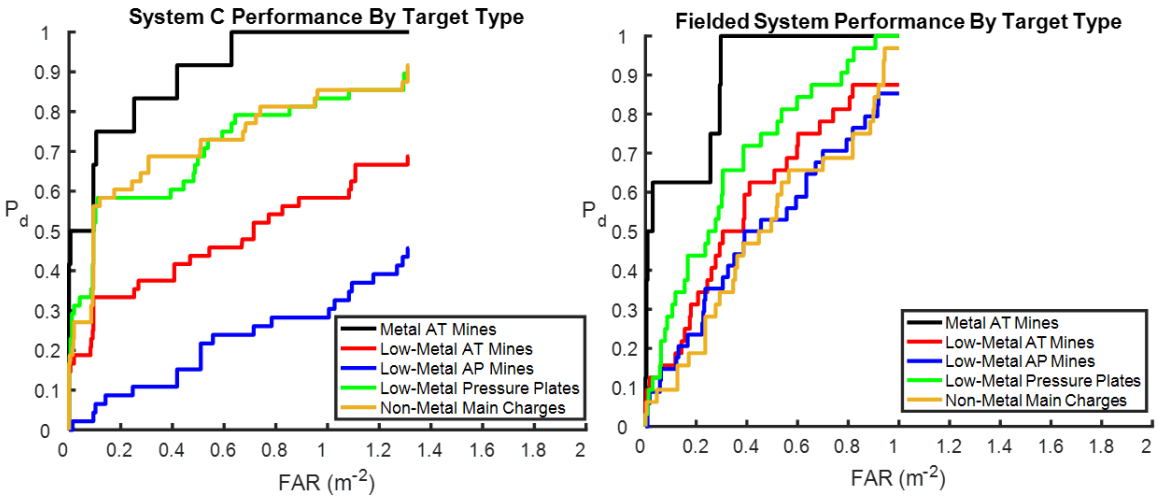

Figure 5.27: System C and Fielded System Performance by Target Type

Both systems detect all Metal AT Mines, which is the easiest target in this data collection. System C detects about 90% of all Low-Metal Pressure Plates and Non-Metal

Main Charges, while the fielded system detects all or nearly all of those targets. The difference in performance between the systems is driven by the poor performance against Low-Metal AT and AP mines with System C. System C detects about 70% of Low-Metal AT Mines and 45% of Low-Metal AP Mines, while the fielded system detects just over 80% of both target categories.

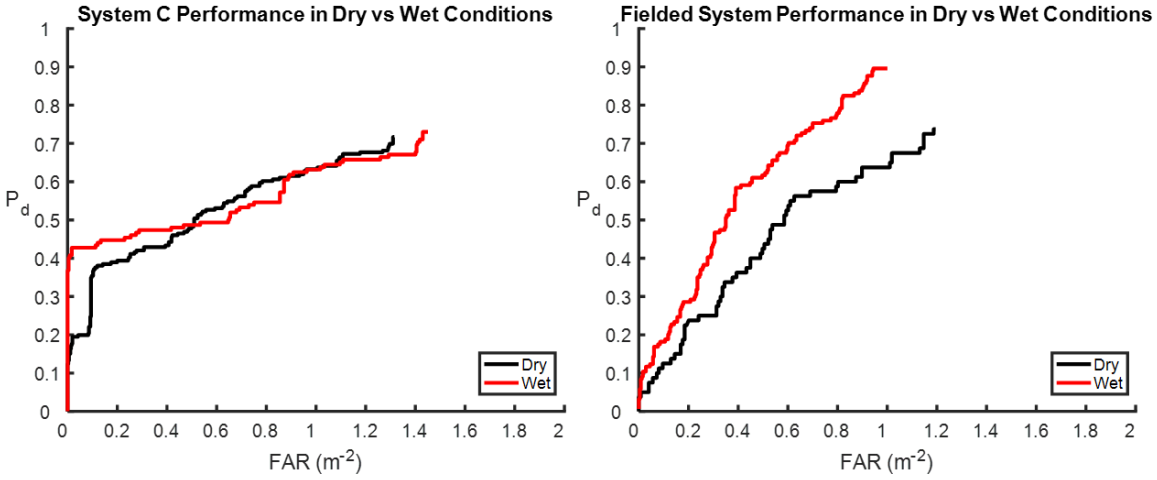

Figure 5.28: System C and Fielded System Performance in Dry vs. Wet Conditions

The performance for each system in wet and dry conditions is plotted in Figure 5.28. For both systems the performance is better in wet conditions than in dry conditions. System A has a similar Pd in both conditions, but the Pd is higher in the low FAR region in wet conditions. The fielded system has a higher Pd and lower FAR in wet conditions than dry conditions. This result is surprising and investigating the performance drivers in wet conditions is part of the proposed future analysis on this data. In wet conditions the

permittivity of the soil increases and thus the wet conditions could potentially have a higher reflection coefficient if the soil permittivity increases to a value such that there is now a bigger difference in permittivity between the target and surrounding soil. However, attenuation also increases in wet conditions so the assumption is that performance degrades in wet conditions for deeply buried targets.

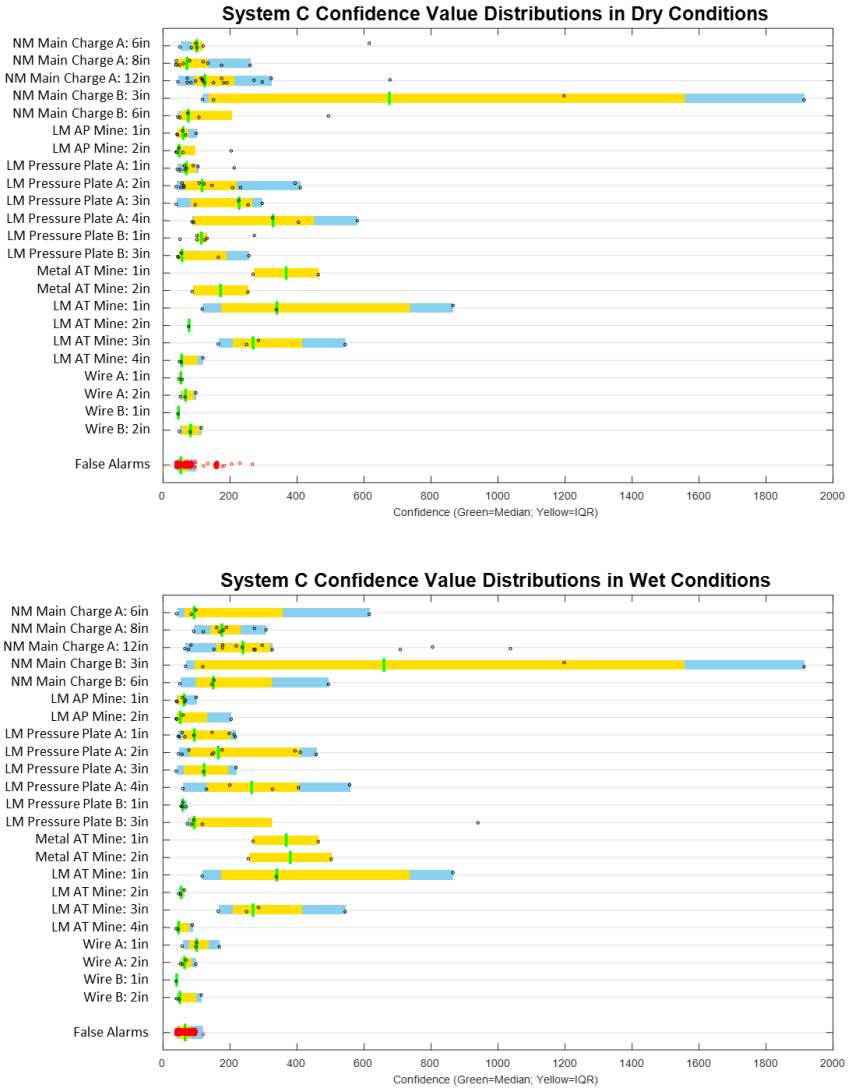

Figure 5.29: System C Confidence Value Distributions in Dry vs. Wet Conditions

System C has fewer high confidence false alarms in wet conditions compared to dry conditions. The confidence value distributions are higher for Non-Metal Main Charges at 6 inches, Low-Metal AP Mines at 2 inches, and Metal AT Mines at 2 inches in wet conditions compared to dry conditions, which results in better performance at low FAR in wet conditions.

The confidence value distributions for the fielded system in wet and dry conditions are in Figure 5.30.

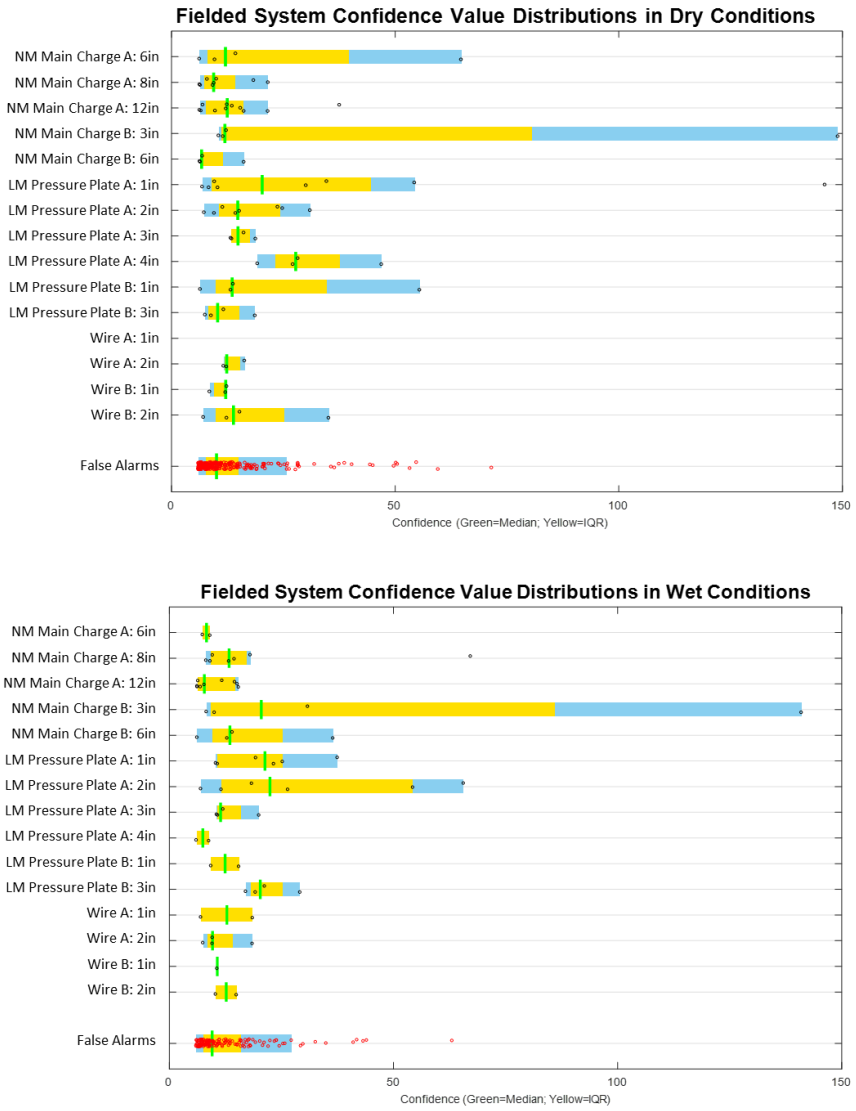

Figure 5.30: Fielded System Confidence Value Distributions in Dry vs. Wet Conditions

The confidence value distributions for most Non-Metal Main Charges decrease in wet soil conditions compared to dry conditions, but the distributions for Low-Metal Pressure Plates and Wire targets increase in wet conditions compared to dry conditions. The median confidence value of the false alarm distributions are similar in both wet and dry conditions, though there are fewer high confidence false alarms in wet soil than dry

soil. The reduction of high confidence false alarms and increased confidence values for a subset of targets is reflected in the improved ROC curve for wet conditions compared to dry conditions.

There were three operators that swung System C during the data collection. The performance for System C is plotted as a function of operator in Figure 5.31.

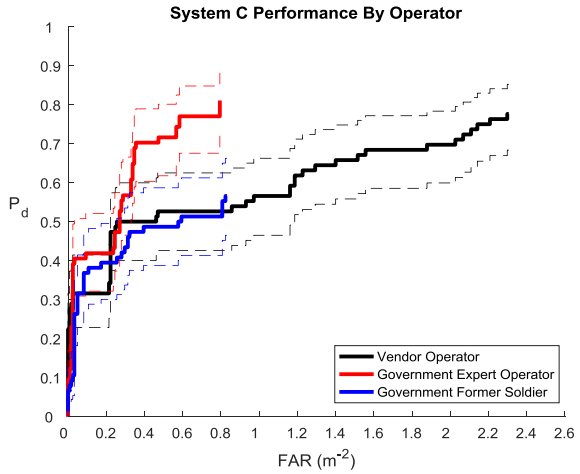

Figure 5.31: System C Performance by Operator

The expert operator has the best performance: he achieves the highest Pd at the lowest FAR. The vendor operator has the second highest Pd, but at a FAR that is three times as high as the two Government operators. The former soldier has a FAR similar to the expert operator, but with about a 30% lower Pd.

5.5 System Comparison

Table 5.1: Pd and FAR by System

System	Total Pd	Total FAR (FA/m^2)	Pd at 0.2 FA/m^2
A	0.68	0.4	0.31
B	1	3.6	0.09
C	0.71	1.3	0.38

Table 5.1 lists the total Pd, total FAR, and the Pd at the FAR of 0.2 false alarms per square meter, which is the FAR limitation for a useable handheld detector. The Pd is highest for System B, but the FAR is also significantly the highest. System A has the lowest total Pd and total FAR, while System C has a similar Pd at nearly three times the FAR. At a FAR of 0.2 false alarms per square meter, System C has a slightly higher Pd than System A and System B has a low Pd of 0.09.

For all systems, the FAR could be reduced if the Ksum metric is used as energy based prescreener that identifies potential threat locations and additional techniques were used at these locations to extract features that have spatial or geometric information which could potentially reduce the FAR.

5.6 Ksum Conclusion

The Ksum metric computes the signal over background better for some systems than others. The Ksum metric works best for radar data that is relatively consistent in response except for over the target location, and thus has very little system noise or subsurface multipath from operator feet. GPR data that has been calibrated to remove

thermal noise and drift, antenna compensations, or other self-induced noise from the system will have better results using the Ksum metric than other systems.

CHAPTER 6: CONCLUSIONS

6.1 Thesis Summary

In this thesis a metric to calculate signal over background, called a Ksum, is applied to data collected with three prototype detectors and a currently fielded system to attain a measure of system performance. The data used in this thesis is Ground Penetrating Radar (GPR) data collected over a three week period with three operators. The target set used for this data collection contains relevant threats and include difficult to detect targets that contain very little or no metal.

The Ksum is applied to each A scan of GPR data, which is the radar response of a single channel at a single scan. Since the prototype systems each had varying levels of relative position information available, the Ksum background was examined using data collected over blank ground and using the scans prior to the operator hitting a trigger to indicate the sensor head is over the target. Potential target locations are identified using a peak picking algorithm to find the local maxima locations and their corresponding values in the Ksum result for the search and localize swings. This peak picking algorithm allows for constraints when choosing the local maxima such as the minimum prominence of a peak, or how much the peak stands out due to its height and relative location to other peaks, as well as the minimum peak width so that only one maxima is chosen for the cases where the response over a large target occurs for many scans.

For the small subset of data collected with System A that had adequate position sensor data, the Ksum is turned into a C scan map of GPR response as the operator swings up to, over, and past the target in a search swing. This C scan map uses the

relative position information to wrap the Ksum result so that it is no longer a single continuous stream of scans, but spatially shows when the sensor head changes direction at the edge of the sweep to advance down the lane. A list of potential target locations are created from the Ksum C scan maps using a blobbing technique, as the response to the target is built up as the operator swings over it multiple times as they advance down the lane.

The performance of each system is evaluated by creating a list of potential target locations in an alarm file and comparing this list to the surveyed ground truth of the targets to determine if each alarm is a detection of a target or a false alarm. The analysis methodology used in this thesis then counts the number of target detections compared to the number of encounters to calculate the probability of detection and counts the number of false alarms per area swept by the operator (false alarm rate). The probability of detection (Pd) and false alarm rate (FAR) are plotted in ROC curves so that the trade-off between Pd and FAR can be observed.

6.2 Data Collection Conclusions

The results of each system during this data collection indicate that each system has a detection capability for difficult to detect targets. Each system has a different trade-off: System A has the lowest false alarm rate and the lowest Pd of nearly 70%, System B detects all targets but has the highest false alarm rate, and System C performance was in between with 70% of targets detected at a higher FAR than System A but lower than System B. System A outperformed the currently fielded system at low FAR, but overall detected fewer targets. System B detects more targets than the currently fielded system at

a high FAR, but the currently fielded system has better performance at low FAR. System C outperforms the currently fielded system at low FAR, but the fielded system detects more targets at a higher false alarm rate.

Data was collected before and after rainfall with Systems A and C. All data collected with System B was in wet soil conditions. System A performed better in dry soil compared to after rainfall occurred, especially at low FAR. The fielded system also collected data under dry and wet conditions concurrently with System A and has much less performance dependence on the soil conditions: the Pd is the same for dry and wet conditions, but the FAR in dry soil is lower.

Three operators collected data with each prototype system: a government expert operator, a government former solider operator, and a vendor operated. Each vendor operator had a varying level of experience operating a handheld detector, the vendor operator for System A is a novice with little to no experience, the vendor operator for System B is an expert operator who conducts training for other detectors manufactured by that vendor, and System C was operated by a vendor operator that has some experience but is still a novice. The expert operator performed the best for Systems A and C and the worst for System B. The expert operator results for System B are surprising; the expert operator detects all targets but at a significantly higher FAR than the other operators.

Ksum C scans were only created for the small subset of data collected with System A that had adequate position information. When these results are compared to the

Ksum results using the peak picking algorithm for the same dataset, the Pd is about the same but the Ksum C scan metric performs better at low FAR.

6.3 Proposed Future Work

Proposed future work would examine additional benefits of having position information for the handheld prototype systems. The ability to build up data over the same piece of ground and know its location would likely improve detection of difficult targets since data could be integrated over multiple sweeps. Additionally, metrics or algorithms that utilize shape or geometry information could be used to enhance detection if accurate position information is available. Algorithms such as an Edge Histogram Detector (EHD) [12] [13] or the Hidden Markov Model (HMM) [14] could be used to determine if the suspected threat has a rising, flat, and falling evident in a target response and could be used to reduce false alarms. Position sensor information could also be used to form Synthetic Aperture Radar or SAR images as the sensor moves back and forth over the target and additional radar data is collected to attain a fine-resolution image of the target [10].

Other future work would examine using adaptive signal processing techniques to update the background used for the Ksum as the operator swings the system down an entire lane. This work would improve upon the technique of applying a guard band to determine the background for implementing the Ksum as a more sophisticated algorithm such as Recursive Least Squares (RLS) would do something similar but with more control since a forgetting factor can be chosen to determine which scans of previous data would be used for the background [15].

APPENDICES: MATLAB CODE

A.1 Calculating Ksum

```
%% KSUM Calculation using Trigger Info (if available, else use blank data)


[fn, pathname, filterindex] = uigetfile(...
  {'*.asc', '*asc'; '*.*', 'All Files (*.*)'},...
  'Pick data file(s) please',...
  'C:\Data\HH_DataCollections\');
fid=fopen([pathname fn]);
Filelist = textscan(fid,'%s')
FileList=cellstr(Filelist{1,1});
num_files=length(FileList);
% All 5 swings for one target are read in as a group for Ksum calculation
file_grouping=5;
num_groups=num_files/file_grouping;
count=1;
for k=1:num_groups


  blank_data = load((FileList{count,1}));
  localize_xt=load(FileList{count+1,1});
  localize_dt=load(FileList{count+2,1});
  search_xt=load(FileList{count+3,1});
```

```
search_dt=load(FileList{count+4,1});

BlankPackets=length(blank_data);
NumPackets_dtL=size(localize_dt,2); NumPackets_dtS=size(search_dt,2);
NumPackets_xtL=size(localize_xt,2); NumPackets_xtS=size(search_xt,2);

trigger_dtL = localize_dt(4,:); trigger_logical_dtL=logical(trigger_dtL);
trigger_dtS = search_dt(4,:); trigger_logical_dtS=logical(trigger_dtS);
trigger_xtL = localize_xt(4,:); trigger_logical_xtL=logical(trigger_xtL);
trigger_xtS = search_xt(4,:); trigger_logical_xtS=logical(trigger_xtS);

% Calculate the Mean and Std of Background using button presses
search_dt_button_press=[]; localize_dt_button_press=[];
search_xt_button_press=[]; localize_xt_button_press=[];

for PacketCount=1:NumPackets_dtS-1 %This loop identifies at which packet #
the operator pushes the button
  if trigger_logical_dtS(PacketCount)+trigger_logical_dtS(PacketCount+1)==1
    search_dt_button_press=[search_dt_button_press;PacketCount];
  end
end
```

```
        for PacketCount=1:NumPackets_dtL-1 %This loop identifies at which packet #
the operator pushes the button
          if trigger_logical_dtL(PacketCount)+trigger_logical_dtL(PacketCount+1)==1
            localize_dt_button_press=[localize_dt_button_press;PacketCount];
          end
        end
        for PacketCount=1:NumPackets_xtS-1 %This loop identifies at which packet #
the operator pushes the button
          if trigger_logical_xtS(PacketCount)+trigger_logical_xtS(PacketCount+1)==1
            search_xt_button_press=[search_xt_button_press;PacketCount];
          end
        end
        for PacketCount=1:NumPackets_xtL-1 %This loop identifies at which packet #
the operator pushes the button
          if trigger_logical_xtL(PacketCount)+trigger_logical_xtL(PacketCount+1)==1
            localize_xt_button_press=[localize_xt_button_press;PacketCount];
          end
        end

        N=size(localize_dt,1)-8;

        % Determine the number of "regions" where a region is defined
```

```
        % as an area between operator button presses
        search_dt_numregions=(size(search_dt_button_press,1)+1);
        localize_dt_numregions=(size(localize_dt_button_press,1)+1);
        search_xt_numregions=(size(search_xt_button_press,1)+1);
        localize_xt_numregions=(size(localize_xt_button_press,1)+1);

        search_dt_M=zeros(N,search_dt_numregions);
search_dt_sigma=zeros(N,search_dt_numregions);
        localize_dt_M=zeros(N,localize_dt_numregions);
localize_dt_sigma=zeros(N,localize_dt_numregions);
        search_xt_M=zeros(N,search_xt_numregions);
search_xt_sigma=zeros(N,search_xt_numregions);
        localize_xt_M=zeros(N,localize_xt_numregions);
localize_xt_sigma=zeros(N,localize_xt_numregions);

        Ksum_metric_dtL=zeros(1,NumPackets_dtL);
Ksum_metric_dtS=zeros(1,NumPackets_dtS);
        Ksum_metric_xtL=zeros(1,NumPackets_xtL);
Ksum_metric_xtS=zeros(1,NumPackets_xtS);
        sig_dtL=zeros(N,NumPackets_dtL); sig_dtS=zeros(N,NumPackets_dtS);
        sig_xtL=zeros(N,NumPackets_xtL); sig_xtS=zeros(N,NumPackets_xtS);
        buffer = 50; bckgrd_size=60;
```

```
% Search DT
%The mean and stddeviation is calculated for no button presses
if search_dt_numregions==1
  for i=9:N
  search_dt_M(i,1)=mean(blank_data(i,2:BlankPackets));
  search_dt_sigma(i,1)=std(blank_data(i,2:BlankPackets))/3;
  end
else
%The mean and stddeviation is calculated for all other regions
 for region=1:search_dt_numregions
  for i=9:N
    if region==1
      search_dt_M(i,region)=mean(search_dt(i,(search_dt_button_press(region)-
buffer-bckgrd_size):(search_dt_button_press(region)-buffer)));
      search_dt_sigma(i,region)=std(search_dt(i,(search_dt_button_press(region)-
buffer-bckgrd_size):(search_dt_button_press(region)-buffer)));
    elseif region==search_dt_numregions
      search_dt_M(i,region)=mean(search_dt(i,search_dt_button_press(region-
1)+buffer:search_dt_button_press(region-1)+buffer+bckgrd_size));
      search_dt_sigma(i,region)=std(search_dt(i,search_dt_button_press(region-
1)+buffer:search_dt_button_press(region-1)+buffer+bckgrd_size));
    elseif mod(region,2)==0
```

```
            search_dt_M(i,region)=mean(search_dt(i,(search_dt_button_press(region-1)-
buffer-bckgrd_size):(search_dt_button_press(region-1)-buffer)));
            search_dt_sigma(i,region)=std(search_dt(i,(search_dt_button_press(region-
1)-buffer-bckgrd_size):(search_dt_button_press(region-1)-buffer)));
          else
            search_dt_M(i,region)=mean(search_dt(i,(search_dt_button_press(region)-
buffer-bckgrd_size):(search_dt_button_press(region)-buffer)));
            search_dt_sigma(i,region)=std(search_dt(i,(search_dt_button_press(region)-
buffer-bckgrd_size):(search_dt_button_press(region)-buffer)));
           end
         end
        end
       end
      % Localize DT
       %The mean and stddeviation is calculated for no button presses
      if localize_dt_numregions==1
        for i=9:N
        localize_dt_M(i,1)=mean(blank_data(i,2:BlankPackets));
        localize_dt_sigma(i,1)=std(blank_data(i,2:BlankPackets));
        end
      else
      %The mean and stddeviation is calculated for all other regions
```

```
for region=1:localize_dt_numregions
 for i=9:N
  if region==1

localize_dt_M(i,region)=mean(localize_dt(i,localize_dt_button_press(region)-buffer-
bckgrd_size:localize_dt_button_press(region)-buffer));

localize_dt_sigma(i,region)=std(localize_dt(i,localize_dt_button_press(region)-buffer-
bckgrd_size:localize_dt_button_press(region)-buffer));
  elseif region==localize_dt_numregions

localize_dt_M(i,region)=mean(localize_dt(i,localize_dt_button_press(region-
1)+buffer:localize_dt_button_press(region-1)+buffer+bckgrd_size));

localize_dt_sigma(i,region)=std(localize_dt(i,localize_dt_button_press(region-
1)+buffer:localize_dt_button_press(region-1)+buffer+bckgrd_size));
  elseif mod(region,2)==0

localize_dt_M(i,region)=mean(localize_dt(i,localize_dt_button_press(region-1)-buffer-
bckgrd_size:localize_dt_button_press(region-1)-buffer));
```

```
localize_dt_sigma(i,region)=std(localize_dt(i,localize_dt_button_press(region-1)-buffer-
bckgrd_size:localize_dt_button_press(region-1)-buffer));
                else

localize_dt_M(i,region)=mean(localize_dt(i,localize_dt_button_press(region)-buffer-
bckgrd_size:localize_dt_button_press(region)-buffer));

localize_dt_sigma(i,region)=std(localize_dt(i,localize_dt_button_press(region)-buffer-
bckgrd_size:localize_dt_button_press(region)-buffer));
                end
              end
             end
            end
           % Search XT
            %The mean and stddeviation is calculated for no button presses
            if search_xt_numregions==1
              for i=9:N
              search_xt_M(i,1)=mean(blank_data(i,2:BlankPackets));
              search_xt_sigma(i,1)=std(blank_data(i,2:BlankPackets))/3;
              end
            else
```

```
%The mean and stddeviation is calculated for all other regions
 for region=1:search_xt_numregions
  for i=9:N
   if region==1
    search_xt_M(i,region)=mean(search_xt(i,search_xt_button_press(region)-
buffer-bckgrd_size:search_xt_button_press(region)-buffer));
    search_xt_sigma(i,region)=std(search_xt(i,search_xt_button_press(region)-
buffer-bckgrd_size:search_xt_button_press(region)-buffer));
   elseif region==search_xt_numregions
    search_xt_M(i,region)=mean(search_xt(i,search_xt_button_press(region-
1)+buffer:search_xt_button_press(region-1)+buffer+bckgrd_size));
    search_xt_sigma(i,region)=std(search_xt(i,search_xt_button_press(region-
1)+buffer:search_xt_button_press(region-1)+buffer+bckgrd_size));
   elseif mod(region,2)==0
    search_xt_M(i,region)=mean(search_xt(i,search_xt_button_press(region-1)-
buffer-bckgrd_size:search_xt_button_press(region-1)-buffer));
    search_xt_sigma(i,region)=std(search_xt(i,search_xt_button_press(region-
1)-buffer-bckgrd_size:search_xt_button_press(region-1)-buffer));
   else
    search_xt_M(i,region)=mean(search_xt(i,search_xt_button_press(region)-
buffer-bckgrd_size:search_xt_button_press(region)-buffer));
```

```
                search_xt_sigma(i,region)=std(search_xt(i,search_xt_button_press(region)-
buffer-bckgrd_size:search_xt_button_press(region)-buffer));
              end
             end
            end
           end
          % Localize XT
           %The mean and stddeviation is calculated for no button presses
          if localize_xt_numregions==1
            for i=9:N
            localize_xt_M(i,1)=mean(blank_data(i,2:BlankPackets));
            localize_xt_sigma(i,1)=std(blank_data(i,2:BlankPackets));
            end
          else
          %The mean and stddeviation is calculated for all other regions
           for region=1:localize_xt_numregions
            for i=9:N
              if region==1

localize_xt_M(i,region)=mean(localize_xt(i,localize_xt_button_press(region)-buffer-
bckgrd_size:localize_xt_button_press(region)-buffer));
```

```
localize_xt_sigma(i,region)=std(localize_xt(i,localize_xt_button_press(region)-buffer-
bckgrd_size:localize_xt_button_press(region)-buffer));
        elseif region==localize_xt_numregions

localize_xt_M(i,region)=mean(localize_xt(i,localize_xt_button_press(region-
1)+buffer:localize_xt_button_press(region-1)+buffer+bckgrd_size));

localize_xt_sigma(i,region)=std(localize_xt(i,localize_xt_button_press(region-
1)+buffer:localize_xt_button_press(region-1)+buffer+bckgrd_size));
        elseif mod(region,2)==0

localize_xt_M(i,region)=mean(localize_xt(i,localize_xt_button_press(region-1)-buffer-
bckgrd_size:localize_xt_button_press(region-1)-buffer));

localize_xt_sigma(i,region)=std(localize_xt(i,localize_xt_button_press(region-1)-buffer-
bckgrd_size:localize_xt_button_press(region-1)-buffer));
        else

localize_xt_M(i,region)=mean(localize_xt(i,localize_xt_button_press(region)-buffer-
bckgrd_size:localize_xt_button_press(region)-buffer));
```

```
localize_xt_sigma(i,region)=std(localize_xt(i,localize_xt_button_press(region)-buffer-
bckgrd_size:localize_xt_button_press(region)-buffer));
            end
          end
         end
        end

        %this large for loop loops over all packets with a sub loop that loopsM
        %over all time bins. The sub loop calculates all the signifcance values
        %which are added up in the main for loop for each packet.
        search_dt_index=1; search_xt_index=1; localize_dt_index=1;
localize_xt_index=1;

        search_dt_final_button_press=size(search_dt_button_press,1);
        localize_dt_final_button_press=size(localize_dt_button_press,1);
        search_xt_final_button_press=size(search_xt_button_press,1);
        localize_xt_final_button_press=size(localize_xt_button_press,1);

        for PacketCount=1:NumPackets_dtL
         if localize_dt_index>localize_dt_final_button_press
           localize_dt_index=localize_dt_final_button_press+1;
```

```
elseif PacketCount>localize_dt_button_press(localize_dt_index);
   localize_dt_index=localize_dt_index+1;
end

for timebins=9:N
  sig_dtL(timebins,PacketCount)=(localize_dt(timebins,PacketCount)-
localize_dt_M(timebins,localize_dt_index))/(localize_dt_sigma(timebins,localize_dt_ind
ex));
end
Ksum_metric_dtL(1,PacketCount)=(1/N)*sum(sig_dtL(:,PacketCount).^2);
end

for PacketCount=1:NumPackets_dtS
if search_dt_index>search_dt_final_button_press
  search_dt_index=search_dt_final_button_press+1;
elseif PacketCount>search_dt_button_press(search_dt_index);
   search_dt_index=search_dt_index+1;
end
for timebins=9:N
  sig_dtS(timebins,PacketCount)=(search_dt(timebins,PacketCount)-
search_dt_M(timebins,search_dt_index))/(search_dt_sigma(timebins,search_dt_index));
end
```

```
 Ksum_metric_dtS(1,PacketCount)=(1/N)*sum(sig_dtS(:,PacketCount).^2);
end

for PacketCount=1:NumPackets_xtL
 if localize_xt_index>localize_xt_final_button_press
  localize_xt_index=localize_xt_final_button_press+1;
 elseif PacketCount>localize_xt_button_press(localize_xt_index);
   localize_xt_index=localize_xt_index+1;
 end
 for timebins=9:N
  sig_xtL(timebins,PacketCount)=(localize_xt(timebins,PacketCount)-
localize_xt_M(timebins,localize_xt_index))/(localize_xt_sigma(timebins,localize_xt_ind
ex));
 end
 Ksum_metric_xtL(1,PacketCount)=(1/N)*sum(sig_xtL(:,PacketCount).^2);
end


for PacketCount=1:NumPackets_xtS
 if search_xt_index>search_xt_final_button_press
  search_xt_index=search_xt_final_button_press+1;
 elseif PacketCount>search_xt_button_press(search_xt_index);
```

```
            search_xt_index=search_xt_index+1;
        end
        for timebins=9:N
          sig_xtS(timebins,PacketCount)=(search_xt(timebins,PacketCount)-
search_xt_M(timebins,search_xt_index))/(search_xt_sigma(timebins,search_xt_index));
        end
        Ksum_metric_xtS(1,PacketCount)=(1/N)*sum(sig_xtS(:,PacketCount).^2);
      end


    % Place all Ksum values into a struct to be saved into a .mat file
      Ksum.dtL=medfilt1(Ksum_metric_dtL);
Ksum.dtL_Trigger=trigger_logical_dtL;
      Ksum.dtS=medfilt1(Ksum_metric_dtS); Ksum.dtS_Trigger=trigger_logical_dtS;
      Ksum.xtS=medfilt1(Ksum_metric_xtS); Ksum.xtS_Trigger=trigger_logical_xtS;
      Ksum.xtL=medfilt1(Ksum_metric_xtL);
Ksum.xtL_Trigger=trigger_logical_xtL;
      if count < 10
        file=FileList{count,1};
        Ksum_MatFile=[file(1:end-6),'_Ksum_Trigger.mat'];
      else
        file=FileList{count,1};
        Ksum_MatFile=[file(1:end-7),'_Ksum_Trigger.mat'];
```

```
  end
  save(Ksum_MatFile,'Ksum');
  count=count+5;
end
```

A.2 Pinning Position Sensor Data

```
% Reads in a lookup file of a position sensor data file and the
% corresponding ground truth coordinates for respective grid for pinning the
% position sensor data
[fn, pathname, filterindex] = uigetfile(...
  {'*.asc', '*asc'; '*.*', 'All Files (*.*)'},...
  'Pick data file(s) please','C:\Data\HH_DataCollections\');
fid=fopen([pathname fn]);
Filelist = textscan(fid,'%s%s')
PosSens_FileList=cellstr(Filelist{1,1});
GT_FileList=cellstr(Filelist{1,2});
num_files=length(PosSens_FileList);
% Define direction for pinning position sensor data. Choices are XT or DT
Search_direction='DT';
  for file_count=1:num_files
    load(PosSens_FileList{file_count,1});
    fidtlane=fopen(GT_FileList{file_count,1});
```

```
xdata=textscan(fidtlane,'%d64%f%f%*f%s%*[^\n]','delimiter',',','commentstyle','//');
        IDs=xdata{1,1}; Northings=xdata{1,2}; Eastings=xdata{1,3};
        % Find the first swing edge to determine rotation angle
        [pks, locs]=findpeaks(x,'MinPeakProminence', 0.5);
        % Use BOLR and EOLR for XT Search and BOLL and BOLR for DT Search
        BOLL=[Northings(1) Eastings(1)]; BOLR=[Northings(2) Eastings(2)];
        EOLR=[Northings(3) Eastings(3)];
        if strcmp(Search_direction,'XT')
          lane_vect=EOLR-BOLR;
        elseif Sstrcmp(Search_direction,'DT')
          lane_vect=BOLR-BOLL;
        end
        SwingStartXT=[y(1) x(1)]; FirstSwingEndXT=[y(locs(1)) x(locs(1))];
        FirstSwing_vect=FirstSwingEndXT-SwingStartXT;
        % Save x and y data into a matrix
        z = [x;y];
        % Rotate x and y data

t=acos((dot(FirstSwing_vect,lane_vect))/(sqrt((FirstSwing_vect(1)^2+FirstSwing_vect(2)
^2))*sqrt((lane_vect(1)^2+lane_vect(2)^2))));
        z_Rot = [cos(t) -sin(t); sin(t) cos(t)]*z;
```

```
figure; plot(x,y,'b');hold on; plot(z_Rot(1,:),z_Rot(2,:),'r');
Coords=[z_Rot(1,:)+BOLR(2);z_Rot(2,:)+BOLR(1)];
translation=[z_Rot(1,1);z_Rot(2,1)];
Coords_final=Coords-translation;
% Plot pinned position data and save figure
figure; plot(Coords_final(1,:),Coords_final(2,:)); hold on;
plot(Eastings,Northings,'ko');
figname=PosSens_FileList{file_count,1};
figname=[figname(1:end-4),'_Pinned.fig'];
savefig(figname)
num_scans=length(x);
GoodData=ones(1,length(x)-1);
diffx=diff(x);
for i=1:num_scans-1
 if abs(diffx(:,i))>0.1
 GoodData(:,i)=0;
 end
end
save(PosSens_FileList{file_count,1}, '-append', 'Coords_final','GoodData');
end
```

REFERENCES

[1] C. Woody, "A dangerous weapon from wars that are long over is still wreaking havoc around the world," 18 08 2016. [Online]. Available: http://www.businessinsider.com/land-mines-still-dangerous-around-the-world-and-used-by-isis-2016-8.

[2] "iCasualties," 2009. [Online]. Available: http://icasualties.org/oef/. [Accessed 20 03 2016].

[3] D. J. Daniels, Ground Penetrating Radar, London: Institution of Electrical Engineers, 2004.

[4] J. M. H. S.-H. H. L. W. D. a. C. J. R. Timothy W. Miller. Brian Borchers, "Effects of soil physical properties on GPR for landmine detection," 2002.

[5] C. M. a. A. Murk, "Complex dielectric constant of dry sand in the 0.1 to 2 GHz range," Bern, 2010.

[6] F. P. a. C. Hoover, "Simulant Mines Overview and Technical Data," Alexandria, 1998.

[7] S. A. V. H. H. P. a. K. T. Jan Igel, "From Soil Measurements to Detector Performance- How to Predict Soil Influence on EMI and GPR Sensors," in *AMEREM*, Ottawa, 2010.

[8] A. I. J. M. Mohammed Metwaly, "Evaluating some factors that affect feasiility of using ground penetrating radar for landmine detection," *Applied Geophysics*, vol. 4, no. 3, pp. 221-230, 2007.

[9] T. P. M. a. G. S. Smith, "Land Mine Detection Using a Ground-Penetrating Radar Based on Resistively Loaded Vee Dipoles," *IEEE Transactions on Antennas and Propagation*, vol. 47, no. 12, p. 12, 1999.

[10] R. J. Sullivan, Radar Foundations for Imaging and Advanced Concepts, Edison: SciTech, 2004.

[11] E. M. Rosen, "Assessment of down-looking GPR sensor for landmine detection," in *SPIE*, Orlando, 2005.

[12] H. Frigui and A. Khalifa, "Fusion of Multiple Algorithms for Detecting Buried Objects using Fuzzy Interference," in *SPIE*, Baltimore, 2014.

[13] H. a. G. Frigui, "Detection and discrimination of lande mines in ground penetrating radar based on edge histogram descriptors and a possibilistic k-nearest neighbor classifier," *Fuzzy Systems, IEEE Transations*, pp. 185-199, 2009.

[14] P. Gader, M. Mystkowski and Y. and Zhao, "Landmine detection with ground penetrating radar using hidden markov models," *Geoscience and Remote Sensing*, pp. 1231-1244, 2001.

[15] P. S. R. Diniz, Adaptive Filtering, New York: Springer, 2013.

BIOGRAPHY

Marie Talbott (formerly Marie Fishel) graduated from George Mason University with a Bachelor of Science in Physics and Electrical Engineering in December 2011. Marie is a Research Associate at the Institute for Defense Analyses, where she has worked since 2011 while pursuing her Master of Science in Electrical Engineering.